Carbon Nanofibre Purification

Process Design, Modelling and Analysis of Carbon Nanofibre Purification with Acid Leaching

MSc Thesis Report

Killian Hendrikus Gerardus van Oers

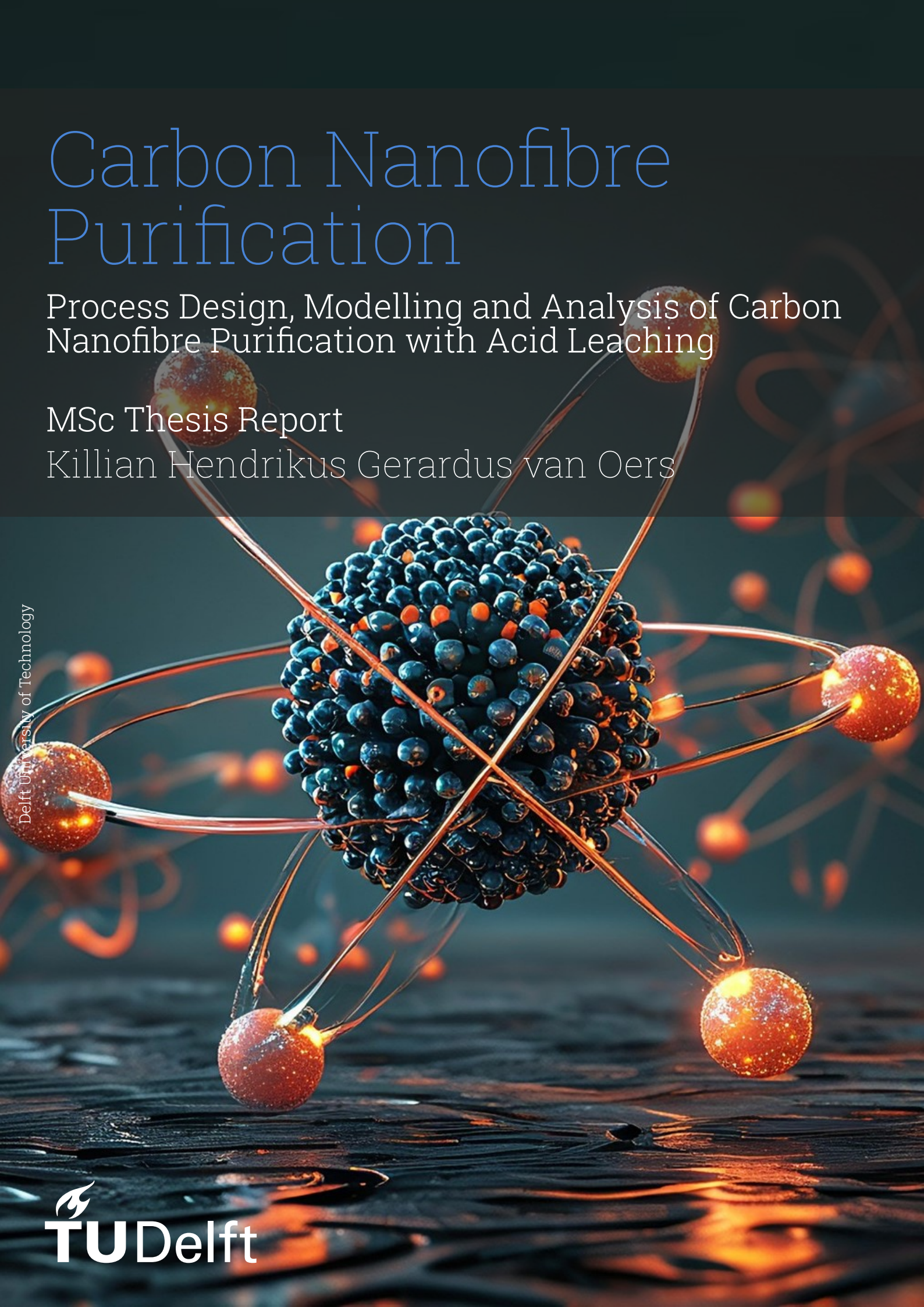

Delft University of Technology

TU Delft

Carbon Nanofibre Purification

Process Design, Modelling and Analysis of Carbon Nanofibre Purification with Acid Leaching

by

Killian Hendrikus Gerardus van Oers

Student number:	5124719
Supervisors:	Ir. P.B. Tamarona
	Prof. Dr. Ir. T.J.H. Vlugt
	Dr. Ir. M. Ramdin
Thesis Committee:	Ir. P.B. Tamarona
	Prof. Dr. Ir. T.J.H. Vlugt
	Dr. Ir. M. Ramdin
	Dr. Ir. R.M. Hartkamp
Course:	ME55035 ME-EFPT MSc Thesis
Faculty:	Faculty of Mechanical Engineering, Delft
Department:	Process & Energy

TU Delft

Preface and Acknowledgements

This paper provides the research for my master's thesis in mechanical engineering, which I have been working on for the past 11 months. It all started during high school, in which I was able to work on all kinds of technical project thanks to the technasium study program. This influenced my choice for the bachelor in mechanical engineering at TU Delft, which I managed to complete successfully in 3 years. Following the bachelor program, I decided to pursue a master's in mechanical engineering, specifically the energy, flow and process engineering track. The process industry and the many challenges it faces really interest me.

The master's thesis started with an extensive literature review. Many hours were spent in the library, reading through article after article trying to find important information and looking for literature gaps. Although diving into literature is not my favourite task, I managed to pull through and I am grateful I did so. Following the literature review, I started working on the process design, building a Python and Aspen model and conducting acid leaching experiments. The process design proved to be a very iterative process, in which I kept running into new problems when I changed the design slightly. Building the Python and Aspen model helped me to improve my understanding of both massively. Conducting the acid leaching experiments together with Panji Tamarona was also very insightful and taught me how precise you need to work when carrying out experiments. Nearing the end of the thesis, I actually enjoyed writing this report. Although it was a lot of work, it was never boring.

To complete the master's thesis, I required the help of numerous people. Without their help, the master's thesis would not be possible. First, I would like to express my gratitude to my supervisors for their assistance during my master's thesis: Panji Tamarona, Thijs Vlugt and Mahinder Ramdin. Panji helped me a ton by providing detailed feedback on the literature review, helping me with the code or calculations whenever I got stuck and we collaborated with the acid leaching experiments. Especially the latter has been a long process so far, with many problems we encountered and had to solve. Thijs and Mahinder provided me with a lot of guidance and valuable feedback both during and outside of our numerous progress meetings and their expertise helped me to improve the end result. I am grateful for all of their help.

I want to express my sincerest gratitude to Chenna Rao Borra, who helped Panji and me in setting up the acid leaching experiments. Although we live on the other side of the world, we managed to make online meetings possible. Chenna always managed to come up with solid solutions for the problems we encountered and provided us with further advice on the experiments. Without Chenna, we would not have the current results of the acid leaching experiments.

I would like to thank Michel van den Brink for his assistance in the lab. Michel conducted the ICP analysis on the samples for us, ordered the required materials and sorted the equipment out and helped us detail the experimental procedure. In addition, I would like to thank Prasad Gonugunta for carrying out the XRF analysis on the CNF samples and thank both Prasad and Ruud Hendrix for carrying out the XRD analysis on the samples. Their help is much appreciated.

My gratitude goes out towards my family: my father Henry, mother Margo't and brother Kevin. Their support throughout my life and studies allowed me to write this master's thesis and become the person I want to be in life. From the bottom of my heart: thank you.

I would also like to extend my gratitude towards my roommates, my friends, my fellow board members and my football team members as the time spent with them gave me great joy during the last 6.5 years of my life.

Killian Hendrikus Gerardus van Oers,
Delft, December 2025

Abstract

Catalytic methane pyrolysis (CMP) is a potential method to produce clean hydrogen without direct COx emissions, but is not cost-competitive with current hydrogen production techniques yet. A strategy to increase the cost-competitiveness is to purify and sell the nanocarbon by-product. This paper outlines the process design, modelling and analysis of purifying carbon nanofibre (CNF), produced by CMP, with acid leaching.

CNF produced by CMP with a Ni-SiO_2 catalyst was used for this study and initially contains 4700 ppm of nickel. The baseline scenario of the designed process has a production capacity of 20,000 tonnes per year and includes acid leaching with HCl, liquid removal and post-treatment steps. The techno-economic analysis showed a Levelized Cost of Purification (LCOP) of 10.09 $/kg and a Net Present Value (NPV) of 1.48 billion $ for the baseline scenario. The process is very profitable due to the assumed high selling price of 25 $/kg. However, the conversion of nickel is only equal to 5.15 %, leaving 4460 ppm of nickel in the CNF product while the desired nickel content is below 300 ppm. The low conversion indicates that the quality of the CNF product is barely improved and that the assumed selling price is probably too high. The acid leaching kinetics are modelled using literature on acid leaching with HCl of nickel from a Ni-Al_2O_3 spent catalyst. Acid leaching experiments of nickel from CNF with H_2SO_4 showed a more positive average nickel conversion of 70.9 % so far. The leaching kinetics still have to be determined for a variety of acids and will be necessary to model the leaching more accurately.

Sensitivity analyses showed that the impact of the acid waste price on the LCOP was the largest of the economic parameters with ±2.5 $/kg variation, followed by the electricity price. The acid feed price also had a significant impact on the LCOP. The high impact of the acid waste and feed price showed a need for the implementation of an acid recycle. A Monte Carlo analysis indicated a robust process design under economic uncertainties. The mean of the LCOP was equal to 10.12 $/kg and the standard deviation was equal to 0.90 $/kg.

Two improved design cases of the baseline scenario are presented. The first includes changes to the reactor temperature, residence time, acid molarity, ratio of CNF feed to acid feed and the inclusion of an acid recycle. The conversion is improved to 61.04 % with an LCOP of 24.68 $/kg. The second design case builds upon the first and includes further changes to the residence time and ratio of CNF feed to acid feed. Furthermore, the reactor setup is changed to three reactors placed in series for the second design case. The conversion is increased to 93.95 %, leaving only 285.66 ppm of nickel in the CNF product. The LCOP is equal to 21.84 $/kg, but a total of 90 reactors are required. While the process is profitable and the nickel content in the product is below 300 ppm, questions arise whether the second improved design is practical.

Nomenclature

Abbreviations

Abbreviation	Definition
AC	Activated carbon
Al	Aluminium
Al_2O_3	Aluminium oxide
Ar	Argon
Aspen	Advanced System for Process Engineering
ASTM	American Society for Testing and Materials
Bi	Bismuth
C	Carbon
Ca	Calcium
$CaCO_3$	Calcium carbonate
CAPEX	Capital expenditure
CB	Carbon black
CCOP	Cash cost of production
CEMNPs	Carbon-encapsulated metal nanoparticles
CEPCI	Chemical Engineering Plant Cost Index
CF	Cash flow
CH_4	Methane
Cl	Chlorine
CMP	Catalytic methane pyrolysis
CNF	Carbon nanofibre
CNM	Carbon nanomaterial
CNO	Carbon nano-onion
CNP	Carbon nanoparticle
CNT	Carbon nanotube
CO	Carbon monoxide
Co	Cobalt
COD	Crystallography Open Database
CoMo-Cat	Cobalt-molybdenum catalyst
CO_x	Oxycarbon
CO_2	Carbon dioxide
CPI	Consumer price index
CS_2	Carbon disulfide
CSTR	Continuously-stirred-tank-reactor
Cu	Copper
DMF	Dimethylformamide
DSO	Direct salary overhead
DWCNTs	Double-walled carbon nanotubes
D&E	Design and engineering
FC	Fixed capital
FCOP	Fixed costs of production
Fe	Iron
$FeCl_2$	Iron(II) chloride
FOB	Free on board
GNF	Graphene nanofibre
GPO	General plant overhead

Abbreviation	Definition
H_2	Hydrogen
H_2O	Water
H_2O_2	Hydrogen peroxide
H_2SO_4	Sulfuric acid
HCl	Hydrochloric acid
HIDE	Hydrothermally initiated dynamic extraction
HiPCO	High-pressure carbon monoxide
HNO_3	Nitric acid
ICDD	International Centre for Diffraction Data
ICP	Inductively coupled plasma
Ir	Iridium
IRR	Internal rate of return
ISBL	Inside battery limits investment
LCOP	Levelized cost of purification
LMTD	Log mean temperature difference
Mg	Magnesium
MgO	Magnesium oxide
Mo	Molybdenum
MSI	Metal-support interaction
Mt	Megatonnes
MWCNTs	Multi-walled carbon nanotubes
Na	Natrium
ND	Nanodiamond
NH_3	Ammonia
NH_4	Ammonium
Ni	Nickel
NO_2	Nitrogen dioxide
NPV	Net present value
O_2	Oxygen
OPEX	Operational expenditure
OSBL	Offsite costs or Outside battery limits investment
PBT	Payback time
Pd	Palladium
PFP	Preliminary fixed production
PFR	Plug flow reactor
PSD	Particle size distribution
P&R	Patents and royalties
RH	Relative humidity
ROI	Return on investment
ROR	Rate of return
R&D	Research and development
S	Sulphur
Sb	Antimony
Sc	Scandium
SDS	Sodium dodecyl sulfate
Sell&Market	Selling and marketing
SEM	Scanning electron microscopy
Si	Silicon
SiO_2	Silicon dioxide
SMR	Steam methane reforming
SO_4	Sulphate
SWCNTs	Single-walled carbon nanotubes
S&M	Supervision and management
SSHE	Scraped surface heat exchanger

Abbreviation	Definition
STD	Standard deviation
USD	US Dollars
VCOP	Variable cost of production
XRD	X-ray diffraction
XRF	X-ray fluorescence
Zn	Zinc
ZrO_2	Zirconium(IV)oxide

Symbols

Symbol	Definition	Unit
A	Area	m^2
C	Cost	$
C_0	Initial investment	$
C_{total}	Total investment	$
c_{dust}	Dust concentration in the air	μg m^{-3}
c_p	Heat capacity at constant pressure	kJ kg^{-1} K^{-1} or J kg^{-1} K^{-1} or kJ mol^{-1} K^{-1}
CF	Cash flow	$
D	Diameter	m
E	Energy	kWh
E_a	Activation energy	kJ mol^{-1}
F_i	Cost factor	
$F_{\text{acid solution}}$	Ratio of acid feed volumetric flow rate over the CNF feed mass flow rate	
$\dot{F}$	Filtration rate	kg m^{-2} hr^{-1}
f	Safety factor	
f_i	Installation factor i	
H	Enthalpy	kJ·mol^{-1}
h	Specific enthalpy	J kg^{-1} or kJ kg^{-1}
I	Interest rate	
k	Pre-exponential factor	Consistent with reaction rate
L_f	Location factor	
m	Mass	kg or tonne
$\dot{m}$	Mass flow rate	kg hr^{-1}
N_i	Number of i	
$\dot{N}$	Normal volumetric flow rate	N m^3 s^{-1}
n	Mole concentration	mol
$\dot{n}$	Molar flow rate	kmol hr^{-1}
$P_{\text{cumulative}}$	Cumulative net profit	$
P_{gross}	Gross profit	$
P_i	Production of i	tonnes per year
p	Pressure	atm, bar or kPa
$\dot{Q}$	Heating or cooling rate	kW
R	Universal gas constant	kJ mol^{-1} K^{-1}
R_i	Revenue of i	$
R^2	Coefficient of determination	
r	Reaction rate	kmol s^{-1} m^{-3}
S_i	Size	

Symbol	Definition	Unit
T	Temperature	°C or K
T_i	Income tax	$
T_p	Tax to be paid	$
T_r	Tax rate	
t	Time	years
U	Overall heat transfer coefficient	W m^{-2} K^{-1}
V	Volume	m^3
V_i	Price of i	$/tonne
$\dot{V}$	Volumetric flow rate	m^3 hr^{-1}, L s^{-1} or m^3 per year
W	Monthy salary	$ per month
X	Conversion	
X_i	Cepci index in year i	
α	Pre-exponential factor	Consistent with reaction rate
Δ	Difference	
η	Efficiency	
ι	Submergence factor	
Λ	Heat of dissolution	kJ kg^{-1}
λ	Heat of ...	kJ kg^{-1}
μ	Mean	
ξ	Depreciation factor	
ρ	Density	kg m^{-3}
$\sum$	Summation	
σ	Standard deviation	
Υ	Steam generator rating	MMBtu hr^{-1}
χ	Concentration	kmol m^{-3}
ψ	Absolute humidity	kg water per kg air

Contents

List of Figures

List of Tables

1

Introduction

Hydrogen is a great energy carrier and a clean fuel, therefore it receives a lot of attention.[1] Currently, the global demand for hydrogen is ever increasing. In 2023 the hydrogen demand equalled 97 Megatonnes (Mt). The demand is expected to grow to 100 Mt in 2024 and close to 150 Mt in 2030.[2] The refining and industry sectors are currently responsible for almost all hydrogen demand.[2] Hydrogen is largely produced by techniques which emit a large amount of greenhouse gases. In 2023, CO_2 emissions related to hydrogen production equalled 920 Mt.[2] Steam methane reforming (SMR) and coal gasification are responsible for 96 % of the hydrogen production.[3] SMR and coal gasification emit 11 and 26 kg CO_2 per kg of H_2 respectively.[4] The increasing CO_2 levels play a vital role in global warming. Concentrations have risen to 412 ppmv in 2018, as compared to 275 ppmv before the year 1800.[5] To battle global warming and climate change, the European Union has the ambition to be climate neutral by 2050. Therefore, it is important to replace current hydrogen production techniques with low-emission and net zero ones.

A possible process to replace current hydrogen production techniques is catalytic methane pyrolysis (CMP). CMP can produce clean hydrogen without direct COx emissions and creates a possibly valuable carbon by-product.[6] CMP is not a 100 % green process, since it uses natural gas to produce hydrogen and carbon. Therefore, CMP is considered to be a bridging-technology.[3] A current issue with CMP is the deposition of the carbon on the catalyst, which leads to catalyst deactivation.[6] Furthermore, CMP is not cost-competitive with current hydrogen production techniques yet. A strategy to increase the cost-competitiveness is to purify and sell the carbon by-product, of which the price depends on the type and purity. Different types of nanocarbon can form in CMP: carbon nanofibres (CNFs), carbon nanotubes (CNTs), carbon black (CB) and also amorphous carbon. CNT has the highest selling price, followed by CNF and CB.

Nanocarbons have many applications in different fields of technology. Nanocarbons can be used in the biomedical field for multiple purposes, such as tissue engineering, biomedical imaging, cancer therapy and drug delivery.[6,7] Nanocarbons can also be used for the creation of high-strength composites. Specifically CNTs and CNFs can improve the physio-mechanical properties of composite materials.[8] In addition, nanocarbons can be used in water purification applications, which includes the potential removal of pathogens and adsorption of hazardous water contaminants.[9] Other applications of nanocarbons encompass: use as anodes in lithium-ion batteries[8,10]; supercapacitors[6,8,10]; sensors[6,8,10,11]; energy storage[6,8]; catalyst supports[11,12]; field emission devices[12,13]; fuel cells[10,13] and hydrogen storage.[7,12]

A specific CNF mentioned in literature is from research by Hadian et al.[14]. Through CMP with a Ni-SiO_2 catalyst, CNF is formed. The formed CNFs have a fish bone structure diameters between 15 to 80 nm and around 70 g of carbon per g of catalyst is formed with a catalyst lifetime of 12 h at 550 °C. Physical samples of the CNFs have been obtained.

There are only a few studies in current literature which have managed to combine the production of nanocarbons, specifically through CMP, and the purification of nanocarbons.[1,15–17] Furthermore, a detailed nanocarbon purification process for CMP obtained nanocarbons combined with simulation

through a commercial simulation tool is still missing. The combination of both could provide an in-depth optimisation and techno-economic analysis of the purification process of CMP obtained nanocarbons. Furthermore, research into CMP could be advanced and the research will potentially help to make CMP more cost-competitive.

The aim of the study is: *The design and modelling of a conceptual process for the continuous purification of nanocarbon produced by catalytic methane pyrolysis and to determine its economic viability.* This leads to the main research question of the study: *How to design and model a conceptual process for the continuous purification of nanocarbon produced by catalytic methane pyrolysis and how to determine its economic viability?* The specific nanocarbon that is the basis of the purification process is CNF produced by CMP with a Ni-SiO_2 catalyst. To answer the main research question, the following sub-questions have been formulated:

1. What nanocarbon types originate from catalytic methane pyrolysis, what is the current state of the nanocarbon market and what are the nanocarbon prices and quality requirements?
2. What methods are available for nanocarbon purification & processing and how can these methods be incorporated in a design for a nanocarbon purification plant?
3. What is the economic viability of the conceptual nanocarbon purification process and how to estimate it with the help of a commercial simulation tool?
4. What are the key parameters that influence the process plant's economic viability?

The structure of the report is as follows. Chapter 2 describes the theoretical background in the form of a literature review. Chapter 3 highlights the research plan, followed by the discussion of the acid leaching experiments of nickel from CNF in Chapter 4. Chapter 5 discusses the process design and the equipment calculations. Afterwards, Chapter 6 details the techno-economic calculations used in the model. Chapter 7 outlines the input for Aspen, the curve fitting of the acid leaching kinetics and the input for the techno-economic and sensitivity analysis. Chapter 8 covers the results of the research and includes a discussion. Finally, Chapter 9 contains a conclusion and recommendations for future research.

To effectively search for useful literature, a search plan is developed. The three main methods used to find literature are the snowball method, citation searching and keyword searching. Retrieved literature is stored in a reference manager and categorised in order to maintain a clear overview. First off the snowball method is applied to literature reviews to find literature on the topics of CMP and nanocarbon purification. The reviews are important because many relevant sources are contained within. Note that the snowball method is also applied to other sources and is not limited to application on the literature reviews. The main literature reviews that were used for the snowball method are:

- Hantoko, D.; Khan, W. U.; Putra, A. F. P.; Shoaibi, A. A.; Chandrasekar, S.; Hossain, M. M. Industrial & Engineering Chemistry Research 2024, 63, 18869–18878.
- Sánchez-Bastardo, N.; Schlögl, R.; Ruland, H. Industrial & Engineering Chemistry Research 2021, 60, 11855–11881.
- Agboola, A.; Pike, R.; Hertwig, T.; Lou, H. Clean Technologies and Environmental Policy 2007, 9, 289–311
- Hou, P.-X.; Liu, C.; Cheng, H.-M. Carbon 2008, 46, 2003–2025
- Pangestu, M.; Malaibari, Z.; Muhammad, A.; Al-Rowaili, F.; Zahid, U. Energy & Fuels 2024, 38, 13514-13538

Secondly, citation searching is applied to the most important and most cited retrieved sources using Scopus. This resulted in 17 new relevant sources. It is important to note that many of the resulting sources from the citation search are either not useful for the research question or have already been retrieved in different ways. Furthermore, keyword searching using Scopus is carried out as a means to find sources on very specific topics and to try to maximize the amount of relevant literature that is retrieved. Table 1.1 gives an overview of the keyword search. Table 1.1 includes the keywords that were used, the search area and the amount of new relevant sources that were retrieved. Note that keyword searching was applied after the snowball method and citation searching. Hence, many of the relevant sources were already retrieved.

Table 1.1: Overview of the keyword search queries for the literature search. The table includes in which area of articles is searched and the amount of new relevant sources that were retrieved.

Keywords	**Searched area**	**New relevant sources**
Catalytic AND decomposition AND methane	Article title	13
Catalytic AND methane AND cracking	Article title	4
Growth AND mechanism AND nanotubes AND methane AND pyrolysis	Article title	0
Methane AND pyrolysis AND carbon AND nanotubes	Article title	2
Methane AND splitting	Article title	0
Methane AND decomposition AND catalytic AND purification	Article title	1
Purification AND carbon AND nanotubes AND methane	Article title	1
Methane AND carbon AND nanotubes AND purification	Keyword/Title/Abstract	1
Economic AND analysis AND methane AND catalytic	Article title	1

2

Literature Review

This chapter details the literature review of the research. Section 2.1 discusses CMP, nanocarbons and the catalysts used in CMP. Section 2.2 details research into processes for purification of nanocarbons produced by CMP and existing methods for the purification of nanocarbons. Section 2.3 outlines the nanocarbon market analysis followed by a brief literature review of techno-economics in Section 2.4. Section 2.5 provides the outlook of the literature review on the research.

2.1. Catalytic Methane Pyrolysis, Nanocarbons and Catalysts

2.1.1. Reaction Mechanics of Catalytic Methane Pyrolysis

CMP follows the chemical reaction in Equation 2.1. Methane is decomposed into hydrogen and valuable solid nanocarbon. It is important to note that there are no CO_x emissions during the reaction. The decomposition of methane is an endothermic reaction, meaning energy should be supplied for the reaction to commence. The standard enthalpy of the reaction is equal to $\Delta H = 74.85$ kJ·mol^{-1} at 0 °C and $\Delta H = 91.7$ kJ·mol^{-1} at 1000 °C.[18] The energy requirements are the result of the strong C-H bonds of methane that need to be broken.

$$CH_4(g) \Longrightarrow 2H_2(g) + C(s) \tag{2.1}$$

There are two proposed reaction mechanisms. The first mechanism is the molecular adsorption mechanism and the second is the dissociative adsorption mechanism.[3] Figure 2.1 visualises both mechanisms. In the molecular adsorption mechanism, methane is adsorbed on the catalyst surface and then dissociated in multiple steps. In the case of the dissociative adsorption mechanism, adsorption and the first step of methane dissociation occur simultaneously. The dissociation reactions that follow after are no different from the molecular adsorption mechanism.[3,19]

2.1.2. Nanocarbon Types

Nanocarbons are a valuable by-product of CMP which have many outstanding qualities, such as high mechanical strength, optical characteristics and significant conductivity.[20] Because of the outstanding qualities, nanocarbons are used in a variety of applications and are a valuable material.

There are many different types of nanocarbons, which can be put into different groups based on dimension, as shown in Figure 2.2. First off are zero-dimensional nanocarbons, which are nanocarbons that are either a single point or have no extended dimensions.[20] Among zero-dimensional nanocarbons are fullerenes, carbon nano-onions (CNOs), nanodiamonds (ND) and carbon-encapsulated metal nanoparticles (CEMNPs).[20]

There also are one-dimensional nanocarbons, which include CNTs.[20] CNTs are a type of carbon nanofilament and exist in different forms: Single-walled carbon nanotubes (SWCNTs), double-walled

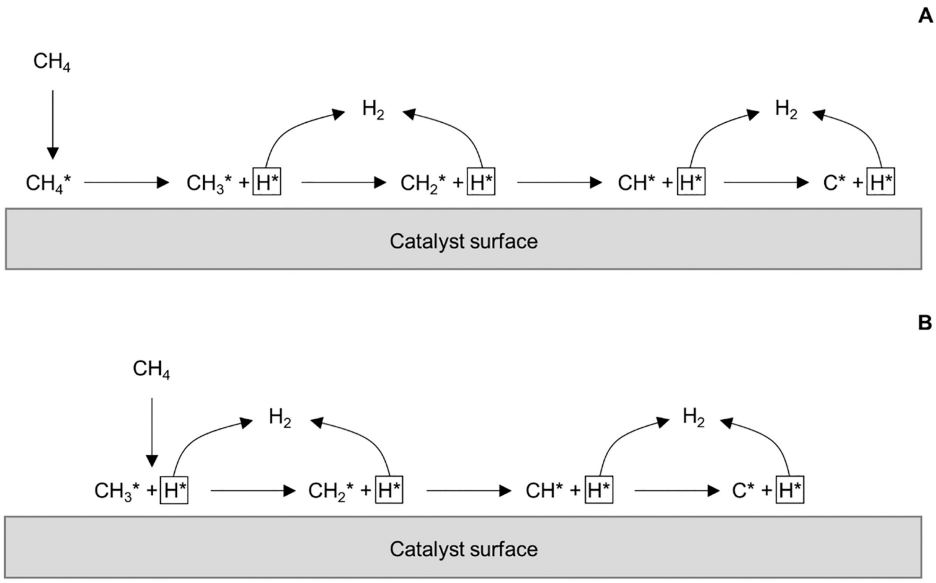

Figure 2.1: Molecular adsorption mechanism (A) and dissociative adsorption mechanism (B) for CMP. For A, methane first adsorbs on the catalyst surface and then follows a series of dissociation reaction steps. For B, the adsorption of methane on the catalyst surface and the first dissociation step occur simultaneously. The dissociation steps that follow are similar to those in A.[a]

carbon nanotubes (DWCNTs) and multi-walled carbon nanotubes (MWCNTs).[21] SWCNTs have a wall of one atom thick, whereas MWCNTs are multiple SWCNTs stacked upon each other.[21] There are multiple structures of CNTs, including a tubular, herringbone, bamboo and amorphous structure.[20] CNTs have superior mechanical, thermal, electrical and biological properties. CNTs have high axial strength and stiffness.[22] The tensile strength of CNTs is much higher compared to that of steel, at least about a factor of 15.[8,17,22] In addition, CNTs have very low electrical resistance[22] and superior current density.[8] Furthermore, research indicates that CNTs have very high thermal conductivity,[22] however other reports indicate that the experimental thermal conductivity is equal or lower to that of diamond.[8] It has also been reported that CNTs have high resistance to both bases and acids.[12] Additionally, CNTs are chemically stable and biologically compatible.[22]

In addition, there are also two-dimensional nanocarbons, which are all based on graphene. Two-dimensional nanocarbons tend to be longer, wider, up to the millimetre scale and have a thickness of a few atomic layers. Furthermore, two-dimensional nanocarbons have the ability to absorb light of all wavelengths and have fantastic transport properties for electrons.[20]

Another type of nanocarbon is CNF. CNFs are different from CNTs, as the stacking of graphene sheets is different, leading to more edge sites on the outer wall of CNFs.[23] CNFs are polycrystalline and 2D planar hexagonal networks.[3] CNFs have a thickness of nanometres and a length scale in micrometres.[23] Furthermore, CNFs are seemingly larger than CNTs, have more defects and are less ordered.[24] Measurements of the Young's moduli show that multilayered CNTs are much stronger than CNFs.[25] In addition, CNFs that are formed at high temperatures tend to have closer diameters to the metal particles, whereas those formed at low temperatures have diameters which are smaller than the metal particle.[26] Figure 2.3 shows multiple types of CNTs and CNFs. GNF is short for graphene nanofibre and the herringbone structure is also referred to in literature as the fish-bone structure. It is characterised by the angle that the graphene planes have compared to the central axis.[27]

[a]"Reaction Mechanisms Proposed for the Catalytic Methane Pyrolysis" by Nuria Sánchez-Bastardo, Robert Schlögl and Holger Ruland is licensed under CC BY 4.0. (https://creativecommons.org/licenses/by/4.0/) URL: https://pubs.acs.org/doi/full/10.1021/acs.iecr.1c01679 / original figure

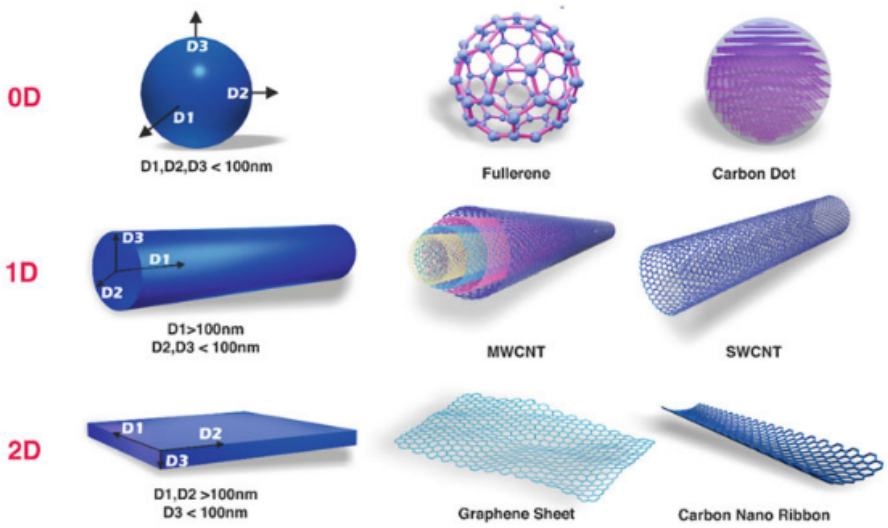

Figure 2.2: Different types of nanocarbons based on dimension. 0D nanocarbons include fullerenes, CNOs, NDs, carbon dots and CEMNPs. 1D nanocarbons includes CNTs. 2D nanocarbons includes graphene sheets, carbon nano ribbons and CNFs.[b]

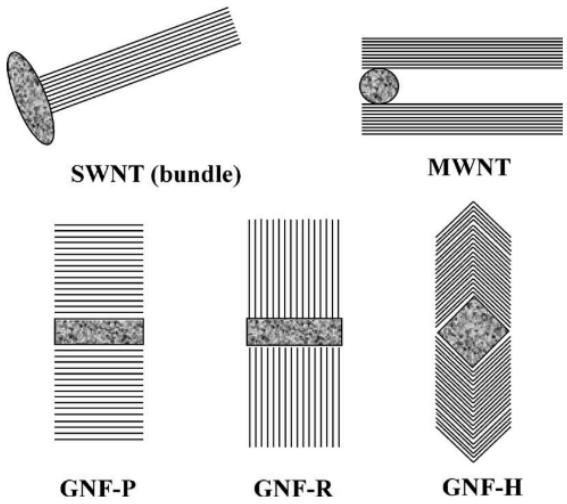

Figure 2.3: Various types of CNTs and CNFs. The CNTs showed are a SWCNT and a MWCNT. The CNFs have different structures. GNF-P indicates a CNF with a platelet structure, GNF-R indicates a CNF with a ribbon structure and GNF-H indicates a CNF with a herringbone structure. GNF is short for graphene nanofibre and a herringbone structure is also commonly referred to as a fish-bone structure.[c]

2.1.3. Nanocarbon Growth Mechanisms in Catalytic Methane Pyrolysis

In order to describe the growth of filamentous carbon, there are two generally accepted models: the tip-growth model and the base-growth model,[29] as shown in Figure 2.4. Tip-growth occurs when the interaction between metal and support is weaker.[15,30,31] A gas containing carbon decomposes at the top of the metal particle, after which it dissolves and then diffuses downward through the metal catalyst particle.[27,31] This leads to the accumulation of carbon at the back end of the metal, which

[b]Reproduced with permission from Springer Nature, from Industrial Scale Production, Commercialization, and Global Market of Functionalized Carbon Nanostructures.[20] Punetha, M.; Bhagat, J.; Pathak, R.; Bhatt, S.; Sanghani, P.; Punetha, V. D. 2024; permission conveyed through Copyright Clearance Center, Inc.

[c]Reproduced with permission from Elsevier, from Carbon nanotubes and nanofibers in catalysis.[28] Serp, P.; Corrias, M.; Kalck, P. 2003; permission conveyed through Copyright Clearance Center, Inc.

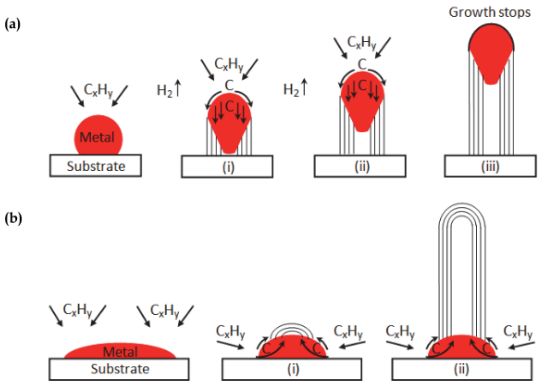

Figure 2.4: Tip-growth model (a) and base-growth model (b) for the growth of filamentous nanocarbons. In the case of the tip-growth model, the carbon decomposes at the tip of the metal catalyst, diffused downward through the catalyst and accumulates in-between the support and the catalyst, lifting the catalyst up from the support. In the case of the base-growth model, the carbon accumulates at the top of the metal catalyst and grows up from the catalyst. The catalyst remains attached to the support.[d]

causes the metal to detach from the support.[3] Specifically for CNTs, a big disadvantage of tip-growth is when acid or base treatment is applied for separation of the CNTs and metal particles.[32] The acid or base treatment dissolves the metal particles, resulting in the catalyst being sacrificed. In the case of base-grown nanocarbon filaments, the interaction between catalyst and support is stronger.[31] Carbon accumulates at the tip of the metal catalyst particle, causing the nanocarbons to form on top of the metal, which stays attached to the support.[3] For CNTs, an advantage of base-growth is that it leads to easier harvesting.[32]

The metal loading is an important factor when it comes to which growth model is active. It appears that an increase in metal loading leads from base growth to tip growth and it leads to larger filaments.[29] Besides the metal loading, the size of the metal catalyst particles also affects the formation of nanocarbons.[6,33–35] In the case of Ni-based catalysts, small nickel particles lead to formation of encapsulated carbon and thus rapid catalyst deactivation, whereas larger nickel particles lead to increased formation of CNTs.[6] Figure 2.5 shows the mechanisms for both large and small nickel particles. Furthermore, a metal catalyst is considered inactive when the metal particles are too small or too large.[29]

2.1.4. Catalysts for Catalytic Methane Pyrolysis

The role of catalysts in CMP is to reduce the activation energy, leading to a lower required reaction temperature.[6] In non-catalytic methane pyrolysis, the required temperature to obtain sufficient methane conversion rates is above 1000 °C.[36] With using catalysts, the required temperature can be lowered to in-between 500 and 1000 °C. The type of catalyst influences to what extent the temperature can be lowered. Another possible goal of adding a catalyst is to change the carbon morphology.

The first type of catalysts for CMP are metal based catalysts. The most popular are the transition metals nickel (Ni) and iron (Fe).[15] Cobalt (Co) is another option, but not a lot of research has been conducted into Co based catalysts due to the high price, toxicity and the lower activity compared to Ni.[3,15] Ni-based catalysts show the highest activity, followed by Fe- and Co-based.[15] However, Fe-based catalysts have better conversion rates and stability than Ni catalysts at higher temperatures.[6,15] The catalysts can be either supported or unsupported and the use of promoters is also frequently reported.

The second type of catalysts for CMP are carbon based catalysts. Carbon based catalysts are less active compared to metal based catalysts, but carbon based catalysts have better stability and show a longer lifetime.[3] Furthermore, carbon based catalysts are cheaper[3,6] and are resistant to sulphur poisoning,[6,37] but the operating temperature of carbon based catalysts is higher.[6,37] The carbon product deposited on the carbon catalyst helps sustain the catalytic activity, as the carbon product has a self-

[d]"Carbon Nanotube Synthesis and Growth Mechanism" by Mukul Kumar is licensed under CC BY-NC-SA 3.0. (https://creativecommons.org/licenses/by-nc-sa/3.0/) URL: https://www.intechopen.com/chapters/16802 / original figure

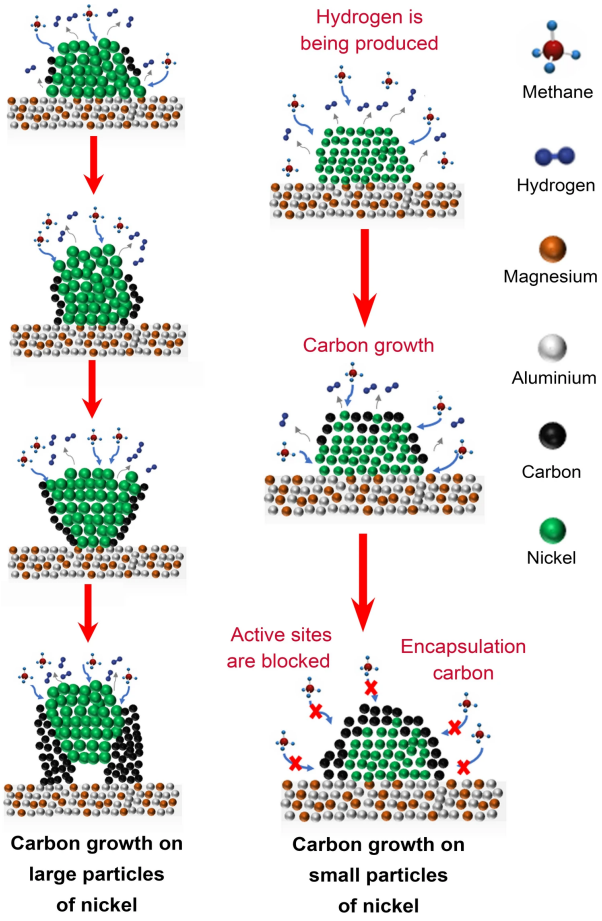

Figure 2.5: Carbon growth mechanisms for large nickel and small nickel particles. In the case of large nickel particles, the carbon forms a filamentous nanocarbon before the catalyst is eventually deactivated by carbon encapsulation. In the case of small nickel particles, carbon quickly encapsulates the catalyst leading to rapid catalyst deactivation.[e]

catalysing effect.[15,35] However, unwanted by-products, like larger hydrocarbons, can be created and hinder the activity.[6]

Many types of carbon materials can be used as catalyst: activated carbon (AC), carbon black (CB), CNTs, fullerenes, graphite, biochar and mesoporous carbon. The most popular are AC and CB.[3] AC and CB show higher activity and better stability compared to ordered nanocarbons.[6,37] Amorphous carbon contains many high-energy sites.[3] High-energy sites are the largest share of active sites for carbon catalysts and hence the amount of high-energy sites determines the activity level.[3] When comparing AC to CB, AC has higher initial methane conversion, but deactivates faster which means CB shows better long-term stability.[6,19,38] An advantage of carbon based catalysts compared to metal based catalysts is that the created nanocarbons require no purification steps for the removal of metal impurities.

There are many recent articles that give overviews of catalysts researched for CMP. Although much research has already been conducted into catalysts for CMP, a best catalyst has yet to be found. Table 2.1 gives an overview of catalyst materials frequently used in CMP. Using a metal catalyst will very often lead to the formation of filamentous nanocarbon. Among the filamentous nanocarbon are SWCNTs, DWCNTs, MWCNTs and CNFs. Using a carbon catalyst will almost always lead to the formation of CB and some amorphous carbon. It is important to note that the properties in Table 2.1 are a generalisation. Specific types of catalysts can therefore deviate from the information given in Table

[e]Fig.2 from "Carbon–neutral hydrogen production by catalytic methane decomposition: a review" by Dwi Hantoko, Wasim Ullah Khan, Ahmed I. Osman, Mahmoud Nasr, Ahmed K. Rashwan, Yahya Gambo, Ahmed Al Shoaibi, Srinivasakannan Chandrasekar and Mohammad M. Hossain is licensed under CC BY 4.0 (https://creativecommons.org/licenses/by/4.0/). URL: https://link.springer.com/article/10.1007/s10311-024-01732-4 / original figure

2.1. A promising specific catalyst is Ni-SiO_2. Research by Hadian et al.[14] shows that mainly CNFs are formed, with a purity of 96 %. The formed CNFs have a fish bone structure, diameters between 15 to 80 nm and around 70 g of carbon per gram of catalyst is formed with a catalyst lifetime of 12 h at 550 °C. A problem with Ni based catalysts is rapid catalyst deactivation above 600 °C. The conversion and activity are therefore only high initially and drop off due to the catalyst deactivation.

Table 2.1: Comparison of catalysts used in CMP. Four catalysts are compared: nickel, iron, cobalt and carbon.

Catalyst	Activity	Deactivation rate	CH_4 Conversion	Price	Toxic	Operating temperature	Source
Nickel (Ni)	High	Rapid above 600 °C	High	Moderate	Yes	500-700 °C	[3, 5, 6, 15, 19, 29, 35, 37, 38]
Iron (Fe)	Good	Low/Moderate	Moderate	Low	No	700-950 °C	[3, 5, 6, 19, 29, 35, 37, 38]
Cobalt (Co)	High	Moderate	High	High	Yes	750-950 °C	[3, 6, 15, 19, 29, 35, 37, 38]
Carbon	Moderate	Low	Moderate	Low	No	800-1000 °C	[3, 5, 15, 29, 35, 37]

2.2. Nanocarbon Purification

2.2.1. Processes for Purification of Produced Nanocarbons

In current literature, there are a few studies which combine the production and purification of nanocarbons into a single research paper. Some include process simulation, others do not. An example is the separation process designed by Parmar et al.[16] Parmar et al. used a 60%Ni-5%Cu-5%Zn/Al_2O_3 catalyst in a fluidized bed reactor. During the process, CNTs with a length of 5 μm and outer diameter of 60-80 nm were created. After a certain amount of time, separation of the carbon from the catalysts took place. Ultrasonication in combination with a neodymium magnet is applied for the separation. This partially regenerates the catalyst. The remaining carbon is removed and the catalyst is fully regenerated by recalcining at 750 °C in air. The catalyst regained its full activity after each regeneration and it provides over 90 % initial methane conversion for up to five reaction-regeneration cycles with a high selectivity towards CNTs. Figure 2.6 shows the process for the separation and regeneration. The efficiency for separation is 45-50 % for 70 wt% carbon in the catalyst and 25-30 % for 30 wt%.

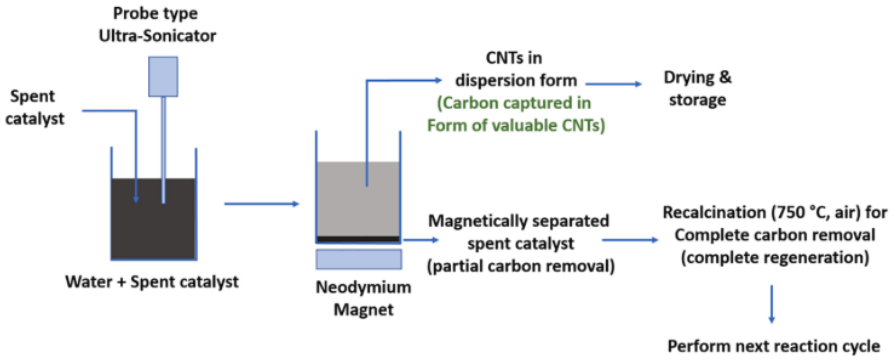

Figure 2.6: CNT and metal catalyst separation process by Parmar et al.[16] The catalyst is mixed with water and ultrasonicated. After ultrasonication, the CNT and metal are separated from each other by a neodymium magnet. The CNT is dried and stored and the metal catalyst is regenerated by recalcination.[f]

A second example for the separation of the nanocarbon from the metal catalyst and subsequent regeneration is reported by Wang et al.[1] A 10Ni-1Pd/CNT catalyst was used in a vertical fixed bed reactor of 12 cm in diameter and 44.5 cm in length for CMP. Figure 2.7 shows the process cycle developed by Wang et al.[1] In the fixed bed reactor, hydrogen and nanocarbons are formed. The nanocarbons produced for a Ni-Pd/CNT catalyst are mainly CNFs. In the case of a Ni/CNT catalyst, MWCNTs are mainly produced. The catalyst is removed from the nanocarbon by acid leaching. The leached catalyst is then recovered and re-used. During regeneration, a small part of the formed nanocarbon is used as a

[f]Reproduced with permission from Elsevier, from Blue hydrogen and carbon nanotube production via direct catalytic decomposition of methane in fluidized bed reactor: Capture and extraction of carbon in the form of CNTs.[16] Parmar, K.; Pant, K.; Roy, S. 2021; permission conveyed through Copyright Clearance Center, Inc.

catalyst support. The report shows that the properties of the carbon product remain unchanged after five cycles.

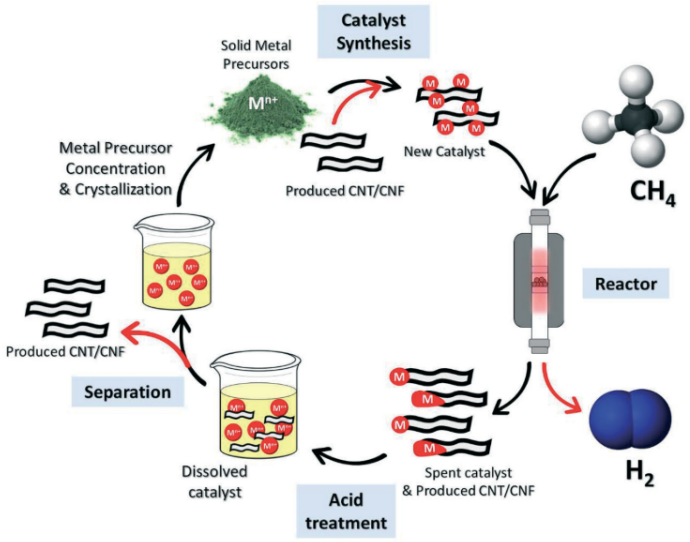

Figure 2.7: Cyclic thermocatalytic decomposition process by Wang et al.[1]. The catalyst and nanocarbon are treated with an acid and then separated. The metal catalyst is then regenerated, with CNT or CNF as a support, and fed back into the reactor.[g]

Another process for the separation of the nanocarbon from the metal catalyst and the subsequent catalyst regeneration is developed by Ahmad et al.[15] A Fe-based catalyst is used in a continuous fluidized bed reactor for CMP at 600 °C. The spent catalyst along with the nanocarbon is fed to a magnetic separator. In the magnetic separator 80 % of the carbon is separated, while 20 % remains deposited on the catalyst. The catalyst is then fed to an air combustor, where the remaining carbon is burned at 800 °C and 1 bar. This last step releases CO_2. Figure 2.8 shows the Aspen Plus model of the CMP process with the separation and regeneration steps.

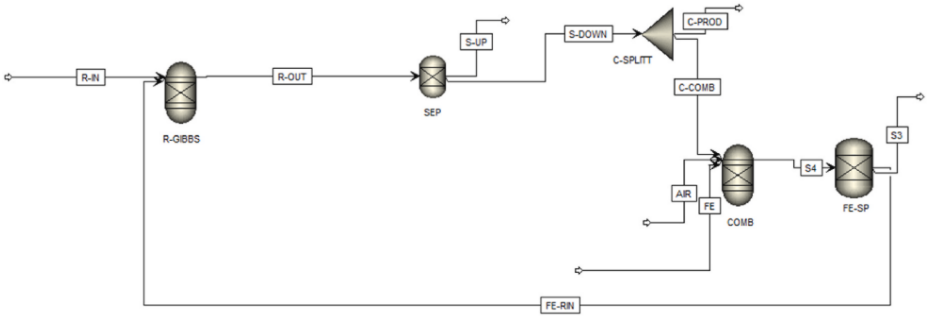

Figure 2.8: Aspen Plus model of CMP with carbon separation and catalyst regeneration. R-GIBBS represents the fluidized bed reactor, after which a magnetic separator separates 80 % of the carbon from the catalyst. The magnetic separator is represented by the SEP and C-SPLITT blocks. The carbon product leaves to stream C-PROD and the catalyst along with 20 % of the carbon deposited is fed to an air combuster. After the air combustor, the metal catalyst is regenerated in the FE-SP unit and fed back to the reactor.[h]

[g]Reproduced with permission from Royal Society of Chemistry, from Catalytic Decomposition of Methane into Hydrogen and High-Value Carbons: Combined Experimental and DFT Computational Study in Catalysis Science & Technology.[1] Wang, I.-W.; Dagle, R.; Khan, T.; Lopez-Ruiz, J.; Kovarik, L.; Jiang, Y.; Xu, M.; Wang, Y.; Jiang, C.; Davidson, S.; Tavadze, P.; Li, L.-L.; Hu, J. 2021; permission conveyed through Copyright Clearance Center, Inc.

[h]Reproduced with permission from Elsevier, Catalytic cracking of methane to hydrogen and carbon: Scale-up perspective in International Journal of Hydrogen Energy.[15] Ahmad, A.; Hamdani, I. R.; Srinivasakannan, C.; Al Shoaibi, A.; Hossain, M. M. 2024; permission conveyed through Copyright Clearance Center, Inc.

Agboola et al.[17] designed two processes for production of CNTs using catalytic vapor deposition which both include the purification of nanocarbon and regeneration of the catalyst. The first process includes a high-pressure carbon monoxide (HiPCO) reactor called the CNT-PFR process. The second process includes a cobalt-molybdenum catalyst (CoMoCat) reactor called the CNT-FBR process. Both have a production capacity of 5000 tonnes of nanotubes per year.

For the CNT-PFR process based on the HiPCO reactor, the produced CNTs contain metal particles and amorphous carbon. Figure 2.9 shows the process flow diagram of the CNT-PFR process. First, amorphous carbon is removed through oxidation in an oxidizer. This does not affect the structure of the CNTs. Furthermore, the Fe particles in the outer carbon layers are exposed and the Fe particles are oxidized into iron oxide. This means the Fe particles can now be easily removed by acid treatment. The following step is acid treatment in a tank with 12 % HCl. The iron oxide forms $FeCl_2$ and water and is dissolved. Afterwards, filtration, washing with de-ionized water and drying at 80 K is applied to obtain the final product. The final product contains 97 mol% CNT and 3 mol% Fe. The solution containing $FeCl_2$ is treated in a column for acid regeneration and in a centrifuge separator to obtain the HCl. The HCl is then recirculated back into the process. The NPV is 609 million dollar and the (ROR) is 37.4 %. The selling price of the CNT is 38 \$/kg, which is produced at a rate of 595 kg hr^{-1}.

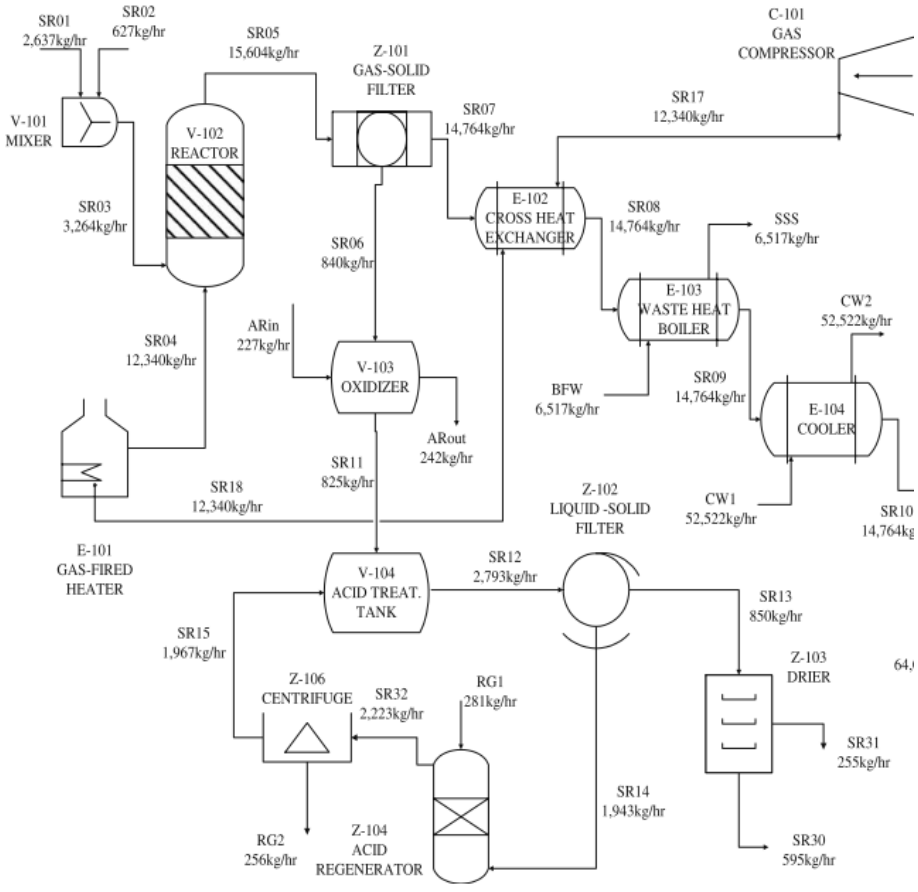

Figure 2.9: Process flow diagram of the CNT-PFR process. The reactor produces CNTs containing metal particles and amorphous carbon. The CNT is fed to a gas-solid filter, after which the CNT is fed to the V-103 oxidizer to remove amorphous carbon. Following the oxidation, acid treatment is applied to remove the metal particles from the CNT. Filtering with a liquid-solid filter and drying in a drier are applied as post-treatment steps to obtain the final CNT product. The acid is regenerated with an acid regenerator and centrifuge by removing the created metal oxides.[i]

[i]Reproduced with permission from Springer Nature, Conceptual design of carbon nanotube processes in Clean Technologies and Environmental Policy.[17] Agboola, A.; Pike, R.; Hertwig, T.; Lou, H. 2007 ; permission conveyed through Copyright Clearance Center, Inc.

For the CNT-FBR process based on the CoMoCat reactor, the reaction takes place at 950 °C with a Co-Mo catalyst on a silica support. Figure 2.10 shows the process flow diagram of the CNT-FBR process. The produced CNTs remain attached to the catalyst and are first washed with 2 M sodium hydroxide solution in a leaching tank. This breaks the attachment of the CNT with the silica. The next step is to apply froth flotation with an inorganic surfactant in an air medium to trap the CNTs. The CNTs are then treated with a 12 % HCl solution, which dissolves remaining metal particles and turns the metal particles into metalchlorides. By filtering and then drying at 800 K the final product is obtained. It contains 97 mol% CNT, 1.5 mol% Co and 1.5 mol% Mo. As with the CNT-PFR process, acid regeneration happens to recirculate the HCl back into the process. Furthermore, the slurry from the froth flotation column is sent to a filter to separate the catalyst particles and support from the remaining waste. The catalyst is then regenerated. The NPV is 753 million dollar and the ROR is 48.2 %. The selling price of the CNT is 25 \$/kg with a production rate of 595 kg hr^{-1}.

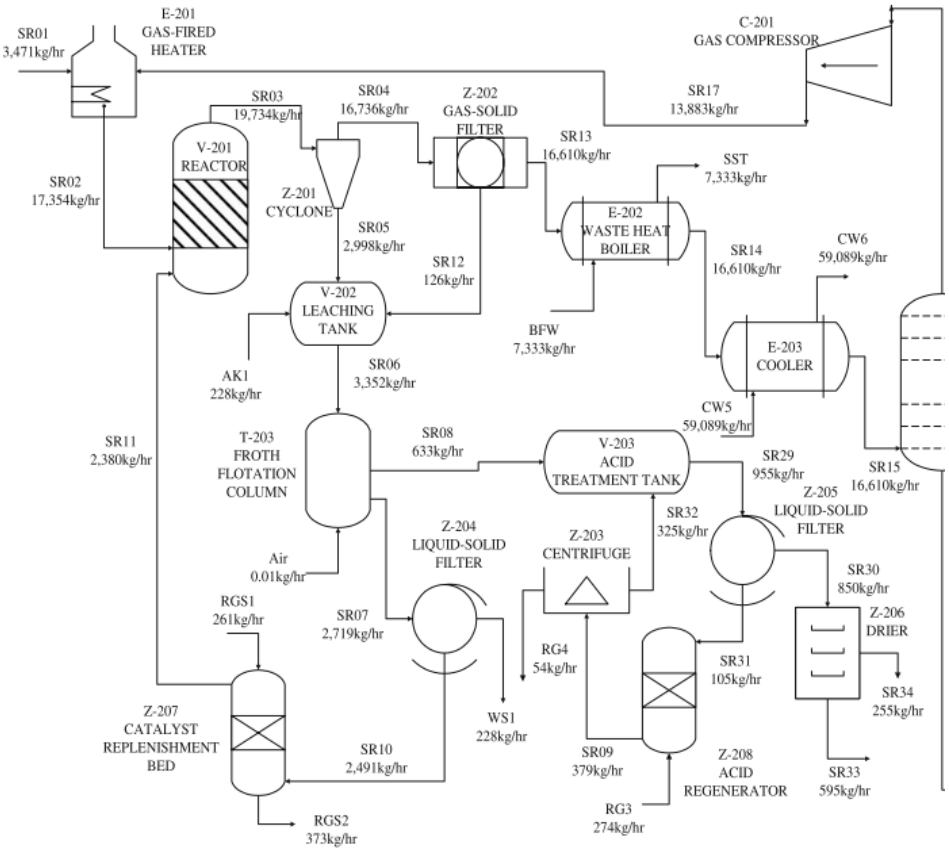

Figure 2.10: Process flow diagram of the CNT-FBR process. The reactor is based on a CoMoCat reactor in which CNT is produced with a Co-Mo catalyst on a silica support. The CNTs remain attached to the catalyst and are fed to a cyclone and gas-solid filter to remove the gas. After the removal of the gas, acid leaching with a 2 M sodium hydroxide solution is applied to break the attachment of the CNT with the silica. The next step is froth flotation with an inorganic surfactant in an air medium to trap the CNTs. The CNTs are then treated with a 12 % HCL solution to dissolve the remaining metal particles. Filtering and drying are applied as post-treatment steps to obtain the final CNT product. The acid is regenerated with an acid regenerator and centrifuge, which remove the created metalchlorides. The metal catalyst is regenerated after froth flotation and filtering with a catalyst replenishment bed.[j]

[j]Reproduced with permission from Springer Nature, Conceptual design of carbon nanotube processes in Clean Technologies and Environmental Policy.[17] Agboola, A.; Pike, R.; Hertwig, T.; Lou, H. 2007 ; permission conveyed through Copyright Clearance Center, Inc.

2.2.2. Existing Methods for Purification of Nanocarbons

A variety of methods for the purification of nanocarbons exists. In Section 2.2.1, purification processes for produced nanocarbons were highlighted. The studies all included either a process flow diagram, process simulation or both. However, research into the purification of nanocarbons does not limit itself to those produced by CMP nor does all research contain modelling or detailed sketches. This section gives a full overview of the purification methods for nanocarbons. Purification methods include both physical, chemical and a combination of both. Methods such as acid treatment and magnetic separation focus on the removal of the metal catalyst, whereas other methods such as oxidation focus on the removal of carbonaceous impurities.

Acid treatment
First off is acid treatment, which can be applied to remove the metal catalyst from the carbon nanomaterial and can also remove carbonaceous impurities. Often, it is accompanied by prior oxidation or sonication in order to expose the metal catalyst surface,[17] as this makes the acid treatment process easier. After acid treatment, the purified carbon nanomaterials have to be washed in order to neutralize the remaining acid and subsequently dried. This can be achieved with deionized water or e.g. methanol, ethanol and drying in an oven. The advantage of using acid treatment is that it is very effective at removing metal impurities from carbon nanomaterials (CNMs), which leads to a high purity. The downside is that is can also attack the CNMs.[39]

A general reaction for acid treatment is given in Equation 2.2. The metal reacts with the acid to form a metal-oxide or metal-nitrate with one or more by-products. HCl and HNO_3 are the most common acids for the acid treatment of nanocarbons. Equation 2.3 shows the reaction of Ni with HCl and Equation 2.4 shows the reaction of Ni with HNO_3. The reaction of Fe with HCl is given by Equation 2.5 and the reaction of Fe with HNO_3 is given by Equation 2.6.

$$\text{metal} + \text{acid} \Longrightarrow \text{metaloxide/metalnitrate/metalchloride} + \text{byproducts} \tag{2.2}$$

$$\text{Ni} + 2\text{HCl} \Longrightarrow \text{NiCl}_2 + \text{H}_2 \tag{2.3}$$

$$\text{Ni} + 4\text{HNO}_3 \Longrightarrow \text{Ni(NO}_3)_2 + 2\text{H}_2\text{O} + 2\text{NO}_2 \tag{2.4}$$

$$\text{Fe} + 2\text{HCl} \Longrightarrow \text{FeCl}_2 + \text{H}_2 \tag{2.5}$$

$$\text{Fe} + 6\text{HNO}_3 \Longrightarrow \text{Fe(NO}_3)_3 + 3\text{H}_2\text{O} + 3\text{NO}_2 \tag{2.6}$$

Rahatwan et al.[40] applied HNO_3 to remove the Fe-Co-Mo/MgO catalyst from CNTs synthesised in a fluidized bed reactor from a LPG carbon source. A purification column containing a filter was used, which was kept at 50-70 °C for 2 h. Afterwards, the CNTs were washed with distilled water and dried in an oven at 100-120 °C for 120 min. The last step removes 5 % water leftovers. The purity of the CNTs increased from 94.85 % to 99 %. The production plant can produce up to 250 kg per year.

Chiang et al.[41] applied both HNO_3 and HCl to remove the metal catalyst from SWCNTs. The first step is cleaning with HNO_3, followed by washing with methanol. The latter removes the soluble residue from the HNO_3 cleaning. Carboxyl acids were then removed by refluxing in water for a few hours, followed by oxidation in 5 % O_2/Ar at 300 °C and 500 °C. Then, an HCl solution was applied to extract the catalyst, followed by drying in vacuum at 150 °C. SWCNTs with a purity of 99.9 % were obtained. Wang et al.[42] combined acid treatment with supercritical fluid extraction to purify SWCNTs synthesised through the HiPCO process. The SWCNTs are first treated by either bulk electrolysis or by combining acid treatment with sonication in a mixture containing HNO_3 and H_2O. The second step is the supercritical fluid extraction using Sc-CO_2. The final result is that over 98 % of the iron is removed.

Harutyunyan et al.[43] used HCl to remove metal catalyst particles from SWCNTs synthesised by the arc-discharge technique. First, microwave heating is applied to remove the carbon shell. This leads to CO and CO_2 emissions. The next step is to treat the SWCNTs with 4 M HCl for multiple hours to remove the metal catalyst. Before purification, the SWCNTs contain 20 to 40 wt% of metal catalyst particles and after purification the SWCNTs contain only 0.2 wt% of catalyst particles.

Wang et al.[32] applied HNO_3 to remove the metal catalyst from CNTs synthesised over 9Ni-1Fe/SiO_2 in methane decomposition. The CNTs were first refluxed in 3 M HNO_3 for 1 to 2 days at 120 °C with

magnetic stirring. The residue is then filtered and washed with deionized water. The CNTs are then dried at 120 °C for 16 hours. Results indicate that the metal catalyst along with the support is removed after acid treatment for 2 days. Furthermore, the structure of the CNTs is unaffected. Refluxing for a longer period of time at a higher temperature results in full removal of the metal catalyst. However, CNTs are also attacked by the acid.

Ferromagnetism
Magnetism is another method that can be used to remove metal impurities from CNMs. Ahmad et al.[15] designed a process which uses a magnetic separator to separate the nanocarbon and metal catalyst. Parmar et al.[16] combined ultrasonication and a neodymium magnet to separate the carbon and catalyst. Thiên-Nga et al.[44] uses ferromagnetism. SWCNTs are suspended in toluene or a soap solution. Then, the SWCNTs are distributed in 30 % HNO_3. By mixing with inorganic nanoparticles, such as ZrO_2 and $CaCO_3$, in addition to applying ultrasonication, the magnetic particles are removed from the carbon shells. The metal particles can then be removed by using a magnet. The SWCNTs are then exposed to a chemical treatment and filtering. Results show that a large part of the metal particles were removed. A downside of the method is that some defects are introduced on the CNTs.

Kang and Park[45] used magnetophoretic purification to remove iron particles from SWCNTs. A SWCNT solution is passed through a microchannel on which a magnetic field is applied. The iron particles are attracted by the magnetic force and so the iron moves to areas with higher magnetic-flux density. The SWCNTs are obtained via the outlet. Not all SWCNTs are recovered, as some were removed in the process. A purity of over 98 % was obtained.

Functionalisation
Georgakilas et al.[46] reported on a purification method which involves the functionalisation of the nanotubes. SWCNTs are functionalised in a dimethylformamide (DMF) suspension by 1,3 dipolar cycloaddition of azomethine ylides. This results in the SWCNTs becoming more soluble, while the metal particles remain unaffected. The SWCNTs and amorphous carbon are dissolved in the DMF. The next step is to remove amorphous carbon through a precipitation process by adding diethyl ether. The last steps are a thermal treatment at 350 °C and annealing at 900 °C to remove the functional groups from the CNTs. The results indicate that only 0.4 wt% iron particles remained, from starting with 26 wt%. The advantage of applying functionalisation is that the electronic structure of the surface stays intact.[39] However, it is ineffective if there are many impurities.[39]

High temperature annealing
High temperature annealing can be used to remove metal particles, specifically in the hollow core or at the tip of CNTs.[39] Research indicates that annealing above 1400 °C works for the removal of metal impurities from both SWCNTs and MWCNTs. Furthermore, it can change the CNTs such that the diameter is enlarged or that structural defects are removed.[39] The disadvantage of high temperature annealing is that carbon impurities are still present and are now harder to remove. Thus, this method is best suited for the removal of residual metal from CNTs or when there are a small amounts to none carbon impurities in the CNTs.[39]

Zhang et al. used thermal annealing in combination with filtration to purify MWCNTs. First, thermal annealing at 2600 °C is conducted during one hour in an argon atmosphere. The metal particles and structural defects are removed. The next step was to solute the MWCNTs in ethanol containing a dispersing agent and then applying sonication. In addition, filtration was applied multiple times to further purify the MWCNTs. Results show that the MWCNT yield is around 90 %.

Filtration
Filtration is a technique based on size separation and can be applied to remove a variety of impurities from CNTs. Metal particles, fullerenes and polyaromatic carbons can be removed.[17] A disadvantage is that is is time-consuming.[39]

Bandow et al.[47] used microfiltration to purify SWCNTs. The SWCNTs are first submerged in CS_2, followed by filtering to remove fullerenes and polyaromatic carbons. The remaining solid on the filter is sonicated in 0.1 % surfactant. This suspension is then exposed to microfiltration, where the metal particles pass through and the SWCNTs stay behind. Results show that over 90 wt% of SWCNTs is achieved and the yield is around 70 %. The downside of this method is that it is not a continuous process.[48]

Bonard et al.[49] applied filtration assisted by ultrasonication to purify MWCNTs. First, 2.5 g of Sodium dodecyl sulfate (SDS), 500 mL of distilled water and 50 mg of MWCNTs are suspended. Then sonication is applied, followed by sedimentation and centrifugation to rid graphitic particles which are larger than 500 nm. The remaining suspension is filtrated under the influence of sonication. The final residue contains 87 wt% CNTs after one filtration step and over 90 wt% after two steps.

Shelimov et al.[48] also combined ultrasonication with filtration and managed to make the process continuous. The SWCNTs are submerged in toluene, as this removed fullerenes. After submerging in toluene, the SWCNTs are soluted in methanol and filtration assisted by ultrasonication is applied. After filtration, the residue is treated with 6M H_2SO_4 to remove metal traces from the ultrasonication. Results show that 150 mg of SWCNT soot was purified to over 90 % purity with a yield of 30 to 70 wt%. The possible downside of using ultrasonication is that it may damage the CNTs.[48]

Centrifugation
Centrifugation is a purification method which can be applied to remove amorphous carbon and CNPs from SWCNTs.[39] At low speeds, amorphous carbon is removed and at high speeds CNPs are removed. A disadvantage of applying centrifugation is that prior treatment of CNTs with HNO_3 is necessary. This introduces functional groups which have to be removed later on.

Oxidation
Oxidation is often applied as a purification method to remove carbonaceous impurities and helps expose the surface of the metal catalyst.[17] The yield of oxidation is poor under normal circumstances, as there is a high change that CNTs are also oxidized.[17] Another disadvantage of oxidation is the release of CO and CO_2.

Hydrothermally initiated dynamic extraction (HIDE)
Hydrothermally initiated dynamic extraction (HIDE) is a purification method that causes collisions, resulting in graphitic nanoparticles and CNSs being removed from the soot.[39] Furthermore, metals are exposed as the surrounding graphitic layers are broken.[39]

Tohji et al.[50] combined HIDE with other purification methods to purify SWCNTs synthesised by the arc discharge method. First HIDE is applied, followed by filtering and then drying at 333 K. After dying, fullerenes are removed by applying toluene Soxhlet extraction. The last steps are burning at 743 K to remove amorphous carbon and acid treatment with 6 M HCl to remove metals. Results show that SWCNTs with 95 wt% were obtained.

Sato et al.[51] reported a purification process of MWCNTs which also combines HIDE with other purification techniques. First, grinding in a mortar occurs and then the sample is sonicated in distilled water. After sonication, the MWCNTs are filtered to remove large graphites. Then, HIDE occurs at 373 K. Following the HIDE treatment, a surfactant was added to disperse the MWCNTs and then the MWCNTs were centrifuged. The suspension obtained from the centrifugation was then filtered, washed and dried. The last step was to burn carbon impurities at 973 K. Results show that MWCNTs with a purity close to 100 % are obtained.

Multi-step methods
Under multi-step methods fall purification procedures that combine chemical with physical methods and that do not directly fall under one of the aforementioned categories.

In research by Hernadi et al.[52] CNTs were synthesised through catalytic decomposition by using Co/SiO_2 and Fe/SiO_2 catalysts. First, the metal particles are dissolved by submerging the CNTs in 30 % HNO_3. Then foltration is applied, followed by washing with distilled water and acetone. The next step was ultrasonication in an organic solvent. The best solvent proved to be a mixture of n-hexane with acetone and iso-propanol. Then, the CNTs are evaporated to dryness and as last step the amorphous carbon is removed by hydrogenation at 900 °C. Results show a yield of around 1 %.

Hou et al.[53] reported a multi-step purification method with bromination. MWCNTs synthesised through catalytic decomposition are first dispersed by ultrasonication and heat treatment. Then, the MWCNTs are submerged in bromine water at 90 °C. This helps to remove the amorphous carbon and carbon nanocapsules by decreasing the oxidation resistance of those. Furthermore, the damage to the MWCNTs is low. The remaining MWCNTs are heated at 520 °C for 45 min in air. Afterwards, acid treatment in 5 M HCl is applied to remove the iron catalyst particles. After acid treatment, washing

with de-ionized water and drying in an oven for 12 h at 150 °C occurs. Results show that a yield of 50 wt% is obtained.

Wang et al.[54] combined acid treatment with ultrasonication and gas treatment to purify SWCNTs produced by catalytic decomposition with a Co catalyst. SWCNTs are first refluxed with 2.6 M HNO_3 to remove the metal catalyst particles. Then the SWCNTs are ultrasonicated to improve dispersion, filtered and washed. The next step is to again apply ultrasonication, but this time in a H_2SO_4/H_2O_2 solution at 30 to 40 °C. This cuts and polishes the SWCNTs. After the ultrasonication, filtering and washing occurs again. Finally, heating at 1000 °C in NH_3 occurs to remove carbonaceous impurities. Results show an increase in purity from 60 % to 70 % to 98 %.

Li et al.[55] described a multi-step method of purifying SWCNTs produced by catalytic decomposition of methane and benzene. First, the produced SWCNTs are submerged in benzene for a week, after which fullerenes and catalyst precursors can be removed. The SWCNTs are then washed with de-ionized water and ultrasonicated in HCl. Acid treatment is conducted to remove the iron catalyst particles, followed by filtering. The next step is freezing in liquid nitrogen and applying more ultrasonication. The last steps are washing with de-ionized water and finally drying the SWCNTs. Results show that 75 mg of SWCNTs with 95 wt% purity are obtained from 200 mg starting product.

Montoro et al.[56] used a multi-step purification process for the purification of SWCNTs produced by the arc-discharge method. The first step is to expose the SWCNTs to toluene, followed by extraction to remove fullerenes and other soluble impurities. The SWCNTs are then washed with acetone and dried. The amorphous carbon is removed through oxidation with 10 % H_2O_2. The SWCNTs are submerged in the H_2O_2 solution and ultrasonication occurs. Then, by refluxing, filtration, washing and finally drying in air, the amorphous carbon is removed. The next step is the removal of the metal catalyst particles. The SWCNTs are treated with HNO_3, after which the SWCNTs are sonicated in SDS with HNO_3 and HF to improve the dispersion. Afterwards, filtering, washing and drying occur. The last step is to remove graphitic impurities and metal particles which are difficult to access. The SWCNTs are dispersed in SWS, followed by sonication and then filtering multiple times. Afterwards, washing and drying occurs again. The results show that a SWCNT yield of 25 % is obtained along with high purity.

Liu et al.[57] developed a method for purifying SWCNTs synthesised by catalytic decomposition. The first step is refluxing in 2.6 M HNO_3 to remove metal catalyst particles. After refluxing, washing and ultrasonication are applied. This is followed by filtering, washing and then drying. The following step is aimed at cutting the SWCNTs by applying ultrasonication in $(NH_4)2S_2O_8/H_2SO_4$, followed by washing and drying. The last step is heating in NH_3 at 1000 °C to remove carbonaceous impurities. Results show that the purity of the final product is above 95 % and the weight loss in the last step is around 60 %.

Li et al. tried to purify DWCNTs synthesised by CMP with a Co/MgO catalyst. First, the SWCNTs are treated with HCl. It appears that this is efficient for removing MgO, but not for removing Co. Furthermore, the carbonaceous impurities are also still present. After the acid treatment, the sample is filtered, washed with distilled water and dried at 150 °C. Oxidation can not be applied as a next step, because above 650 °C the DWCNTs are also oxidized and below that the carbonaceous impurities are not oxidized. Therefore, oxidation in air seems to be impossible for the removal of carbonaceous impurities from DWCNTs.

Kim and Luzzi[58] used magnetic filtration combined with acid treatment and oxidation to purify SWCNTs synthesised by a laser method. By first applying oxidation in air and a HNO_3 treatment and then applying magnetic purification, a final catalyst content of 2.2 wt% from 11.7 wt% was achieved. Even better results were achieved when air oxidation, HCl treatment and magnetic purification were combined. The final metal catalyst content equalled 0.3 wt%. For both methods, the yield is 50 %. When comparing magnetic filtration with oxidation or acid treatment, it achieves higher purity SWCNTs with a similar yield.

2.2.3. Acid Leaching of Nickel

Experiments conducted by Parhi et al.[45] study the acid leaching of Ni from Ni-Al_2O_3 spent catalyst using hydrochloric acid. Ni reacts with hydrochloric acid according to the reaction in Equation 2.7.

$$Ni + HCl \rightarrow Ni^{2+} + Cl^{-} + H_2 \tag{2.7}$$

In the acid leaching experiments, 0.2 or 0.4 g of catalyst is added to 500 ml of hydrochloric acid mixture. The temperature, acid concentration residence time, stirring speed and the particle size of the catalyst are all varied to determine the impact on the effectiveness of the leaching. The experimental results show that a higher temperature is beneficial to the conversion of the Ni. A temperature of 353 K at 1 M acid concentration yields the highest conversion, 97 %, and is also the highest temperature tested. Increasing the acid concentration is also beneficial to the Ni conversion. However, increasing the acid concentration above 1 M has diminishing effects compared to the difference in Ni conversion between acid concentrations of 1 M and lower. Leaching at 323 K with 0.025 M acid concentration leads to 35 % Ni conversion after 180 min while leaching at 323 K with 1 M acid concentration leads to 80 % conversion after 180 min. Another important factor is the residence time of the spent catalyst in the acid mixture. A longer residence time leads to higher Ni conversion, with the Ni conversion increasing steeply up until 60 min and stagnating after 180 min. In addition, a higher stirring speed and smaller particle size also increase the Ni conversion. The leaching results show that the reaction is dictated by the shrinking core model. It is important to note that the experiments do not show Ni leaching from nanocarbon. The results are still important, as the results do show the effectiveness of Ni removal through acid leaching and provide kinetic data.

2.3. Nanocarbon Market Analysis

The carbon price is influenced by the type of carbon and the purity. A higher purity means a higher selling price. CNTs are typically the most expensive, followed by CNFs and finally carbon black. Table 2.2 gives an overview of the nanocarbon market per nanocarbon type.

CB has a price of 400 to 1000 $/tonne for ASTM grade and can even be up to 2000 $/tonne for specialty grade.[3,59] The global market demand stood at 12 million tonnes in 2014 and is expected to grow to 16.4 million tonnes in 2022.[59] A more recent report states a price for carbon black between 350 and 1250 $/tonne.[60] The price is affected by the purity, absolute density, bulk density, particle size and surface area of the carbon black. The market is predicted to grow by 9 % per year.[60] Research by Lucintel[61] shows that the carbon black market stood at a valuation of 22.5 billion $ in 2023 and is predicted to grow to 36 billion $ in 2027. Mordor Intelligence Research & Advisory[62] indicate that the market size is 24.10 billion $ in 2025 and is expected to grow to 31.87 billion $ in 2030.

The CNF price ranges from 25,000 to 113,000$/tonne.[59] The global market demand stood at 70,000 tonnes in 2016 and is expected to grow to 100,000 tonnes in 2020. The market value was around 2.15 billion $ in 2015 and is expected to be 4.2 billion $ in 2022.[59] Another report indicates that the CNF market was valued at 0.872 billion $ in 2021 and is expected to be 3.48 billion $ in 2027. The CAGR is 25.93 % over 2022-2030.[20] BBC research indicates that in 2018 the CNF market stood at a valuation of 0.927 billion $ and is predicted to grow to 4.3 billion $ in 2023.[63]

The CNT price ranges from 100,000 to 60,000,000$/tonne.[59] The price range is due to the variation in purity levels.[64] The global market demand stood at 5,000 tonnes in 2014 and is expected to grow to 20,000 tonnes in 2022. The market value is expected to be 3.4 billion $ in 2022 or 5.6 billion $ in 2020 according to different researches.[59] According to Yang et al.,[60] it will surpass a value of 1 billion $ in 2023 and is expected to grow by 9.6 % per year to reach 2.45 billion $ in 2033. The estimate from Yang et al. is on the low side. Other research estimates a valuation of 6.63 billion $ and a predicted grow to 20.31 billion $ in 2030.[65] Research by Statista indicates a total market value of 6.49 billion $ in 2021, with an expected grow towards 13.5 billion $ in 2026. The European market is expected to grow from 1.52 billion $ to 3.09 billion $ in the same period.[66]

Table 2.2: The market for carbon black, carbon nanofibres and carbon nanotubes.

Nanocarbon type	Price range	Market demand in 2020/2022	Market value in 2022/2023	Future market value
Carbon black	400 to 1000 $/tonne[59]	16.4 million tonnes in 2022[59]	22.5 billion $ in 2023[61]	31.87 billion $ in 2030[62]
Carbon nanofibre	25,000 to 113,000$/tonne[59]	100,000 tonnes in 2020[59]	4.2 billion $ in 2022[59]	3.48 billion $ in 2027[59]
Carbon nanotube	100,000 to 60,000,000$/tonne[59]	20,000 tonnes in 2022[59]	3.4 billion $ in 2022[59]	20.31 billion $ in 2030[65]

Information of carbon products sold by companies and webshops is also important to determine the price of the carbon products. Table 2.3 gives an overview of carbon products sold by various companies and online webshops. The prices are per certain amount of g or kg, the prices per tonne are not available via companies and online webshops. Figure 2.11 shows the normalized prices per g of the carbon products in Table 2.3. An important conclusion from the literature is that the price per gram drops as the total quantity of the purchase goes up. An example is the CNF of >95 % purity by Nanografi.[67] Purchasing thousand times 1 g would cost $27,000 whereas purchasing one time 1 kg only costs $1480. The literature also shows that the price range for CNFs of $25,000 to $113,000 per tonne is realistic. Furthermore, the prices of CNTs and CNFs indeed confirm that CNTs are more expensive than CNFs. Within the different categories of CNTs there is also a variation in price, as SWCNTs are more expensive than MWCNTs. In addition, the price generally increases as the purity goes up for CNTs, SWCNTs and MWCNTs. The price for CNF does not show the same increase with purity, which is caused by the CNF with >95 % purity sold by US Research Nanomaterials INC.

The Ni concentration in the CNF is also very important to consider, as the application of the CNF can depend on the Ni concentration. Furthermore, Ni can pose health risks to humans and be toxic to the environment.[68,69] Therefore a low Ni concentration is desired. Through inquiries, the following conclusions hold for the Ni concentration:

- 100-300 ppm of Ni: tolerated for most industrial use cases
- 10-100 ppm of Ni: tolerated for composites, energy storage and catalysts
- <10 ppm of Ni: electronics, sensors and biomedical applications

Table 2.3: Carbon products sold by various companies and online webshops. Prices, purity and specifications are indicated per product.

Carbon product	Purity	Price	Specifications	Source
CNF	>99.9 %	$195/25g $1970/kg	50-150 nm diameter, 1-15 μm length	Nanografi[70]
CNF	>98 %	$124-157/25g	Black powder, trace metals	Sigma Aldrich[71,72]
CNF	>95 %	$65/g $185/5g $589/25g	200-600 nm diameter, 20-50 μm length	US Research Nanomaterials INC[73]
CNF	>95 %	$27/g $124/25g $1480/kg	50-150 nm diameter, 1-15 μm length	Nanografi[67]
CNF	>95 %	$540/100g $2997/kg $2592/kg, at least 5 kg	200-600 nm diameter, <50 μm length	Inquiry
CNF	>85 %	$144/25g	CNF is clustered	ACS material[74]
CNT	>99 %	$550/25g	1.6 nm diameter, > 5 μm length	Inquiry
CNT	>85 %	$450/25g $3800/kg	1.6 nm diameter, > 5 μm length	Inquiry
SWCNT	>96 %	€215/g		Nanografi[75]
SWCNT	>95 %	$185/g $1260/10g $5364/50g	1-2 nm diameter, 5-30 μm length	Inquiry
SWCNT	>92 %	€100/g		Nanografi[76]
SWCNT	>90 %	$140/g $975/10g $4125/50g	1-2 nm diameter, 5-30 μm length	Inquiry
SWCNT	>65 %	€70/g		Nanografi[77]
MWCNT	>98 %	$63/5g $100/10g $540/100g	30-50 nm diameter, 10-30 μm length	Inquiry
MWCNT	>95 %	$150/100g $450/500g $2970/10kg	20-40 nm diameter, 10-30 μm length	Inquiry

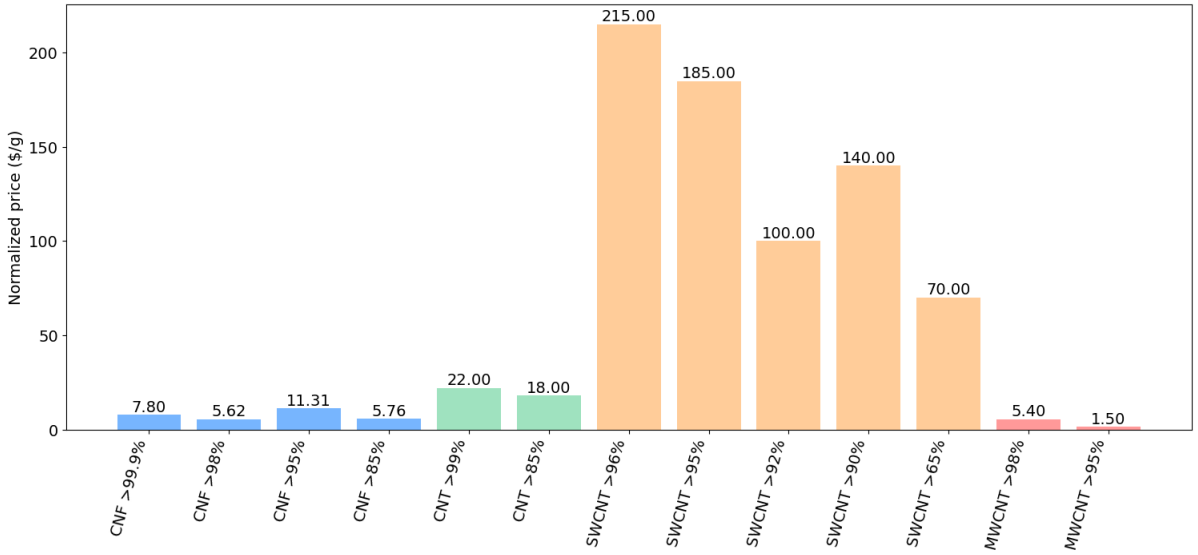

Figure 2.11: Normalized prices per gram for CNF, CNT, SWCNT and MWCNT based on Table 2.3. For CNF and CNT the price per 25 g and for MWCNT the price per 100 g is converted to per g, for SWCNT the price per g is taken. The price generally increases as the purity goes up for CNTs, SWCNTs and MWCNTs. The price for CNF does not show the same increase with purity, caused by CNF with >95 % purity sold by US Research Nanomaterials INC.

2.4. Techno-economic Analysis

A techno-economic analysis is required to determine the economic viability of the CNF purification process. A techno-economic analysis consists of multiple parts: the capital expenditure (CAPEX), the operational expenditure (OPEX), revenues and profits and finally the economic evaluation of the project.

Capital expenditure consists of two parts: the fixed capital costs and the working capital. The fixed capital costs consist of the following components, according to Towler & Sinnott[78]:

- Inside battery limits investment (ISBL): The ISBL consists of direct and indirect field costs. Among the direct field costs are all the major equipment, items in bulk such as wiring, pipes et cetera, civil works and installation labour and supervision. Among the indirect field costs are construction insurance, labour benefits and burdens, miscellaneous overhead, field expenses and services and finally construction costs such as temporary water, construction et cetera.
- Offsite costs (OSBL): OSBL consists of additions to the plant infrastructure. These include laboratories, offices, emergency services, power generation plants and more.
- Design and engineering costs (D&E): consists of the cost for detailed design, procurement, construction supervision, bonding, administrative charges and the profit of the contractor(s).
- Contingency charges: consists of extra costs that are added to allow for uncertainty regarding the cost estimate. It also can help to cover small project scope changes, unexpected problems and labour disputes.

According to Towler & Sinnott[78], the working capital is an additional investment to the fixed capital for maintaining plant operations. This additional investment is needed during the whole length of plant operation, but is recovered once the plant shuts down. Working capital involves the raw material, spare parts, product and by-product inventory, cash on hand, money owed by customers and money that is owed to suppliers.

Operational expenditure involves costs during the plant operation, and will always be there as long as the plant is operational. The OPEX can be divided into two categories: the variable and the fixed production costs. According to Towler & Sinnott[78], the variable production costs include:

- Raw materials

- Utilities
- Consumables
- Effluent disposal
- Packaging and shipping

The fixed production costs are different compared to the variable production costs, as the fixed costs are not dependent on the production rate of the plant. According to Towler & Sinnott[78], the fixed production costs include:

- Operating labour
- Supervision
- Direct salary overhead
- Maintenance
- Property taxes and insurance
- Rent costs of the land
- General plant overhead
- Allocated environmental charges
- Royalty payments and license fees
- Capital charges
- Research and development
- Sales and marketing

The revenues originate from selling the products and by-products of the process. The gross profit is the revenues of the main product, subtracted by the total cash cost of production (CCOP). The net profit is obtained by subtracting the costs of the taxes from the gross profit.[78]

The economic performance of a project for building and operating a process plant can be evaluated using multiple parameters. First, it is important to determine the cash flow of a project per year. The cash flow per year, CF_{i}, is equal to the gross profit minus the tax paid and minus the capital cost in that same year. In addition, the Net Present Value (NPV) is a very useful economic parameter. Equation 2.8 shows the calculation of the NPV, where the NPV is the summation of the present values of future cash flows.[78] The time value of money is taken into account. Furthermore, the annual variation in expenses and revenues are accounted for,[78] which are dependent on the interest rate I and the project lifetime t.

$$\mathrm{NPV} = \sum_{i=1}^{i=t} \frac{CF_i}{(1+I)^i} \tag{2.8}$$

Another important parameter is the Levelized Cost of Purification (LCOP), which indicates the price to purify a certain amount of product. A logical unit for the LCOP is \$/kg or \$/tonne. The LCOP is calculated using Equation 2.9. The LCOP is the sum of the discounted OPEX and CAPEX in each year divided by the sum of the discounted production in each year.

$$\mathrm{LCOP} = \frac{\sum_{t=1}^{t}(\mathrm{CAPEX}_{\mathrm{Discounted}} + \mathrm{OPEX}_{\mathrm{Discounted}}}{\sum_{t=1}^{t} P_{\mathrm{CNF,Discounted}}} \tag{2.9}$$

Following the LCOP, the Payback Time (PBT) gives insight in the required time for the plant to become profitable. The PBT is a function of the average annual cash flow. A shorter payback time means that the plant is generally more profitable. The PBT is calculated using Equation 2.10.[78] The total investment, C_{total}, is divided by the average of the calculated annual cash flows, $CF_{\mathrm{average,\ annual}}$.

$$\text{PBT} = \frac{C_{\text{total}}}{CF_{\text{average, annual}}} \tag{2.10}$$

The Return on Investment (ROI) is also an important economic parameter. The ROI shows how much money is made off the plant compared to its initial investment. The ROI is calculated using Equation 2.11.[78] The cumulative net profit, $P_{\text{cumulative}}$, is the sum of the cash flow of each year. The initial investment, C_0 is equal to the fixed capital costs and t_{lifetime} represents the plant lifetime in years.

$$\text{ROI} = \frac{P_{\text{cumulative}}}{t_{\text{lifetime}} \cdot C_0} \tag{2.11}$$

The Internal Rate of Return (IRR) indicates the required interest rate for the plant in the case that the NPV is equal to zero at the end of the project lifetime.[78] The IRR is determined by solving Equation 2.12 for I'.[78]

$$\text{NPV} = \sum_{i=1}^{i=t} \frac{CF_i}{(1+I')^i} = 0 \tag{2.12}$$

2.5. Outlook

The goal of the literature research is to find relevant literature related to the following research question: *How to design, model and determine the economic viability of a conceptual process for the continuous purification of nanocarbons produced by catalytic methane pyrolysis?*

The literature review shows that the current state of knowledge on purification techniques does not include a detailed nanocarbon purification process for CMP combined with a commercial simulation tool to carry out a techno-economic analysis. Therefore, the research objective is valid. However, the current state of knowledge does include many nanocarbon purification methods. Methods to remove the metal catalyst are: magnetism, acid treatment, functionalisation, high temperature annealing and filtration. Acid treatment is the most efficient and preferred method, followed by magnetism. Purification techniques to remove carbon impurities from nanocarbons are: oxidation, centrifugation, HIDE, bromination, benzene treatment, filtration and acid treatment. There is no clear preference yet for a method, only oxidation is unwanted because of the COx emissions. A few methods exist which are used to help expose the surface of the metal catalyst and make acid treatment easier: ultrasonication, oxidation and HIDE. Furthermore, filtration, washing and drying are applied after most techniques for post-treatment.

Current literature on the carbon market indicates a CB price between 400 and 1000 $/tonne, a CNF price of between 25,000 and 113,000 $/tonne and a CNT price between 100,000 to 600,000,00 $/tonne.[59] All of the nanocarbon markets are expected to grow significantly towards 2030. The price of the nanocarbons increases as the purity increases. An important aspect of the purity is the Ni content. The maximum Ni content in the CNF depends on the application and can be as low as <10 ppm. The desired maximum nickel content is at least below 300 ppm.

For further research, the following recommendations follow from the literature review:

- To further the understanding of CMP, the exact reaction mechanism that occurs should be determined. It is less relevant for research into the purification of nanocarbons and therefore it is not considered.
- Further research into catalysts for CMP should be conducted to increase the stability and lifetime. However, this is not covered in this research.
- Assume a Ni-Based or Fe-based catalyst for the CMP process from which the to be purified nanocarbons originate. Ni- and Fe-based catalysts are preferred over carbon catalysts because of the lower operating temperatures and the production of filamentous nanocarbon, which is more

valuable than CB. Specifically, the Ni-SiO_2 catalyst from research by Hadian et al[14] is assumed because of its promising results and available data. This means that CNFs have to be purified.

- When a Ni-based catalyst is assumed for the CMP process from which the nanocarbons originate, the desired amount of nickel remaining in the nanocarbon product after purification should be below 300 ppm.
- If acid treatment is used as a purification method, it is important to look into the regeneration of the acid and metals if possible. This could potentially reduce the costs of the process.
- Calculate at least the NPV, LCOP, PBT, ROI and IRR of the designed process plant to determine the economic viability.

3

Methodology

In this chapter, the methodology is highlighted. The required output of the study is a process design for the purification of nanocarbon, specifically CNF, with acid leaching, a techno-economic analysis of the process design and the mapping of key parameters influencing the viability of the process plant. The main objective of the process design is a baseline scenario, with possibly a few alternatives to improve the process. The baseline scenario is the benchmark of the CNF purification process plant. The techno-economic analysis is class 4, meaning the accuracy is ±30 %. A class 4 estimate is based on limited cost data and design detail, which is the case in this study. The study is both a design challenge as well as explorative. The process design was carried out with help of literature and the hierarchy approach. A commercial simulation tool along with a coding language was used to model the process design, carry out the techno-economic analysis and to map the key parameters by performing a sensitivity analysis.

A Ni-SiO_2 catalyst was assumed for the CMP process from which the nanocarbons originate, which means that CNFs with a fish-bone structure and diameters between 15 to 80 nm had to be purified. Analysis of the composition of the particular CNFs was required. Since the process design provides a lay-out for the purification of CNF, possibly only minor adjustments had to be made to acquire a purification process design for other nanocarbon types. The CMP process is also out of scope. Experiments on the leaching of Ni from the particular CNFs were required in order to determine the effectiveness of leaching and the leaching kinetics. First, preliminary experiments with H_2SO_4 as acid were conducted to test whether the leaching of Ni from CNF is effective at all. In addition, part of the experiments with varying the acid concentration were conducted. Experiments with varying temperature, residence time and levels of sonication have not been conducted yet.

Data necessary for the design of equipment, that is part of the purification process, was gathered from relevant literature. Relevant literature includes technical data, experiments and descriptions of equipment that were utilized to accurately determine or help determine design parameters of the equipment. If required data on equipment was not available, reasonable estimates had to be made. Data and correlations for the techno-economic analysis were mainly extracted from techno-economic books describing process plant economics. Data for the techno-economics was also gathered from other literature, businesses and governmental organizations in order to retrieve accurate economic numbers.

For the process design, first a simple flow sheet was created. The simple flow sheet only outlines the necessary steps and processes. The basis of the process design is the use of acid leaching for the purification of the CNF. The simple flow sheet provides a foundation for a detailed process design, in which all equipment is specified, recycle structures are incorporated and where equipment integration and necessary process utilities are included. During the process design, it was important to keep alternatives open and consider all options carefully. The nanocarbon process design was realised with the help of the hierarchy approach as described by Dimian et al.[79] and Douglas.[80] It is important to note that the hierarchy approach is considered a helpful tool and was not strictly followed. The hierarchy approach includes the following steps:

- Input of information and batch versus continuous

- Reaction type and the input-output structure
- Recycle structure
- Structure of the separation system
- Equipment integration and heat exchanger network

The commercial simulation tool Aspen Plus V12 was used to model, simulate and optimize the process. A flow sheet was created in Aspen Plus where equipment was added and designed, reactions were specified, input streams were defined and other necessary details were also added. Next to Aspen Plus, Python was used for modelling the techno-economic calculations and is coupled to Aspen Plus. By coupling Python and Aspen Plus, Python was able to forward input to Aspen Plus. Aspen Plus would then run the simulation(s) and Python would retrieve the output of the simulations. Finally, the techno-economic and sensitivity analysis were conducted via Python using the output from Aspen Plus. Python was also used to model equipment, that is not included in the Aspen Plus model, and was used to run sizing calculations for equipment for which Aspen Plus did not provide the size accurately. Other relevant calculations to the model were also added to Python. The techno-economic equations that were used in the model are mainly retrieved from techno-economic books describing process plant economics. Equations that were used for the sizing of equipment are either retrieved from literature or derived with logic.

Important parameters to determine the economic viability are the NPV, LCOP, PBT, ROI and IRR. For the sensitivity analysis, a Monte Carlo analysis and a tornado plot were required. A Monte Carlo analysis of the LCOP tested the robustness of the process design. The tornado plot showed which economic parameters have the largest impact on the LCOP. Other relevant sensitivity analyses, such as the effect of process parameters on the LCOP and conversion, were also included. In addition to economic parameters, the nickel conversion showed if the process is effective for the removal of nickel from CNF. The desired amount of nickel in the final product is below 300 ppm.

4

Acid Leaching Experiments

The goal of the acid leaching experiments is to study the effectiveness and determine the kinetics of acid leaching for removing Ni from CNF. Specifically, the removal of Ni from CNFs from research by Hadian et al. was studied.[14] The effectiveness of various acids, acid concentrations, temperatures, residence times and sonication was studied. In this study, only preliminary and part of the acid concentration experiments were conducted. Preliminary experiments were conducted to test whether the acid leaching of nickel from CNF is effective and whether to continue with further experiments to determine the acid leaching kinetics. The acid leaching experiments were conducted in collaboration with P.B. Tamarona.

First off the analysis of the received samples is discussed in Section 4.1 followed by a description of the procedures of the acid leaching experiments in Section 4.2. Section 4.3 discusses the results of the acid leaching experiments. The samples before and after leaching were analysed using various analysis methods: X-ray Fluorescence analysis (XRF), Inductively Coupled Plasma analysis (ICP), Scanning Electron Microscopy analysis (SEM) and finally X-ray Diffraction analysis (XRD). XRF and ICP were used to measure how effective the leaching process to extract the Ni and other impurities from the nanocarbons is. XRD was used to characterize the structure and species of the nanocarbons, including trace amounts of catalyst. XRD was used before and after the acid leaching process, determining whether there is a shift in carbon forms or metal content. Finally, SEM was used to compare the structural condition of nanocarbons before and after the acid leaching process. The SEM image shows whether the acid has any effect on the nanocarbon structure.

4.1. CNF Samples Analysis

It is important to analyse the CNF samples that are used during the experiments. The samples originate from CMP with a Ni-SiO_2 catalyst from the Multiphase Reactors Group of the Department of Chemical Engineering at Eindhoven University of Technology.[14] Four analysis methods are used: X-ray Fluorescence analysis (XRF), Inductively Coupled Plasma analysis (ICP), Scanning Electron Microscopy analysis (SEM) and finally X-ray Diffraction analysis (XRD).

Table 4.1 shows the results of XRF and ICP, which are used to measure the contents of the CNF samples. The XRF results show that the CNF is 98.567 % carbon and that 1.154 wt% of Ni is present. The ICP results only show the metal concentrations and indicate that only 0.47 wt% of Ni is present. This is a difference of 0.684 wt% with the XRF results and in the context of the experiments it is a significant difference. ICP is generally considered to be more accurate, as XRF analysis only shows the contents of a thin surface layer. Therefore, the ICP analysis results are deemed to be the ground truth.

Table 4.1: XRF and ICP results of the CNF samples originating from CMP with a Ni-SiO_2 catalyst. The XRF concentration and absolute error are shown in wt%. The ICP concentration is shown in ppm and wt%.

Component	XRF concentration (wt%)	XRF absolute error (wt%)	ICP concentration (ppm)	ICP concentration (wt%)
C	98.567			
Ni	1.154	0.03	4700	0.47
Si	0.133	0.01	290	0.029
Mg	0.032	0.005	638	0.0638
Al	0.015	0.004	133	0.0133
Fe	0.005	0.002	33	0.0033
Ca	0.003	0.002	33	0.0033
S	0.001	0.001		
Bi			29	0.0029
Cu			98	0.0098
Na			57	0.0057
Zn			39	0.0039
SO_4			26	0.0026
Sb			13	0.0013
Ir			17	0.0017

SEM is applied to the CNF samples to determine the internal structure, morphology and compositional contrast. Figure 4.1 shows the SEM results. The upper two images show that the CNF structures are clearly visible and that the diameters are in-between 15 and 80 nm. The bottom two images show that impurities are visible on the carbon.

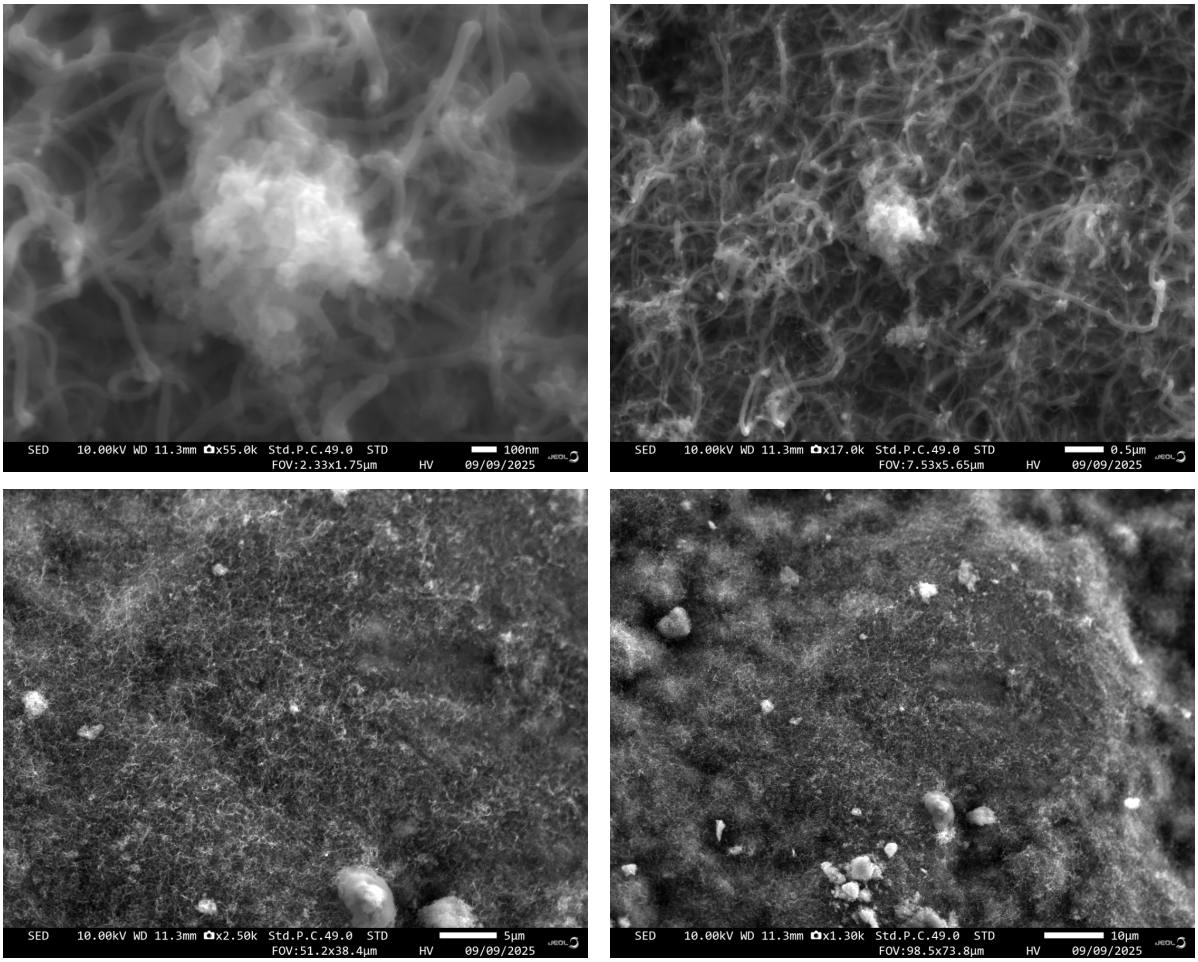

Figure 4.1: SEM results of the CNF samples retrieved from CMP with a Ni-SiO_2 catalyst. In the upper two images, the CNF structures are clearly visible. In the bottom two images, impurities are visible on the carbon.

Figure 4.2 shows the XRD results of the CNF samples. XRD is used to provide information about the crystallographic structure, chemical composition, and physical properties of the CNF samples. The black pattern represents the measured XRD pattern after background subtraction. The coloured sticks indicate the intensities and peak positions of possibly present crystalline phases. The ICDD pdf5 and COD databases are used. The results show that both carbon and nickel are present in the CNF samples.

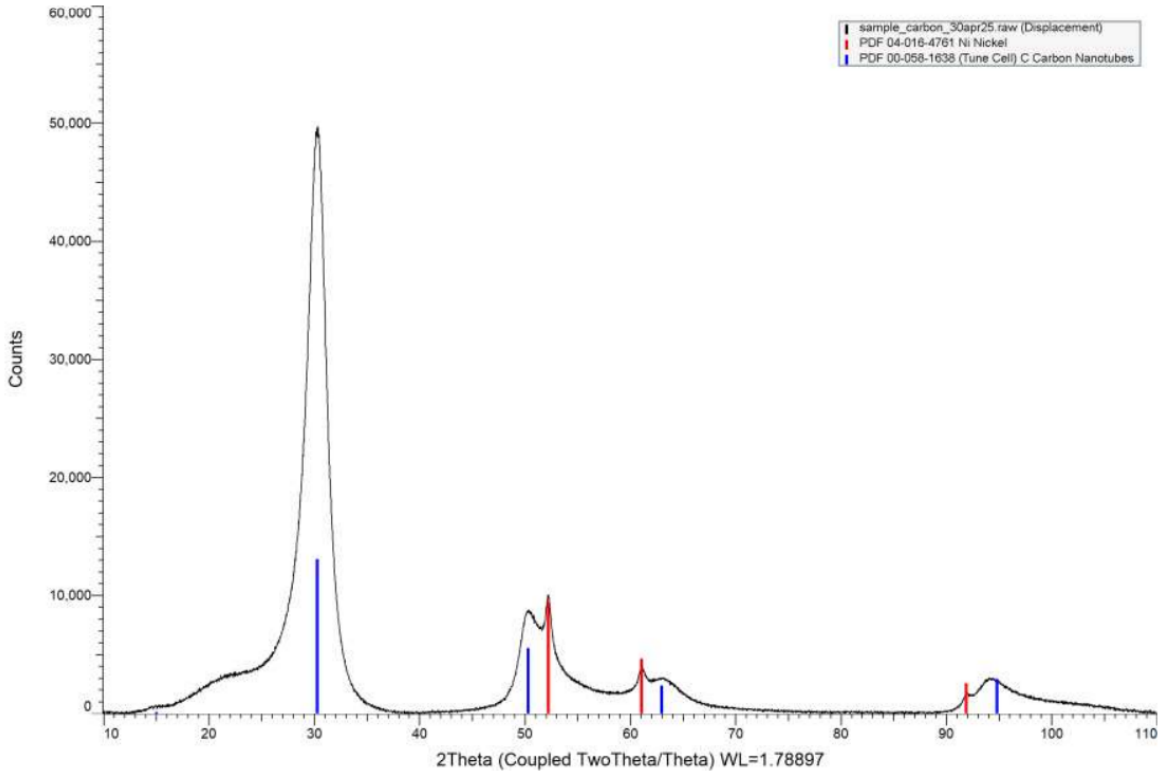

Figure 4.2: XRD results of the CNF samples retrieved from CMP with a Ni-SiO_2 catalyst. The black pattern represents the measured XRD pattern after background subtraction. The coloured sticks indicate the intensities and peak positions of possibly present crystalline phases. The ICDD pdf5 and COD databases are used.

4.2. Acid Leaching Experimental Procedures

This section gives an overview of the general acid leaching procedure and the acid leaching experiments. The full description of the procedure and experiments is in Appendix A. Various experiments are to be conducted: preliminary experiments, acid concentration experiments, temperature and residence time experiments, and lastly experiments to determine the effect of the sonication. The temperature and residence time, and sonication experiments are out of scope for this study, because of problems encountered during sample analysis and time restrictions. The experiments are carried out using various acids: HCl, H_2SO_4 and HNO_3.

The general experimental procedure of the experiments is as follows. The first step is to prepare the acid mixture with the required molarity. Afterwards, 1 mL of the acid mixture is added to a 2 mL vial with a hole at the top. This step is repeated for a total of n vials. The vials are added to a thermoshaker and heated to the desired temperature. Once the required temperature has been reached, 0.2 g of the CNF sample is added to each of the vials. The vials are left in the thermoshaker for a certain time period at the desired temperature with a stirring speed of the thermoshaker of 550 rpm. After the specified time period, the vials are removed from the thermoshaker. The acid and CNF are then filtered using a funnel with a filter paper on top. The CNF is the residue and the acid is the filtrate. The CNF is then washed multiple times with hot water and subsequently dried at 120 °C for 4 hours. After drying the CNF, multiple analyses methods are applied to the CNF samples: XRF, XRD, SEM and ICP. The CNF samples are also weighed after the experiments. The acid filtrate is also weighed

and ICP analysis is conducted on the acid filtrate to determine the Ni content in the filtrate.

The first set of experiments are the preliminary experiments. The preliminary experiments are conducted to confirm whether the acid leaching of Ni from the CNF samples is effective and whether to continue with the other experiments. The preliminary experiments are conducted using 1 mL of a 4 M H_2SO_4 mixture with 0.25 g of CNF sample in a vial. A total of 8 vials are used. The vials are kept at 70 °C for 4 hours with a thermoshaker stirring speed of 550 rpm. There are four vials that are not sonicated, two are with 20 % sonication and two are with 40 % sonication. If H_2SO_4 proves to be efficient in acid leaching, the preliminary experiments can also be conducted with HCl and HNO_3. The complete description of the preliminary experiments is given in Appendix A.

The next set of experiments are the acid concentration experiments. The goal of the acid concentration experiments is to determine the influence of the acid concentration on the acid leaching of Ni. A total of 24 vials are used. Each vial contains 0.2 g of CNF sample and 1 ml of acid mixture. Each vial is kept at 60 °C for 1 hour in a thermoshaker. Six different values of the acid concentration are used: 1 M up to and including 6 M. For every value of the acid concentration, four vials are used. Hence, the total number of vials is 24. The acid concentration experiments are first conducted with H_2SO_4 and later on with HCl and HNO_3 as well. The complete description of the acid concentration experiments is given in Appendix A.

Temperature and residence time experiments have to be carried out to determine their effect on the acid leaching of Ni. These experiments give insight into the acid leaching kinetics of Ni. Furthermore, sonication experiments have to be carried out to determine the effect of sonication on the acid leaching of Ni. The temperature, residence time and sonication experiments are however out of scope for this study, but the procedures are described in Appendix A.

4.3. Acid Leaching Experimental Results

This section details the results of the acid leaching experiments. The only results available are the compositions of the acid leftovers of the preliminary experiments and part of the acid concentration experiments, both conducted with H_2SO_4. The main reason is a delay caused by the difficulties encountered during the preparation of the CNF sample for the ICP analysis. After the acid leaching procedure, the CNF is dried in an oven. The dry CNF is first burned in an oven at high temperature, around 950 °C. Whether the CNF is first burned or not, the sample is mixed with HNO_3 to digest it for ICP. However, not all of the sample dissolves in the acid. The consequence is that the ICP analysis is potentially inaccurate and provides values for the metal concentrations which are too low. Part of the metals can still be contained in the non-dissolved part of the sample. A potential solution to the problem is to use a microdigester to decompose the solid CNF and prepare the sample for ICP analysis. Once the problem of the ICP sample preparation has been solved, the experiments can continue. The remaining acid concentration, the temperature and residence time as well as the sonication experiments can then be conducted. Because the kinetics of the nickel leaching with acid from CNF have not been determined yet, the next best alternative needs to be used for the modelling of the process plant, therefore the kinetics of nickel leaching from a Ni–Al_2O_3 spent catalyst determined by Parhi et al[81] are used instead.

Table 4.2 shows the conditions at which the experiments have been conducted. P1 to P4S represent the preliminary experiments. B13 to B16 are part of the acid concentration experiments. Figure 4.3 shows the nickel content in ppm (mg/kg) of the acid leftovers of the preliminary and part of the acid concentration experiments. The acid leftover is the acid that remains after the acid leaching of the CNF and the measurements are conducted with ICP. The contents of a control group with unused acid are also measured to show that nickel is initially not present in the acid. The results in Figure 4.3 show that B13 to B16 contain more nickel in ppm than the other acid leftover samples. However, the results first have to be converted to absolute mass and then wt% to be able to tell how much nickel is removed compared to the original CNF sample.

Table 4.2: Overview of the conditions of the preliminary and part of the acid concentration experiments. The mass of the acid leftover is also included. P1 to P4S are the preliminary experiments, B13 to B16 are part of the acid concentration experiments.

Sample	Temperature (°C)	Molarity (M)	Time (hours)	Sonication	Acid sample mass (mg)
P1	70	4	4	no	4100
P2	70	4	4	no	5793
P3	70	4	4	no	4774
P4	70	4	4	no	3033
P1S	70	4	4	20 %	6210
P2S	70	4	4	20 %	3614
P3S	70	4	4	40 %	3860
P4S	70	4	4	40 %	3845
B13	60	4	1	no	960.7
B14	60	4	1	no	981.8
B15	60	4	1	no	983.5
B16	60	4	1	no	1093.1

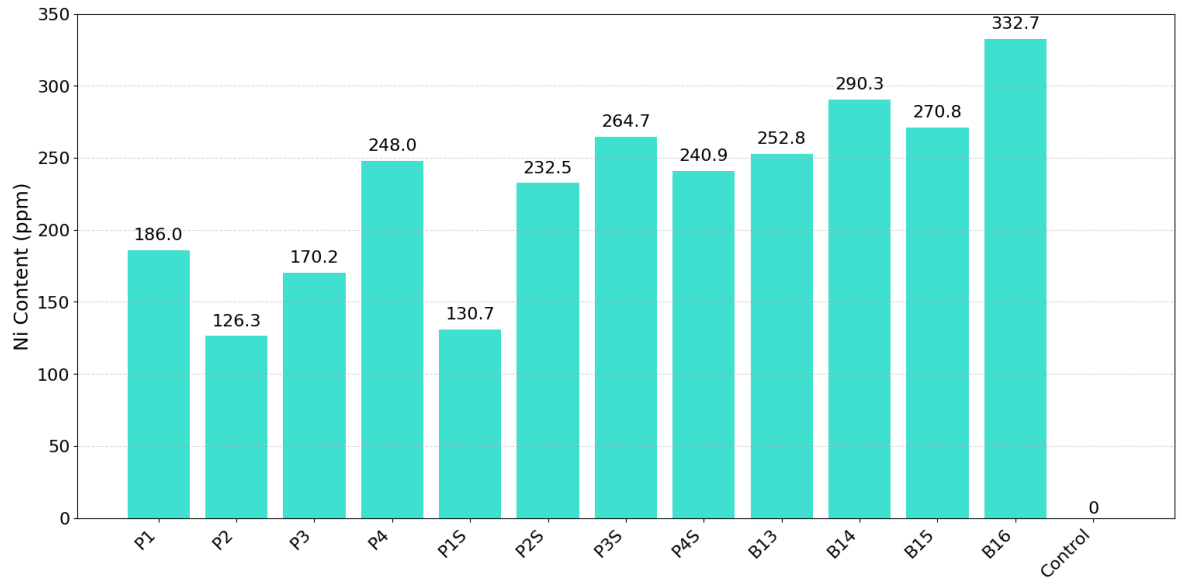

Figure 4.3: Nickel content in ppm of the acid leftovers of the preliminary experiments, P1 until P4S, and part of the acid concentration experiments, B13 until B16. The nickel content is determined with ICP. A control group of unused acid is added to confirm that there is no nickel initially present in the acid.

The content in ppm is converted to mg by multiplying with the mass in kg of each acid sample. The mass of each acid sample in mg is given in Table 4.2. Further division by the initial mass of the carbon sample, which is 250 mg for P1 to P4S and 200 mg for B13 to B16, gives the weight fraction. The results of the wt% of nickel in the acid leftovers versus the original sample are shown in Figure 4.4. The results show that acid leaching is effective for the removal of nickel from CNF, even when the original CNF sample has a low wt% of nickel equal to 0.47. However, the measured Ni concentration in the original sample might not be accurate yet, due to the problems encountered when conducting the ICP analysis. Therefore, no definitive conclusion on the effectiveness of the acid leaching can be drawn. The average nickel conversion of the preliminary experiments is equal to 70.9 %. The conversion of P3S and P4S is equal to 83.0 %, which is the highest achieved for the preliminary experiments. The average conversion of B13 to B16 is equal to 30.8 %. The conclusion is that the preliminary experiments P1 to P4S show better nickel conversion results than B13 to B16. The temperature and especially the residence time are higher for the preliminary experiments, both which seem to positively affect the removal of nickel from the CNF.

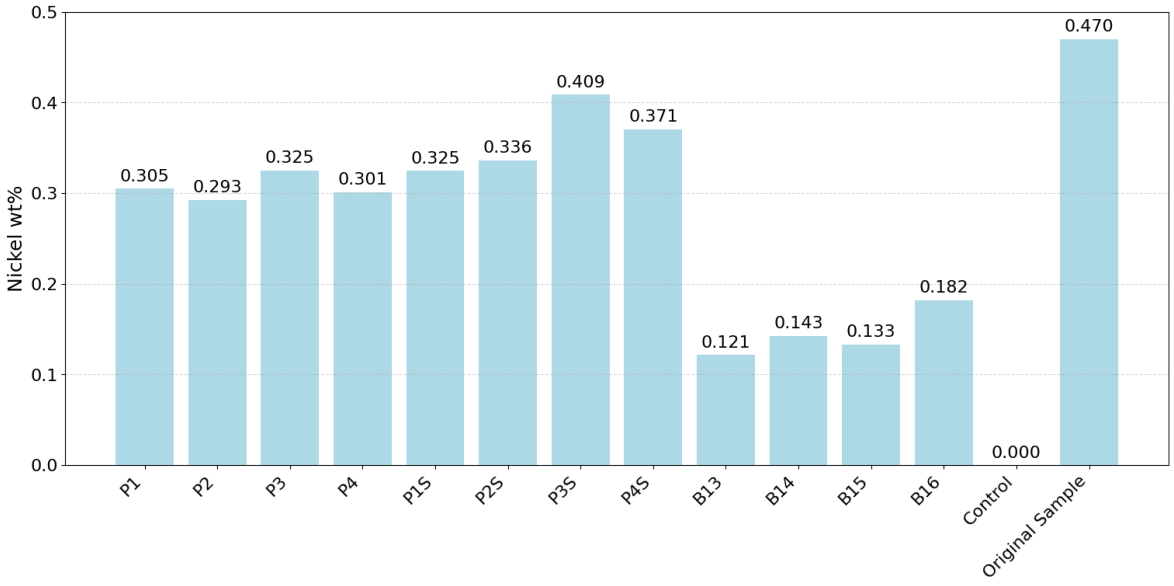

Figure 4.4: Wt% of nickel removed in the preliminary experiments, P1 to P4S, and part of the acid concentration experiments, B13 to B16. The nickel content in the original sample is also shown and a control group of unused acid is added. The preliminary experiments do show a significant removal of the nickel content.

5

Process Design and Equipment Sizing

This chapter describes the process design for the CNF purification process plant. Section 5.1 discusses the design steps and choices for the nanocarbon purification process. The outcome is a process flow sheet for the baseline scenario. Section 5.2 provides the design calculations for sizing of the equipment.

5.1. Process Design and Overview

The process design is executed using the help of the hierarchy approach,[79,80] but not strictly following all steps of the hierarchy approach. In this section, the most important aspects of the process design are discussed.

5.1.1. First Process Flow Sheet Design and Design Choices

The first step of the hierarchy approach is to define whether the process plant is a continuous or batch process. The title of the research states that a 'conceptual process for the continuous purification of nanocarbons...' should be designed. Therefore, the goal is to design a continuous process. Furthermore, it is important to note that the location of the process plant is in the Netherlands. The production capacity of the plant is within reasonable amount of the current CNF market. The market demand for CNF was 100,000 tonnes in 2020.[59] The production capacity of the process plant is assumed to be 20,000 tonnes per year. The nanocarbons, that are purified in the process plant, are CNFs which contain Ni impurities. The analysis of the CNF samples in Chapter 4 shows the composition of the CNF. The carbon content is 99.4173 wt%, the Ni content is 0.47 wt% and the remaining wt% is attributed to various other metallic impurities. Only components that appear in both XRF and ICP are considered and the numbers in the composition are based on only the ICP analysis results. The desired Ni content of the final product is below 300 ppm.

Currently, the most preferred method for the purification of nanocarbon is through acid treatment, as research has already shown.[17,32,40,41,43] In this study, acid treatment is also applied for the purification of the nanocarbon. Common acids are HCl and HNO_3, but H_2SO_4, ammonia based acids or organic based acids could also be an option. The acid used in this process design is HCl, as data on the leaching kinetics of nickel with HCl is available and HCl is a very suitable acid for the leaching. Equation 2.3 shows the reaction of HCl with nickel. It is very important to note that ions often form, such as Ni^{2+} with Cl^-. The ions are usually soluted in the liquid acid that remains.

Because acid treatment is applied, at least filtration, washing and drying need to be applied as post-treatment methods in order to obtain the final CNF product. Filtration separates the solid CNF and liquid acid. Washing removes remaining acid from the CNF and finally drying removes the last bit of liquid water from the CNF. Ultrasonication or crushing could be used prior to the acid treatment to help expose the metal surface. The downside of ultrasonication and crushing is that it can potentially damage the CNFs.

The reaction of Ni with HCl leads to the existence of three phases. CNF is in solid phase, the remaining acid solution with ions is in liquid phase and the H_2 is in gas phase. The gas phase has to be separated from the other two phases prior to the liquid-solid filter. Therefore, an extra separation step is introduced.

Combining the current known process steps, a structure of the first conceptual CNF purification flow sheet is developed, as shown in Figure 5.1. The CNF with the metal impurities and the acid are fed to a reactor. The acid turns the Ni into $NiCl_2$ and H_2. The H_2 gas is removed in a separator and afterwards the filter separates the solid and liquid phase. The CNF is then washed with water to remove any remaining acid and Ni-chloride/oxide. Finally, the CNF is dried to remove the remaining liquid and the final CNF product is obtained. It is important to note that the final product most probably still contains very small amounts of Ni and the other metal impurities, as acid leaching is not 100 % effective in removing the Ni. The desired amount of Ni in the final product is below 300 ppm.

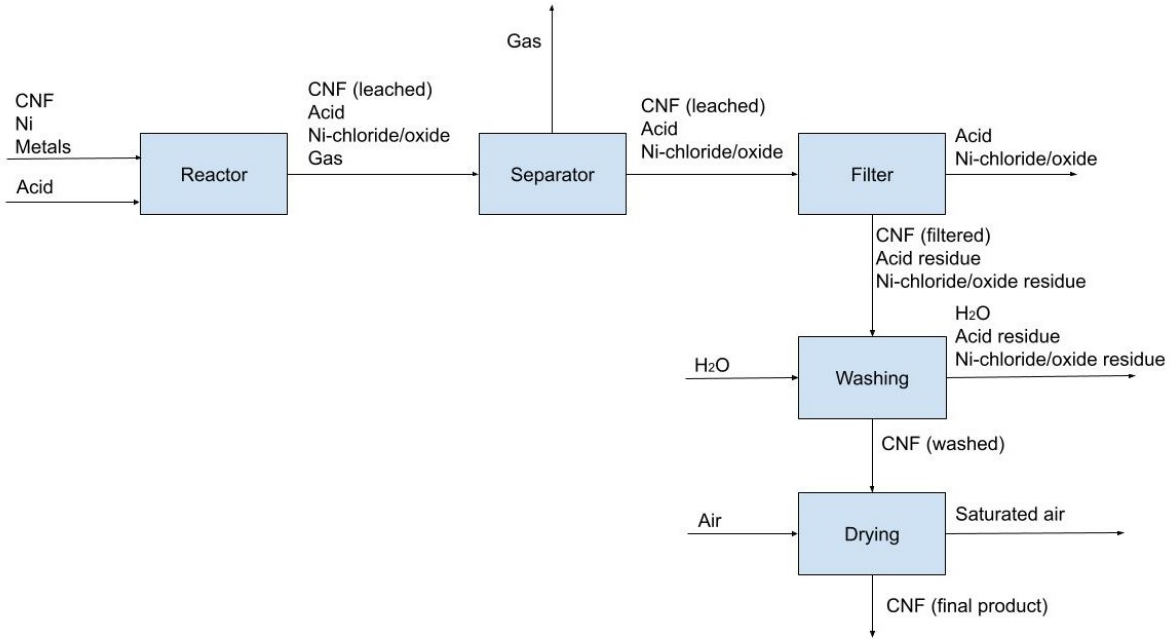

Figure 5.1: Structure of the first conceptual process plant flow sheet. CNF with metal impurities and acid are reacted in a reactor. Afterwards, the gas and remaining acid mixture need to be removed. The CNF is then washed with water to remove any remaining acid and dried afterwards to obtain the final product.

5.1.2. Final Process Flow Sheet and Design Choices

Following the first conceptual flow sheet, more detail was added and a final process flow sheet is retrieved. Equipment is specified, recycle streams are added when needed and equipment integration is necessary. Figure 5.2 shows the final process flow sheet for the baseline scenario. The design choices are discussed in the remainder of this section.

First, constant pressure is assumed along the main stream. In reality, this may be different. The main stream starts with the CNF feed. Under the assumption that the process plant is built directly next to the CMP plant from which it originates, the CNF that enters is around 600 °C. That is too hot for the reactor, so the first step is to cool the CNF down. In order to cool the CNF down to the reactor temperature, which is 80 °C in the baseline scenario, a heat exchanger is necessary. Conventional heat exchangers are difficult to employ, as the CNF is in solid phase. A possible method is to use a solids rotary cooler. The solid CNF enters the drum of the cooler and is indirectly cooled by continuously showering the exterior of the drum with water. The solid CNF that leaves the cooler through stream Main-2 is then at an adequate temperature to enter the reactor.

Another important feed stream is the acid mixture feed for the reactor. The type of acid, concentration of the acid as well as the feed rate can affect the reactor conversion. The acid used is HCl. The

ratio of the mass flow rate of the CNF feed stream to the volumetric flow rate of the acid feed stream is assumed to be 1:10 and the molarity of the feed stream is 2 M. The temperature of the acid feed is assumed to be 20 °C.

The next important step was to define the reactor type. For this particular application, a Continuously-Stirred-Tank-Reactor (CSTR) is deemed fit. In the CSTR, the metal in the CNF reacts with the acid to form $NiCl_2$ and H_2. What remains after the CSTR in stream Main-3 is a three phase system consisting of solid CNF, a liquid containing water, acid, Ni & Cl ions and finally H_2 in the gas phase. To keep the CSTR at a constant temperature of 80 °C, hot steam at 200 °C is used, which is supplied through stream Steam-2.

After the reactor, the H_2 gas needs to be separated from the slurry containing the solid and liquid. An advanced type of three-phase separator, with a gas and a slurry outlet, is used. The slurry is then fed to the liquid removal system, which contains a hydrocyclone, two rotary vacuum drum filters and a washer. The first step of the liquid removal system is the bulk separation of the liquid and solid, for which a hydrocyclone is very suitable. The coarse particles of around 1 mm are also ideal for a hydrocyclone. A hydrocyclone has an underflow, which contains a much more solid concentrated solid. The bulk of the liquid leaves through the overflow via stream Waste-1. Another option for bulk separation is to use a gravity settler. However, a gravity settler is much slower then a hydrocyclone. After the bulk separation, further removal of the liquid is required. A rotary vacuum drum filter is very suitable and is widely used in industry. Although filtration can be a bit slow, it is important to apply in order to remove as much liquid prior to feeding the solid to the washer. Typically, at least 10 % of liquid remains after filtering. Another option is to use a dewatering screen, which contains a slightly tiled vibrating screen to increase the removal of the liquid.

The following step is to feed the main stream to a washer. Washing is very often applied as a post-treatment step for CNF and also for CNT, as shown in Chapter 2. By adding water, as much of the remaining acid as possible is removed. The bulk of the liquid leaves to stream Waste-3, while the slurry leaves to stream Main-7. Because the liquid content of the slurry is increased due to the washing, another rotary vacuum drum filter is required to remove as much liquid mechanically. Again, a dewatering screen is also an option for the mechanical removal of the liquid. Since removing liquid by drying is costly and energy intensive, it is very important to remove as much liquid through other methods.

After the mechanical liquid removal steps, the remaining liquid is removed in a dryer. The problem with drying is that the main stream needs to be heated to 100 °C and the latent heat of vaporisation also needs to be supplied. The latter one costs a lot of energy to supply and it would be inefficient to supply the latent heat of vaporisation with air only. The solution is to add a heat exchanger in-between the second filter and the dryer. This heat exchanger is called the 'slurry heater'. The slurry heater is a scraped surface heat exchanger (SSHE). A SSHE is very suitable for flows containing both solid and liquid as the scraping prevents fouling and clogging. Hot steam at 200 °C indirectly heats the main steam. Following the SSHE, the main stream Main-9 is fed to the dryer. The dryer is a rotary solids dryer. Hot air at 100 °C is supplied to the dryer by stream Air-3 to carry away the vapour. The end result is dry and purified CNF.

The hot air used for drying is taken from the atmosphere. First, the air flows through a bag filter to rid unwanted dust particles. The dust is captured and is disposed of. The air flows through stream Air-2 to the air heater. The air heater heats the hot air to 100 °C using steam at 200 °C. The air heater is assumed to be a plate-frame heat exchanger. After usage in the rotary dryer, the hot air contains water and acid vapour. In order to remove the water and acid from the air, the air is condensed to below the dew point in a condenser using cold water at 20 °C. The clean air leaving through Air-5 can be recycled or released. The condensate is acid waste and leaves through stream Waste-6.

To generate the hot steam used for heating, a pump and steam generator are required. Water flows into the pump. The pump increases the pressure of the water from 1 to 15.54 bar. The steam generator runs on electricity and converts the water into hot steam at 200 °C. The steam is then transported to the CSTR, slurry heater and air heater. After heating, the steam is recycled by letting it return to the water stream, before the water enters the pump.

Water is also used for cooling in the rotary solids cooler, cooling in the air condenser and for removing

acid in the washer. Water used for cooling in the rotary solids cooler and air condenser is recycled by using it for generating steam. Water is also used in the acid mixture feed, but that is not explicitly indicated in the process flow sheet. It is important to mention that not all used steam or water is to be recycled, part of it can be released again. The process flow sheet does however not indicate this. For the sizing and the techno-economic calculations, the recycling of water is not considered. The cost of water is relatively low compared to other operational costs.

The hydrocyclone, vacuum drum filter 1 and 2, washer and rotary dryer all generate waste streams which contain HCl with water. This acid waste is disposed off-site. This means that there are off-site waste disposal costs. Another option would be to treat the acid waste such that the water can safely be released back into the environment or to implement an acid recycle.

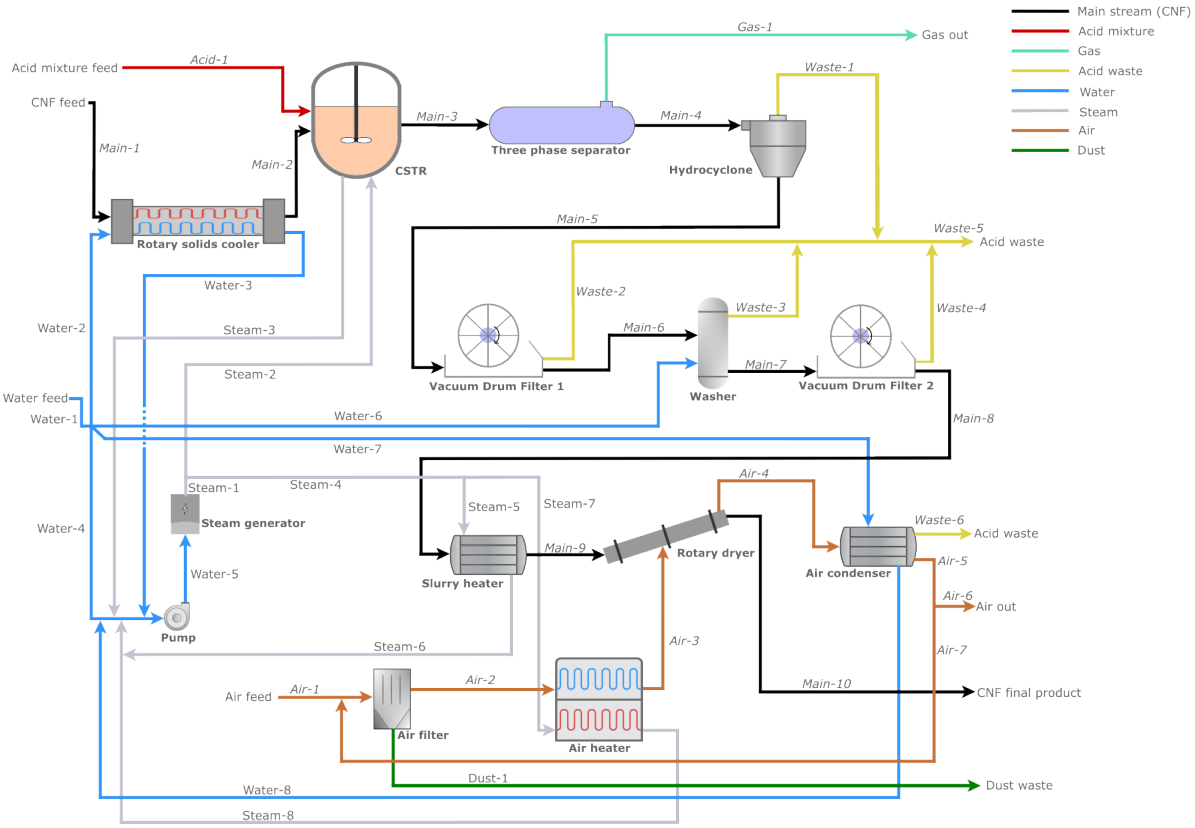

Figure 5.2: Final process flow sheet of the CNF purification process plant. The incoming CNF is fed to the rotary solids cooler to cool the CNF to the reactor temperature, after which it is fed to the CSTR for acid leaching. Following the CSTR, a three phase separator is added to remove the created H_2 gas. The slurry is then fed to a hydrocyclone followed by the first vacuum drum filter for liquid removal, after which it is washed with water. Following the washer, the main steam is fed to the second vacuum drum filter for liquid removal. The main stream is then heated in the slurry heater and finally dried in a rotary dryer. The final product is dry and pure CNF. The air for drying is atmospheric air which is first filtered in an air filter and heated to the desired temperature in the air heater. After drying, the water and acid in the air is condensed and removed. Steam is used for heating and is generated by a steam generator. Water is used for cooling, washing and as supply to the steam generator. A pump brings the water to the desired pressure for the steam generation. Recycle streams of water and steam are shown, but are not taken into account in the model and calculations.

5.2. Equipment Design Calculations

In this section, the design calculations of the equipment are discussed in detail. The equations, important numbers and assumptions for all equipment is given. Note that the research limits itself to a class 4 estimate for the techno-economics, which is ±30 % accurate. The class 4 estimate means that the equipment design and calculations can be rough estimations instead of precise calculations.

5.2.1. Rotary solids cooler

The CNF enters the process plant at 600 °C. The CNF first needs to be cooled down to the CSTR temperature, which is 80 °C in the baseline scenario. A rotary solids cooler is used for cooling the CNF. The incoming water is assumed to be 20 °C and the pressure in the cooler is 1 atm. To calculate the required mass flow of water for the cooler, Equations 5.1 through 5.3 are applied. In Equation 5.1 the temperature of the water leaving the heat exchanger is assumed to be 5 °C lower than that of the solid stream leaving the heat exchanger. The required cooling rate in kW, $\dot{Q}_{\text{cooler}}$, is retrieved from Aspen Plus. Aspen Plus calculates the cooling rate based on Equation 5.2, where $c_{p,\text{CNF}}$ is estimated to be 0.7 kJ kg^{-1} K^{-1}.[82] Furthermore, $\dot{m}_{\text{Main-1,2}}$ is the mass flow rate of the main stream flowing through the solids cooler. Equation 5.3 is applied to calculate the required mass flow of the water in the cooler in kg s^{-1}, where $c_{p,\text{water}}$ is equal to 4.184 kJ kg^{-1} K^{-1}.

$$T_{\text{water,out}} = T_{\text{CNF,out}} - 5 \tag{5.1}$$

$$\dot{Q}_{\text{cooler}} = \dot{m}_{\text{Main-1,2}} \cdot c_{p,\text{CNF}} \cdot (T_{\text{Main-1}} - T_{\text{Main-2}}) \tag{5.2}$$

$$\dot{m}_{\text{Water-2,3}} = \frac{\dot{Q}_{\text{cooler}}}{c_{p,\text{water}} \cdot (T_{\text{Water-3}} - T_{\text{Water-2}})} \tag{5.3}$$

The required area of the cooler in m^2 is calculated using the Log Mean Temperature Difference (LMTD) method in Equations 5.4 through 5.7. The overall heat transfer coefficient, U_{cooler}, is estimated to be 150 W m^{-2} K^{-1}. The value for U_{cooler} is based on literature on heat transfer coefficients for drying and cooling.[83]

$$\Delta T_{1,\text{ cooler}} = T_{\text{Main-1}} - T_{\text{Water-2}} \tag{5.4}$$

$$\Delta T_{2,\text{ cooler}} = T_{\text{Main-2}} - T_{\text{Water-3}} \tag{5.5}$$

$$\Delta T_{\text{lm,cooler}} = \frac{\Delta T_{1,\text{ cooler}} - \Delta T_{2,\text{ cooler}}}{\log \frac{\Delta T_{1,\text{ cooler}}}{\Delta T_{2,\text{ cooler}}}} \tag{5.6}$$

$$A_{\text{cooler}} = \frac{\dot{Q}_{\text{cooler}}}{U_{\text{cooler}} \cdot \Delta T_{\text{lm,cooler}}} \tag{5.7}$$

5.2.2. Continuously Stirred Tank Reactor (CSTR)

The CSTR is used for acid leaching of the CNF with HCl. In the baseline scenario, the reactor temperature is 80 °C, the reactor pressure is 1 atm and the reactor residence time is set to 3 hours. The volume of the CSTR is retrieved from Aspen Plus. The software calculates the volume using Equation 5.8. The volumetric flows of the feed streams of the CSTR in m^3 hr^{-1} are multiplied by the residence time of the reactor in hours, $t_{\text{residence}}$. The required volumetric flow of the acid feed is determined with Equation 5.9 and is used as input. F_{acid} represents the ratio of the acid feed volumetric flow rate over the CNF feed mass flow rate. Unless mentioned otherwise, F_{acid} is equal to 10. The required heat duty for the CSTR is also retrieved from Aspen Plus. The heat duty of the CSTR is provided by hot steam at 200 °C, which is assumed to leave the CSTR at 110 °C after providing heat.

$$V_{\text{CSTR}} = (\dot{V}_{\text{Main-2}} + \dot{V}_{\text{Acid-1}}) \cdot t_{\text{residence}} \tag{5.8}$$

$$\dot{V}_{\text{Acid-1}} = F_{\text{acid solution}} \cdot \dot{m}_{\text{Main-1}} \tag{5.9}$$

$$\dot{Q}_{\text{CSTR}} = \frac{\dot{n}_{\text{Acid-1}} \cdot c_{p,\text{acid}} \cdot (T_{\text{CSTR}} - T_{\text{Acid-1}}) + \dot{n}_{\text{Main-2}} \cdot c_{p,\text{solid}} \cdot (T_{\text{CSTR}} - T_{\text{Main-2}})}{3600} \tag{5.10}$$

5.2.3. Three phase separator

The three phase separator is used to separate the hydrogen from the solid and liquid. The separator is a complicated piece of equipment, which for the sake of the cost estimation, is sized using a simple equation. The volumetric flow rate in L s^{-1} going into the separator is calculated in Equation 5.11 by taking the volumetric flow rate of stream Main-3 in m^3 hr^{-1} and converting it to L s^{-1}. The volumetric flow rate $\dot{V}_{\text{Main-3}}$ is retrieved from Aspen Plus. The calculated volumetric flow rate in L s^{-1} is used later on for the equipment cost calculations. The separator is assumed to be 100 % efficient at removing the H_2 and is assumed to allow no liquid or solid in the gas outlet. Both are important assumptions, especially for Aspen Plus. Any gas left in the slurry streams causes errors with modelling the filters in Aspen Plus.

$$\dot{V}_{\text{separator}} = \frac{\dot{V}_{\text{Main-3}} \cdot 1000}{3600} \tag{5.11}$$

5.2.4. Hydrocyclone

The hydrocyclone is used for bulk separation of the liquid from the solid in the slurry. Two important parameters need to be specified: the fraction of solids to the solid outlet and the liquid load of the solid outlet. Zeng et al. state that around 93 % of solids flows to the solid outlet in the case of hydrocyclone separation for microplastics.[84] Acharya & Ives use a hydrocyclone for removing particulates from a scrubber solution. The hydrocyclone removes approximately 90 % of the particulates greater that 30 μm.[85] Therefore, a value of 0.9 is assumed for the fraction of solids to the solid outlet. For the liquid load of the solid outlet, Mohanty et al. mention that 42.6 % of the incoming water flows to the underflow.[86] The underflow is the stream to which the bulk of the solid flows. The specific case of Mahanty et al. is for the dewatering of silica sand. Svarovsky et al. state that the solids concentration of the underflow of hydrocyclones rarely exceeds 45 to 50 % by volume.[87] Therefore, a value of 0.45 is assumed for the liquid load of the solid outlet. The pressure is assumed to be 1 atm and no temperature across the hydrocyclone are assumed.

The size calculation of the hydrocyclone is, just as for the three phase separator, based on the volumetric flow rate of the incoming process stream. In the case of the hydrocyclone, the incoming stream is Main-4. The volumetric flow rate of Main-4 is in m^3 hr^{-1} and is converted to L s^{-1} in Equation 5.12.

$$\dot{V}_{\text{hydrocyclone}} = \frac{\dot{V}_{\text{Main-4}} \cdot 1000}{3600} \tag{5.12}$$

5.2.5. Rotary Vacuum Drum Filter 1 & 2

Rotary vacuum drum filter 1 is used as an additional liquid removal step after the hydrocyclone. The second filter is necessary to remove as much of the liquid added in the washer. For both filters, two parameters are important for the design: the liquid load of the solid outlet and the fraction of solids to the solid outlet. The liquid load of the solid outlet is set to 0.25, so 25 %. Values for the liquid load typically vary between 20 and 45 % for similar filters.[88] The fraction of solids to the solid outlet is set to 0.9, so 90 %. The fraction of solids to the solid outlet is a high number and is close to what rotary vacuum drum filters can achieve in reality. The temperature change over the filters is assumed to be 0 °C and the operating pressure is 1 atm.

The filters are sized by calculating the required filter area in m^2. For filter 1, Equation 5.13 is used and for filter 2, Equation 5.14 is used. The mass flow of the removed liquid stream is retrieved from Aspen Plus. The mass flow of the removed liquid is divided by the filtration rate $\dot{F}$ of the filter and the submergence rate ι. The submergence rate accounts for the fraction of the filter area that is actually submerged and is taking part in the filtration. The filtration rate is equal 73.24 kg m^{-2} hr^{-1}. The value of the filtration rate is based on filtration rate literature, specifically the value for calcium carbonate.[89] The submergence factor is set to 0.5, which is a design choice.

$$A_{\text{filter1}} = \frac{\dot{m}_{\text{Waste-2}}}{\dot{F} \cdot \iota} \tag{5.13}$$

$$A_{\text{filter2}} = \frac{\dot{m}_{\text{Waste-4}}}{\dot{F} \cdot \iota} \tag{5.14}$$

5.2.6. Washer

The washer is implemented to remove as much of the leftover acid as possible. The amount of water added is set equal to the mass flow rate of the CNF Feed. The amount of water to be added is determined by trial and error and it appeared that about 75 % of the leftover acid is removed. The liquid to solid mass ratio of the solid outlet of the washer is set to 0.3, which is a realistic value in the case of a carbon solid. The mixing efficiency is 0.9, so 90 %.

The size calculation of the washer is based on the volumetric flow rate of the incoming process stream. In the case of the washer, the incoming stream is Main-6. The volumetric flow rate of Main-6 is in $m^3\ hr^{-1}$ and is converted to $L\ s^{-1}$ in Equation 5.15.

$$\dot{V}_{\text{washer}} = \frac{\dot{V}_{\text{Main-6}} \cdot 1000}{3600} \tag{5.15}$$

5.2.7. Slurry heater

The slurry heater is a scraped surface heat exchanger. The slurry heater heats the slurry up to 100 °C and provides the latent heat of vaporisation for the water. It is sized using the LMTD method. The heat duty is retrieved from Aspen Plus. The retrieved value is very similar to calculating the heat duty using Equation 5.16. The sensible heat required to heat the slurry to 100 °C is calculated for the solid and the liquid in the slurry. Where $\dot{n}$ is the flow in $kmol\ hr^{-1}$ and c_p is the heat capacity in $kJ\ kmol^{-1}\ K^{-1}$. The latent heat is calculated by multiplying the latent heat of vaporisation, λ_{latent}, with the mass flow of the liquid in the slurry. Adding the total sensible and latent heat together and dividing by 3600 gives the total heat duty in kW. The latent heat of vaporisation of water is equal to 2260 $kJ\ kg^{-1}$.

$$\dot{Q} = \frac{\dot{n}_{\text{solid}} \cdot c_{p,\text{solid}} \cdot (T_{\text{Main-9}} - T_{\text{Main-8}}) + \dot{n}_{\text{liquid}} \cdot c_{p,\text{liquid}} \cdot (T_{\text{Main-9}} - T_{\text{Main-8}}) + \lambda_{\text{latent}} \cdot \dot{m}_{\text{liquid}}}{3600} \tag{5.16}$$

Equations 5.17 through 5.20 provide the LMTD calculations of the slurry heater, where the area of the slurry heater in m^2 is calculated. The overall heat transfer coefficient $U_{\text{slurry heater}}$ of the slurry heater is equal to 100 $W\ m^{-2}\ K^{-1}$, which is based on literature by Mujumdar.[90]

$$\Delta T_{1,\text{ slurry heater}} = T_{\text{Steam-5}} - T_{\text{Main-8}} \tag{5.17}$$

$$\Delta T_{2,\text{ slurry heater}} = T_{\text{Steam-6}} - T_{\text{Main-9}} \tag{5.18}$$

$$\Delta T_{\text{lm,slurry heater}} = \frac{\Delta T_{1,\text{ slurry heater}} - \Delta T_{2,\text{ slurry heater}}}{\log \frac{\Delta T_{1,\text{ slurry heater}}}{\Delta T_{2,\text{ slurry heater}}}} \tag{5.19}$$

$$A_{\text{slurry heater}} = \frac{\dot{Q}_{\text{slurry heater}}}{U_{\text{slurry heater}} \cdot \Delta T_{\text{lm,slurry heater}}} \tag{5.20}$$

5.2.8. Air filter

The sizing of the air filter is based on the volumetric flow of the dry air entering the air filter. It is important to mention that the recycle stream of air is not considered for the calculations. One can also argue that a recycle stream for air is not necesarry, as air is readily available. The flow of dry air that is required is calculated by Equation 5.21 through 5.23. It is very important to note that the dry air required is input for the model and can not be calculated after running the simulation in Aspen Plus. Therefore, the mass flow rate of the slurry entering the slurry heater first has to be estimated. In

Equation 5.21, the mass flow rate of the solid part of the slurry entering the slurry heater is estimated. Through trial and error, the value of $\dot{m}_{\text{Main-8, solid}}$ is determined to be 0.7255 times that of the mass flow rate of the CNF feed $\dot{m}_{\text{CNF feed}}$. In Equation 5.22 the mass flow rate of the liquid part of the slurry entering the slurry heater is estimated. Through trial and error, the value of $\dot{m}_{\text{Main-8, liquid}}$ appears to be 0.25 times $\dot{m}_{\text{Main-8, solid}}$. Then, Equation 5.23 is used to calculate the required mass flow rate of the dry air to carry away all the vapour in the dryer. The mass flow rate $\dot{m}_{\text{Main-8, liquid}}$ is divided by the difference in absolute humidity of the dry air leaving the dryer $\psi_{\text{Air-4}}$ and entering the dryer $\psi_{\text{Air-3}}$. The mass flow rate $\dot{m}_{\text{Main-8, liquid}}$ is then multiplied by a safety factor f_{dryer} to ensure that there is enough air to carry away all the water vapour. The safety factor f_{dryer} is equal to 1.5. The humidity of the dry air leaving the dryer $\psi_{\text{Air-4}}$ is assumed to be equal to 0.05 kg water per kg air. The value of $\psi_{\text{Air-4}}$ is a design variable. The humidity of the dry air entering the dryer is calculated using 5.24. First, the relative humidity (RH) in the Netherlands is on average equal to 0.77.[91] Furthermore, $p_{\text{saturated}}$ is equal to $2.3393 \cdot 10^3$ at 20 °C.[92] Then, p_v is calculated in kPa with Equation 5.25. Finally, p_v is used to calculate $\psi_{\text{Air-3}}$, where p_{atm} is equal to the atmospheric pressure: 101.325 kPa.

$$\dot{m}_{\text{Main-8, solid}} = 0.7255 \cdot \dot{m}_{\text{CNF feed}} \tag{5.21}$$

$$\dot{m}_{\text{Main-8, liquid}} = 0.25 \cdot \dot{m}_{\text{Main-8, solid}} \tag{5.22}$$

$$\dot{m}_{\text{dry air required}} = \frac{\dot{m}_{\text{Main-8, liquid}}}{\psi_{\text{Air-4}} - \psi_{\text{Air-3}}} \cdot f_{\text{dryer}} \tag{5.23}$$

$$\psi_{\text{Air-3}} = 0.622 \cdot \frac{p_v}{p_{atm} - p_v} \tag{5.24}$$

$$p_v = \text{RH} \cdot p_{\text{saturated}} \tag{5.25}$$

The volumetric flow rate of the dry air in m^3 hr is calculated in Equation 5.26 by dividing the required mass flow rate of dry air by its density at 20 °C. The air density is equal to 1.204 kg m^{-3}. The normal volumetric flow rate $\dot{N}_{\text{Air-1}}$ in Nm^3 s^{-1} is calculated using Equation 5.27, where $p_{\text{air normal}}$ is equal to 101.325 kPa and $T_{\text{air normal}}$ is equal to 0 °C.

$$\dot{V}_{\text{Air-1}} = \frac{\dot{m}_{\text{Air-1}}}{\rho_{\text{air}}} \tag{5.26}$$

$$\dot{N}_{\text{Air-1}} = \dot{V}_{\text{Air-1}} \cdot \left(\frac{p_{\text{dry air in}}}{p_{\text{air normal}}}\right) \cdot \left(\frac{T_{\text{air normal}} + 273.15}{T_{\text{Air-1}} + 273.15}\right) \cdot \frac{1}{3600} \tag{5.27}$$

The generated yearly mass of dust waste, $m_{\text{dust yearly}}$, in tonne per year is calculated using Equation 5.28. The dust concentration in the air is equal to $15 \cdot 10^{-9}$ μg m^{-3} and is based on air quality guidelines provided by the World Health Organization.[93] Furthermore, t_{plant} represents the yearly operating hours and the division by 1000 is the conversion from kg to tonne.

$$m_{\text{dust yearly}} = \dot{V}_{\text{Air-1}} \cdot c_{\text{dust}} \cdot t_{\text{plant}} \cdot \frac{1}{1000} \tag{5.28}$$

5.2.9. Air heater

The air heater is modelled as a plate and frame heat exchanger. The air heater is sized by calculating the required area with the LMTD method. The required heating duty of the air heater is retrieved from Aspen Plus, which calculates the duty by using Equation 5.29. Using Equation 5.30 through 5.33 the area of the air heater in m^2 is determined with the LMTD method. The value for the overall heat transfer coefficient $U_{\text{air heater}}$ is equal to 50 W m^{-2} K^{-1}. The overall heat transfer coefficient is based on the heat transfer of steam to air in finned tubes, based on the air side surface area.[94] The value should lie between 30 and 300 W m^{-2} K^{-1}. The specific heat capacity of air is equal to 1 kJ kg^{-1} K^{-1}.

$$\dot{Q}_{\text{air heater}} = \dot{m}_{\text{Air-2}} \cdot c_{p,\text{air}} \cdot (T_{\text{Air-3}} - T_{\text{Air-2}}) \tag{5.29}$$

$$\Delta T_{1,\text{ air heater}} = T_{\text{Steam-7}} - T_{\text{Air-2}} \tag{5.30}$$

$$\Delta T_{2,\text{ air heater}} = T_{\text{Steam-8}} - T_{\text{Air-3}} \tag{5.31}$$

$$\Delta T_{\text{lm,air heater}} = \frac{\Delta T_{1,\text{ air heater}} - \Delta T_{2,\text{ air heater}}}{\log \frac{\Delta T_{1,\text{ air heater}}}{\Delta T_{2,\text{ air heater}}}} \tag{5.32}$$

$$A_{\text{air heater}} = \frac{\dot{Q}_{\text{air heater}}}{U_{\text{air heater}} \cdot \Delta T_{\text{lm, air heater}}} \tag{5.33}$$

5.2.10. Rotary dryer

The rotary dryer is sized by calculating the area with the incoming volumetric flow rate of stream Main-9 and stream Air-3. First, the mass flow in kg hr^{-1} of the incoming CNF, water and acid is retrieved from Aspen Plus. The mass flow of the incoming dry air is also retrieved from Aspen Plus. The mass flows are converted to the volume flows in m^3 hr^{-1} by diving with the density in Equations 5.34 through 5.36. The density of carbon at 100 °C is 2100 kg m^{-3},[95] the density of water at 100 °C is 958 kg m^{-3} and the density of ideal dry air at 100 °C is 1.92 kg m^{-3}.[96] Under the assumption of a 1 hour residence time, the volume of the dryer can be approximated by summing up the volume flows in Equation 5.37. Using the volume of the dryer, the diameter of the dryer in m^2 is calculated in Equation 5.38 using a rearrangement of the equation for the volume of a cylinder. A length over diameter ratio of 5 is applied.[97,98] Finally, the area of the rotary dryer in m^2 is calculated using Equation 5.39.

$$\dot{V}_{\text{Solid, Main-9}} = \frac{\dot{m}_{\text{Solid, Main-9}}}{\rho_{\text{carbon, 100°C}}} \tag{5.34}$$

$$\dot{V}_{\text{Water, Main-9}} = \frac{\dot{m}_{\text{Water, Main-9}}}{\rho_{\text{water, 100°C}}} \tag{5.35}$$

$$\dot{V}_{\text{Air-3}} = \frac{\dot{m}_{\text{Air-3}}}{\rho_{\text{air, 100°C}}} \tag{5.36}$$

$$V_{\text{dryer}} = \dot{V}_{\text{Solid, Main-9}} + \dot{V}_{\text{Water, Main-9}} + \dot{V}_{\text{Air-3}} \tag{5.37}$$

$$D_{\text{dryer}} = \left(\frac{4 \cdot V_{\text{dryer}}}{5 \cdot \pi}\right)^{\frac{1}{3}} \tag{5.38}$$

$$A_{\text{dryer}} = \frac{\pi \cdot D_{\text{dryer}}^2}{4} \tag{5.39}$$

5.2.11. Air condenser

The air condenser is sized based on a simple shell and tube heat exchanger. The first step is to determine the dew point of the incoming air stream Air-4. Through trial and error in Aspen Plus, the dew point is determined to be around 32 °C. The air is cooled indirectly using water at 20 °C. The temperature of stream Air-4 is assumed to be 100 °C, equal to the drying temperature. In reality, the temperature of stream Air-4 could be a bit lower. The mass flow in kg hr^{-1} of stream Air-4 is retrieved from Aspen Plus and is equal to the mass flow of stream Air-3 plus the mass flow of the water and the acid from stream Main-9. The amount of heat to be removed in the condenser is the sensible heat, the latent heat and the heat of dissolution of the acid combined. The sensible heat to be removed in kJ hr^{-1} is calculated in Equations 5.40 through 5.42. The temperatures of stream Air-5 and Waste-6 are assumed to be equal to the dew point of the incoming air. The specific heat capacity of water vapour is equal to 1.9 kJ kg^{-1} K^{-1} and of HCl is equal to 0.8 kJ kg^{-1} K^{-1}.

$$\dot{Q}_{\text{sensible, air}} = \dot{m}_{\text{Air-4, air}} \cdot c_{p,\text{air}} \cdot (T_{\text{Air-4}} - T_{\text{Air-5}}) \tag{5.40}$$

$$\dot{Q}_{\text{sensible, water}} = \dot{m}_{\text{Air-4, water}} \cdot c_{p,\text{water vapour}} \cdot (T_{\text{Air-4}} - T_{\text{Waste-6}}) \tag{5.41}$$

$$\dot{Q}_{\text{sensible, HCl}} = \dot{m}_{\text{Air-4, HCl}} \cdot c_{p,\text{ HCl vapour}} \cdot (T_{\text{Air-4}} - T_{\text{Waste-6}}) \tag{5.42}$$

The heat to be removed for the condensation of water in kJ hr^{-1} is calculated using Equation 5.43. The latent heat of condensation is equal to the latent heat of vaporisation: 2260 kJ kg^{-1}.

$$\dot{Q}_{\text{latent, condenser}} = \lambda_{\text{latent}} \cdot \dot{m}_{Air-4,water} \tag{5.43}$$

The HCl is condensed by the dissolution of the HCl particles into the water. The dissolution of HCl releases heat, which also needs to be removed. The dissolution heat to be removed in kJ hr^{-1} is calculated with Equation 5.44. The heat of dissolution for HCl into water, $\Lambda_{\text{HCL, dissolution}}$, is equal to 2100 kJ kg^{-1}.[99]

$$\dot{Q}_{\text{HCl dissolution}} = \dot{m}_{\text{Air-4, HCl}} \cdot \Lambda_{\text{HCL, dissolution}} \tag{5.44}$$

The total heat to be removed in the condenser in kJ hr^{-1} is calculated with Equation 5.45.

$$\dot{Q}_{\text{condenser}} = \dot{Q}_{\text{sensible, air}} + \dot{Q}_{\text{sensible, HCl}} + \dot{Q}_{\text{latent, condenser}} + \dot{Q}_{\text{HCl dissolution}} \tag{5.45}$$

The required mass flow of the water used for cooling in kg hr^{-1} is calculated using Equation 5.46. The water leaving the condenser through stream Water-8 is assumed to be equal to the dew point temperature minus 5 °C. It is important to note that the specific heat capacity for water is now for water liquid.

$$\dot{m}_{\text{Water-7}} = \frac{\dot{Q}_{\text{condenser}}}{c_{p,\text{water}} \cdot (T_{\text{Water-8}} - T_{\text{Water-7}})} \tag{5.46}$$

Finally, using the LMTD method, the required area of the condenser in m^2 is calculated in Equations 5.47 through 5.50. The overall heat transfer coefficient $U_{\text{condenser}}$ is equal to 50 W m^{-2} K^{-1}. The overall heat transfer coefficient is based on the heat transfer of water to air in finned tubes, based on the air-side surface area.[94] Since the mass flow of the air is much larger, the overall heat transfer coefficient is mainly based on the air in stream Air-4 and not on the water and acid vapour.

$$\Delta T_{1,\text{ condenser}} = T_{\text{Air-4}} - T_{\text{Water-7}} \tag{5.47}$$

$$\Delta T_{2,\text{ condenser}} = T_{\text{Air-5}} - T_{\text{Water-8}} \tag{5.48}$$

$$\Delta T_{\text{lm,condenser}} = \frac{\Delta T_{1,\text{ condenser}} - \Delta T_{2,\text{ condenser}}}{\log \frac{\Delta T_{1,\text{ condenser}}}{\Delta T_{2,\text{ condenser}}}} \tag{5.49}$$

$$A_{\text{condenser}} = \frac{\dot{Q}_{\text{condenser}}}{U_{\text{condenser}} \cdot \Delta T_{\text{lm,condenser}}} \tag{5.50}$$

5.2.12. Water pump

The water pump is sized based on the mass flow of steam required in the process plant. There are three locations in the process plant which require steam: the air heater, the slurry heater and the CSTR. The mass flow of steam required in the CSTR in kg hr^{-1} is determined by using Equation 5.51. The heating duty is retrieved from Aspen Plus. The specific heat capacity of steam is equal to 2010 J kg^{-1} K^{-1}. A factor of 1000 is included to convert kW to W and a multiplication by 3600 to go from seconds to hours. The calculation of the mass flows of steam required for the slurry heater and air heater are similar to that of the CSTR, see Equations 5.52 and 5.53. Finally, using Equation 5.54 the volume flow of the pump in L s^{-1} is calculated. The required mass flows for steam are summed up and divided by 3600 to convert to kg s^{-1}. Further division by the density of water and multiplication with 1000 gives the pump flow in L s^{-1}.

$$\dot{m}_{\text{Steam-2}} = \frac{\dot{Q}_{\text{CSTR}} \cdot 1000}{c_{p,\text{steam}} \cdot (T_{\text{Steam-2}} - T_{\text{Steam-3}})} \cdot 3600 \tag{5.51}$$

$$\dot{m}_{\text{Steam-5}} = \frac{\dot{Q}_{\text{slurry heater}} \cdot 1000}{c_{p,\text{steam}} \cdot (T_{\text{Steam-5}} - T_{\text{Steam-6}})} \cdot 3600 \tag{5.52}$$

$$\dot{m}_{\text{Steam-7}} = \frac{\dot{Q}_{\text{air heater}} \cdot 1000}{c_{p,\text{steam}} \cdot (T_{\text{Steam-7}} - T_{\text{Steam-8}})} \cdot 3600 \tag{5.53}$$

$$\dot{V}_{\text{Water-5}} = \frac{\dot{m}_{\text{Steam-2}} + \dot{m}_{\text{Steam-5}} + \dot{m}_{\text{Steam-7}}}{3600 \cdot \rho_{\text{water 20°C}}} \cdot 1000 \tag{5.54}$$

5.2.13. Steam generator

The steam generator heats up the incoming water and creates steam electrically. The steam generator is sized with the required energy needed to create the steam. First, using Equation 5.55, the difference in enthalpy between steam at 200 °C and water at 20 °C is calculated using thermodynamic data.[96] Then, the required heating duty in kW to create steam at 200 °C is calculated with Equation 5.56. Using Equation 5.57 the energy required in kWh for heating the steam is calculated, where $\eta_{\text{steam generator}}$ is the efficiency of the steam generator, equal to 0.99 (99 %) and t_{plant} is the amount of plant operating hours in a year. Finally, the steam generator rating in MMBtu hr^{-1} is calculated using Equation 5.58.

$$\Delta_h = h_{g,\text{saturated vapour 200°C}} - h_{f,\text{saturated liquid 20°C}} \tag{5.55}$$

$$\dot{Q}_{\text{steam}} = \frac{\Delta_h \cdot (\dot{m}_{\text{Steam-2}} + \dot{m}_{\text{Steam-5}} + \dot{m}_{\text{Steam-7}})}{3600} \tag{5.56}$$

$$E_{\text{electrical}} = \frac{\dot{Q}_{\text{steam}}}{\eta_{\text{steam generator}}} \cdot t_{\text{plant}} \tag{5.57}$$

$$\Upsilon_{\text{electrical}} = \frac{E_{\text{electrical}}}{1,000,000} \cdot 3412.142 \tag{5.58}$$

5.2.14. Total Plant Size Calculations

There are a few output equations that give information on the total plant size. First off is the yearly CNF production, which is calculated with Equation 5.59. The mass flow of the product stream in kg hr^{-1} is multiplied by the yearly operating hours and divided by 1000 to retrieve the CNF production in tonnes per year. The total acid waste in tonnes per year is calculated in a similar manner with Equation 5.60. Finally, the yearly water consumption is calculated with Equation 5.61. Adding up the required volumetric flow rates in the plant and multiplying with the yearly operating hours results in the the water consumption in m^3 per year.

$$P_{\text{CNF}} = \frac{\dot{m}_{\text{Main-10}} \cdot t_{\text{plant}}}{1000} \tag{5.59}$$

$$\dot{m}_{\text{acid waste}} = \frac{(\dot{m}_{\text{Waste-1}} + \dot{m}_{\text{Waste-2}} + \dot{m}_{\text{Waste-3}} + \dot{m}_{\text{Waste-4}} + \dot{m}_{\text{Waste-6}}) \cdot t_{\text{plant}}}{1000} \tag{5.60}$$

$$\dot{V}_{\text{water yearly}} = (\dot{V}_{\text{water, pump}} + \dot{V}_{\text{water, solids cooler}} + \dot{V}_{\text{water, washer}} + \dot{V}_{\text{water, condenser}}) \cdot t_{\text{plant}} \tag{5.61}$$

6

Techno-Economic Calculations

This chapter details the calculations concerning the techno-economics of the process. First, the CAPEX and OPEX calculations are treated, followed by the calculations for the economic evaluation. A class 4 estimate is carried out, which is ±30 % accurate and is based on limited cost data and design detail.[78] The costs of major equipment are calculated for the year 2023, as that is the most recent year for which the CEPCI index could be retrieved.

6.1. Techno-Economic Calculations

6.1.1. CAPEX Calculations

The CAPEX calculations consist of two parts: the calculation of the fixed capital costs and of the working capital. For the fixed capital costs, the first step is to calculate the ISBL costs using the factorial method described by Towler & Sinnott.[78] The total major equipment cost is estimated and other factors, such as piping and electrical, are then estimated as factors of this total major equipment cost. The calculation for the ISBL costs is given in Equation 6.1.[78], where $\sum_{i=1}^{i=M} C_{e,i,\mathrm{CS}}$ represents the sum of the cost of the major equipment with carbon steel material. The sum is then multiplied by the installation factors, which are showed in Table 6.1.

$$\sum_{i=1}^{i=M} C_{e,i,\mathrm{CS}} \cdot ((1 + f_\mathrm{p}) \cdot f_\mathrm{m} + f_\mathrm{er} + f_\mathrm{el} + f_\mathrm{i} + f_\mathrm{c} + f_\mathrm{s} + f_\mathrm{l}) \tag{6.1}$$

Table 6.1: Installation factors for the ISBL cost calculation for a fluids-solids process, as given by Towler & Sinnott.[78]

Parameter	Value	Description
f_p	0.6	Piping
f_m	1	Materials
f_er	0.5	Equipment erection
f_el	0.2	Electrical
f_i	0.3	Instrumentation and control
f_c	0.3	Civil
f_s	0.2	Structures and buildings
f_l	0.1	Lagging, Insulation, or paint

The estimation of the cost of the major equipment is based on available data and correlations. Important for the estimation of major equipment cost are the CEPCI Index, the scaling law and the linear equipment cost curve equation. The CEPCI Index indicates the relative cost over time. Data for the cost of equipment is usually given for a certain year. Therefore, to update the historical data for

the cost in 2023, Equation 6.2 is applied.[78] C_A and C_B represent the cost in year A and B. X_A and X_B represent the CEPCI index in the respective years.

$$C_A = C_B \cdot \frac{X_A}{X_B} \tag{6.2}$$

Equation 6.3 shows the scaling law,[78] which is applied to equipment for which the cost is given at a certain size and the change in size needs to be regarded. C_A is the cost at the size of S_A. C_B is the cost at the size of S_B for the data that is given.

$$C_A = C_B \cdot (\frac{S_A}{S_B})^n \tag{6.3}$$

Equation 6.4 shows the linear equipment cost curve equation, which can also be used to account for a difference in size of the equipment in question.[78] C_e is the cost of the equipment on a U.S. Gulf Coast basis. Cost constants a and b are given per equipment and n is the exponent, also given per equipment type.

$$C_e = a + b \cdot S^n \tag{6.4}$$

Two main sources are used for data and correlations of the major equipment: Towler & Sinnott[78] and Woods[100]. In Towler & Sinnott[78] the data is given for a CEPCI index equal to 532.9, which is in January 2010. The data is inserted in Equation 6.4 to account for the size and Equation 6.2 needs to be applied to then calculate the cost in 2023. In Woods[100] the given FOB cost is for a CEPCI index equal to 1,000. Equation 6.2 and 6.3 are then applied to calculate the cost in 2023 for the actual size of the equipment. The CEPCI index in 2023 is equal to 800.8.[101] For all the major equipment, the following data is used:

- For the rotary solids cooler no correlation or data has been retrieved. Instead data for a rotary dryer is used, as the dryer is the most comparable to the rotary cooler. Towler & Sinnott[78] gives the following data for a rotary dryer: a = 15,500, b = 10,500, n = 0.9 in range of 11 to 180 m^2. For the calculations the minimum value of the range is set to 7 m^2, otherwise for low values of the flow rate, the equation would not work. Using the data below 11 m^2 is still reasonably accurate.
- The reactor is modelled as a continuously stirred tank reactor (CSTR). For a CSTR, the following data applies: a = 61,500, b = 32,500, n = 0.65 in range of 0.5 to 100 m^3.[78] The data is based on a jacketed and agitated reactor.
- To estimate the costs of the three phase separator, data for a preliminary treatment unit is used. For a volumetric flow rate of 58 L s^{-1} the FOB cost is equal to \$270,000. The range is 1 to 10,000 L s^{-1} and n is equal to 0.64.[100]
- To calculate the cost of the hydrocyclone, the following data is used: for a size of 50 L s^{-1}, the FOB cost is equal to \$38,000. The range is 9 to 1300 L s^{-1} with n = 0.35.[100] In the case the size of the hydrocyclone falls below 9 L s^{-1}, the size is set to 9 L s^{-1}. The cost correlation for the hydrocyclone is not accurate below 9 L s^{-1} and setting the value to 9 L s^{-1} is the most accurate in the case of a small size hydrocyclone.
- The cost correlation used for the rotary vacuum drum filters 1 and 2 is that of a vacuum drum filter. For a vacuum drum filter, the following data applies: a = -73,000, b = 93,000, n = 0.3 in range of 10 to 180 m^2.[78] Using a minimum value of 10 m^2 does not always suffice, so a minimum value of 1 m^2 is applied. Even for such a low value, the cost correlation is still quite accurate.
- In order to estimate the washer cost, data for a mixer-settler is used. For a volumetric flow rate of the incoming feed to be treated of 10 L s^{-1}, the FOB cost is equal to \$30,000 with n = 0.60 for a range of 10 to 100 L s^{-1} and n = 0.22 for a range of 1 to 10 L s^{-1}.[100] Using a minimum value of 10 L s^{-1} does not always suffice, so a minimum value of 1 L s^{-1} is applied. Even for such a low value, the cost correlation is still quite accurate. If the size drops below 1 L s^{-1}, it is set to 1 L s^{-1} for the cost calculation.

- To estimate the cost of the slurry heater, data for a floating head shell and tube heat exchanger is used. The following data applies: a = 32,000, b = 70 and n = 1.2 for a range of 10 to 1000 m^2.[78]
- The cost of the dryer is estimated using data for a rotary dryer. For a rotary dryer, the following data applies: a = 15,500, b = 10,500, n = 0.9 in range of 11 to 180 m^2.[78] For the calculations the minimum value of the range is 7 m^2, otherwise for low values of the flow rate, the equation would not work. Using the data for a size below 11 m^2 is still reasonably accurate.
- The air filter cost is calculated using data from Woods.[100] For a size of 10 N m^3 s^{-1} the FOB cost is equal to $82,000. The size range is 2.5 to 30 N m^3 s^{-1} with n is 0.71. If the size of the air filter is below 2.5 N m^3 s^{-1}, it is set to 2.5 N m^3 s^{-1} for the cost calculation. The data is not accurate below 2.5 N m^3 s^{-1}.
- The cost of the dry air heater is estimated using data for a plate & frame heat exchanger. The following data is used: a = 1,600, b = 210, n = 0.95 in range of 1 to 500 m^2.[78]
- The cost of the air condenser is estimated using data for a floating head shell and tube heat exchanger. The following data applies: a = 32,000, b = 70 and n = 1.2 for a range of 10 to 1000 m^2.[78]
- To estimate the cost of the steam generator, the following data applies: a = 0, b = 110,280 and n = 0.627 for a range of the boiler rating of 10 to 250 MMBtu hr^{-1}.[102] The steam boiler data is based on a CEPCI index of 603.10, which is for the year 2018.[101]
- For the cost calculation of the pump, the following data for a single stage centrifugal pump applies: a = 8,000, b = 240 and n = 0.9 for a range of 0.2 to 126 L s^{-1}.[78]

Using the sizing calculations from Section 5.2, the costs are calculated for the equipment using the cost correlations. It is important to first check that the size of each individual piece of equipment falls within the specified range. If it falls below the minimum, then an error occurs and the calculation stops, except for the equipment where exceptions are made. If the value is above the maximum, an extra unit of that equipment type is added in parallel. The size of each of the two units of that equipment type is half of the total required size. If necessary, more units of a piece of equipment are added. The total required size is divided by the required number of units of that piece of equipment.

Following the calculation of the ISBL costs, the fixed capital costs are calculated using Equation 6.5. Where C_{FC} are the fixed capital costs and C_{ISBL} are the ISBL costs. The OSBL costs are calculated as a percentage of the ISBL costs. OSBLs cost are estimated as 40 % of the ISBL costs. According to Towler & Sinnott,[78] 40 % should be used in the case when details of the plant site are unknown. The design and engineering costs are calculated as a percentage of the ISBL plus OSBL costs. Engineering costs are estimated as 25 % of ISBL plus OSBL costs, as is given for a fluids-solids process by Towler and Sinnott.[78] Contingency charges are also calculated as a percentage of the ISBL plus OSBL costs. The minimum number for the contingency estimate, 10 %, is used.[78] Furthermore, a location factor is added to the fixed capital calculation to account for placing the plant in the Netherlands. According to Towler & Sinnott,[78] most data for plant and equipment is given based on U.S. Gulf Coast basis and a location factor of 1.19 should be used because the plant is located in the Netherlands.

$$C_{\mathrm{FC}} = C_{\mathrm{ISBL}} \cdot (1 + F_{\mathrm{OSBL}}) \cdot (1 + F_{\mathrm{D\&E}} + F_{\mathrm{Contingency}}) \cdot L_{\mathrm{F}} \tag{6.5}$$

Table 6.2: Input parameters for the fixed capital cost calculation

Parameter	Value	Description
F_{OSBL}	0.4	Outside Battery Limits Factor
$F_{\mathrm{D\&E}}$	0.25	Design & Engineering Factor
$F_{\mathrm{Contingency}}$	0.1	Contingency Factor
L_F	1.19	Location Factor

The second part of the CAPEX, the working capital, is calculated as a percentage of the ISBL plus OSBL costs. According to Towler & Sinnott,[78] 5 % is low and is used for simple single product processes and 15 % is used for typical petrochemical plants. For this study, the percentage for the working capital is estimated as 10 % of the ISBL plus OSBL costs, in order to be in-between the 5 % and 15 %.

6.1.2. OPEX calculations

The OPEX calculations consist of two parts: the variable production costs and the fixed production costs. First, the variable production cost calculations are discussed, followed by an explanation of the fixed production costs calculations.

Variable production costs

The variable production costs consist of raw material costs, utilities costs and waste disposal costs. The cost of consumables and packaging & shipping is not considered. The cost of raw materials consists of the cost of HCl. The cost of the CNF that goes into the reactor is not considered, as the levelized cost of purification (LCOP) is to be calculated. The cost of 1 metric tonne of HCl is equal to $112.03 as of June 2025.[103] Multiplying the cost of HCl with the yearly HCl consumption in metric tonnes of the plant gives the total raw material cost.

The cost of utilities consists of the cost for electricity and water. The price for dry atmospheric air is assumed to be zero. The water price is calculated by taking the process water price of 0.067 $ per m^3 and accounting for inflation by using the CPI in the Netherlands.[104] The CPI in April 2008 is equal to 90.55 and the CPI in April 2025 is equal to 136.91.[105] Dividing the CPI in 2025 by the CPI in 2008 gives the correction factor. Applying the correction factor gives a water price of 0.10 $ per m^3. Multiplying the price of a utility with the annual consumption of that utility and adding the costs together gives the total cost of utilities. The water used in the acid mixture is already accounted for in the price of the acid. The recycling of water and steam is not considered in the techno-economic calculations. Therefore, the annual consumption of water in the techno-economic calculations is higher than it would be if the recycle is included. The reason is that the cost of water has a small influence compared to the other operational costs and it is easier to calculate the annual consumption without recycle streams. The prices of the utilities are given below.

- Price of electricity: $0.10/kWh.[106]
- Price of water: $0.10/$m^3$.

The waste disposal costs are calculated for the acid waste and for the dust waste. The cost of acid waste is $316/tonne, which is the median cost of hazardous waste management in the Benelux.[107] The cost of dust waste is $20/tonne, which is the median cost of non-hazardous waste management in the Benelux.[107] The total acid waste cost per year is calculated by multiplying the cost of acid waste with the total acid waste in tonnes per year. The total cost of dust waste is calculated in the same manner, by multiplying the cost of dust waste with the total dust waste in tonnes per year.

The variable cost of production (VCOP) is calculated by summing up the cost of raw materials C_{RM}, the cost of utilities C_{U} and the waste costs C_{W}, see Equation 6.6.

$$C_{\mathrm{VCOP}} = C_{\mathrm{RM}} + C_{\mathrm{U}} + C_{\mathrm{W}} \tag{6.6}$$

Fixed production costs

For the fixed production cost, each of its components is treated individually. First off is the cost of operating labour. According to Towler & Sinnott,[78] for a continuous fluids and solids process, there are 3 shift positions plus 1 shift position for every solids handling section. Assuming there are 5 teams to carry out the shifts, that gives Equation 6.7 for the number of required operators $N_{\mathrm{Operators}}$. The N followed by the equipment name means the number of times that equipment type is present in the plant. The number of operators $N_{\mathrm{Operators}}$ is then multiplied in Equation 6.8 by monthly salary W and 12 months to give the yearly operator costs $C_{\mathrm{Operators}}$. The operator salary is equal to €3270,- per month. This is based on various literature on the average operating salary in the Netherlands.[108–111] The operator salary is converted to USD by multiplying with a conversion factor of 1.1779.[112] This leads to

an operator salary of $3850 per month. Next to the operator costs, are the supervision and management costs $C_{\text{S\&M}}$. These are estimated as 25 % of the yearly operator cost, see Equation 6.9.[78] Furthermore, the direct salary overhead costs C_{DSO} are equal to 60 % of the supervision and management costs plus the yearly operator cost, see Equation 6.10.[78] Summing up the yearly operator costs, supervision and management costs and direct salary overhead costs gives the total labour costs C_{Labour}, see Equation 6.11.

$$N_{\text{Operators}} = 5 \cdot (3 + N_{\text{Solids Cooler}} + N_{\text{CSTR}} + N_{\text{Separator}} + N_{\text{Hydrocyclone}} + N_{\text{Filter}} + N_{\text{Washer}} + N_{\text{Slurry Heater}} + N_{\text{Dryer}}) \tag{6.7}$$

$$C_{\text{Operators}} = W \cdot N_{\text{Operators}} \cdot 12 \tag{6.8}$$

$$C_{\text{S\&M}} = 0.25 \cdot C_{\text{Operators}} \tag{6.9}$$

$$C_{\text{DSO}} = 0.6 \cdot (C_{\text{Operators}} + C_{\text{S\&M}}) \tag{6.10}$$

$$C_{\text{Labour}} = C_{\text{Operators}} + C_{\text{S\&M}} + C_{\text{DSO}} \tag{6.11}$$

The maintenance costs $C_{\text{Maintenance}}$, land rent $C_{\text{Land Rent}}$, property taxes $C_{\text{Property Taxes}}$, insurance costs $C_{\text{Insurance}}$ and the costs for environmental charges $C_{\text{Environmental Charges}}$ are calculated using Equations 6.12 through 6.16. The maintenance costs are equal to 5 % of the ISBL costs.[78] The land rent, property taxes, insurance costs and the costs for environmental charges are all equal to 1 % of the ISBL plus OSBL costs.[78]

$$C_{\text{Maintenance}} = 0.05 \cdot C_{\text{ISBL}} \tag{6.12}$$

$$C_{\text{Land Rent}} = 0.01 \cdot C_{\text{ISBL}} \cdot (1 + F_{\text{OSBL}}) \tag{6.13}$$

$$C_{\text{Property Taxes}} = 0.01 \cdot C_{\text{ISBL}} \cdot (1 + F_{\text{OSBL}}) \tag{6.14}$$

$$C_{\text{Insurance}} = 0.01 \cdot C_{\text{ISBL}} \cdot (1 + F_{\text{OSBL}}) \tag{6.15}$$

$$C_{\text{Environmental Charges}} = 0.01 \cdot C_{\text{ISBL}} \cdot (1 + F_{\text{OSBL}}) \tag{6.16}$$

The general plant overhead C_{GPO}, also known as general and administrative cost, is defined as 65 % of the total labour cost.[78] Equation 6.17 illustrates the calculation of the general plant overhead.

$$C_{\text{GPO}} = 0.65 \cdot C_{\text{Labour}} \tag{6.17}$$

The next step is to calculate a preliminary cash cost of production (CCOP) using Equation 6.18. The preliminary CCOP is calculated by adding the VCOP and preliminary fixed production cost C_{PFP} and dividing them by (1 - 0.07), see Equation 6.18. The preliminary fixed product cost is obtained by summing up the labour cost, maintenance cost, land rent, property taxes, insurance cost, environmental charges and general plant overhead.

$$C_{\text{CCOP, preliminary}} = \frac{C_{\text{VCOP}} + C_{\text{PFP}}}{1 - 0.07} \tag{6.18}$$

Using the preliminary CCOP, the research and development costs, selling and marketing costs and costs for patents and royalties are calculated. The research and development costs $C_{\text{R\&D}}$ are estimated as 3 % of the cash cost of production (CCOP) as shown in Equation 6.19. The selling and marketing costs $C_{\text{Sell\&Market}}$ are estimated as 2 % of the CCOP, see Equation 6.20. Finally, costs for patents and royalties $C_{\text{P\&R}}$ are equal to 2 % of the CCOP, see Equation 6.21. Adding the factors together gives 0.07, which is exactly the factor subtracted from 1 to calculate the preliminary CCOP.

$$C_{\text{R\&D}} = 0.03 \cdot C_{\text{CCOP}} \tag{6.19}$$

$$C_{\text{Sell\&Market}} = 0.02 \cdot C_{\text{CCOP}} \tag{6.20}$$

$$C_{\mathrm{P\&R}} = 0.02 \cdot C_{\mathrm{CCOP}} \tag{6.21}$$

The final fixed production cost (FCOP) is obtained by adding the research and development cost, selling and marketing cost and cost for patents and royalties to the preliminary fixed production cost C_{PFP}. The final CCOP is obtained by summing up the FCOP and VCOP.

6.1.3. Revenues

For the CNF purification process, there is only one product: purified CNF. The revenue of the CNF, R_{CNF}, is calculated using Equation 6.22. The CNF production, P_{CNF}, is equal to the yearly CNF output of the process plant. The CNF price, V_{CNF}, is based on the information provided in Section 2.3. The standard selling price assumed for the CNF is \$25,000 per tonne. This is the minimum value of the range provided in Section 2.3. The minimum value is assumed because the purified CNFs are still clustered together in small particles and to make a safe assumption without overestimating the selling price.

$$R_{\mathrm{CNF}} = P_{\mathrm{CNF}} \cdot V_{\mathrm{CNF}} \tag{6.22}$$

6.1.4. Economic Evaluation

The economic evaluation starts with calculating the cash cost of production, capital costs and revenue in each year of the project. Table 6.3 gives an overview of the costs and income per year of the project. From year 5 and onwards, the costs and income per year are constant.

Table 6.3: Calculation of production, cash cost of production, capital cost and revenue in the early stages of the project

Key figures	Year 1	Year 2	Year 3	Year 4	Year 5 and onwards
$P_{\mathbf{CNF}}$	0	0	30 %	70 %	100 %
$C_{\mathbf{CCOP}}$	0	0	100 % FCOP + 30 % VCOP	100 % FCOP + 70 % VCOP	100 % of FCOP and VCOP
$CAPEX$	30 % of C_{FC}	60 % of C_{FC}	10 % C_{FC} + working capital	0	0
$R_{\mathbf{CNF}}$	0	0	$V_{\mathrm{CNF}} \cdot P_{\mathrm{CNF}}$	$V_{\mathrm{CNF}} \cdot P_{\mathrm{CNF}}$	$V_{\mathrm{CNF}} \cdot P_{\mathrm{CNF}}$

For each year, the gross profit, P_{gross}, is calculated using Equation 6.23.[78] Subtracting the depreciation, ξ, from the gross profit gives the taxable income T_{i}, as shown in Equation 6.24. The depreciation is calculated using Equation 6.25. Depreciation is only involved if the gross profit is larger than zero. Using the taxable income, the tax that needs to be paid, T_{p}, can be calculated with Equation 6.26. Note that the tax to be paid is over the taxable income of the previous year $T_{\mathrm{i,\ previous}}$. The tax rate, T_{r} is equal to the Dutch tax rate: 21 %.

$$P_{\mathrm{gross}} = R_{\mathrm{CNF}} - C_{\mathrm{CCOP}} \tag{6.23}$$

$$T_{\mathrm{i}} = P_{\mathrm{gross}} - \xi \tag{6.24}$$

$$\xi = \frac{C_{\mathrm{FC}}}{t_{\mathrm{lifetime}}/2} \tag{6.25}$$

$$T_{\mathrm{p}} = T_{\mathrm{r}} \cdot T_{\mathrm{i,\ previous}} \tag{6.26}$$

The cash flow, CF, for each year of the project is calculated using Equation 6.27. CAPEX is the fixed capital costs plus the working capital. One important factor for the cash flow is that the working capital is retrieved at the end of the project lifetime.

$$CF = P_{\mathrm{gross}} - T_{\mathrm{p}} - \mathrm{CAPEX} \tag{6.27}$$

The NPV is the summation of the present values of future cash flows.[78]. Equation shows 6.28 the calculation of the NPV.[78] $\mathrm{CF_i}$ is the cash flow in year i, I is the interest rate and t is the project lifetime. Using the calculated cash flows in each year of the project, an interest rate of 10 % and a project lifetime of 20 years, the NPV is calculated.

$$\mathrm{NPV} = \sum_{i=1}^{i=t} \frac{CF_i}{(1+I)^i} \tag{6.28}$$

The levelized cost of purification (LCOP) indicates the price to purify a certain amount of produced CNF. First, the discounted CAPEX, discounted OPEX and discounted production are calculated in Equations 6.29, 6.30 and 6.31. The total OPEX in this study is essentially equal to the CCOP. Where t is the time in years and the interest rate I is equal to 10 %.

$$\mathrm{CAPEX_{Discounted}} = \frac{CAPEX_t}{(1+I)^{t+1}} \tag{6.29}$$

$$\mathrm{OPEX_{Discounted}} = \frac{C_{\mathrm{CCOP},t}}{(1+I)^{t+1}} \tag{6.30}$$

$$\mathrm{P_{CNF,Discounted}} = \frac{P_{\mathrm{CNF},t}}{(1+I)^{t+1}} \tag{6.31}$$

The LCOP is then calculated using Equation 6.32. The LCOP is the sum of the discounted OPEX and CAPEX in each year divided by the sum of the discounted production in each year. The LCOP is expressed in $ per tonne.

$$\mathrm{LCOP} = \frac{\sum_{t=1}^{20}(\mathrm{CAPEX_{Discounted}} + \mathrm{OPEX_{Discounted}})}{\sum_{t=1}^{20} P_{\mathrm{CNF,Discounted}}} \tag{6.32}$$

The PBT is calculated using Equation 6.33.[78] The total investment, C_{total}, is divided by the average of the calculated annual cash flows, $CF_{\mathrm{average,\ annual}}$.

$$\mathrm{PBT} = \frac{C_{\mathrm{total}}}{CF_{\mathrm{average,\ annual}}} \tag{6.33}$$

The ROI is calculated using Equation 6.34.[78] The cumulative net profit, $P_{\mathrm{cumulative}}$, is the sum of the cash flow of each year. The initial investment, C_0 is equal to the fixed capital costs and the plant lifetime t_{lifetime} is 20 years.

$$\mathrm{ROI} = \frac{P_{\mathrm{cumulative}}}{t_{\mathrm{lifetime}} \cdot C_0} \tag{6.34}$$

The IRR is calculated to determine the required interest rate in the case the NPV is equal to zero at the end of the project lifetime. By solving Equation 6.35 for I', the IRR is determined.[78]

$$\mathrm{NPV} = \sum_{i=1}^{i=t} \frac{CF_i}{(1+I')^i} = 0 \tag{6.35}$$

7

Process and Model Simulation

This chapter outlines the process simulation flowchart, Aspen Plus setup and the input for the techno-economic and sensitivity analyses. Section 7.1 details the simulation flowchart and explains the additional steps required for certain analysis, such as Monte Carlo. Section 7.2 details the setup of Aspen Plus, including the property method, flow sheet, feed details and more. Section 7.3 details the reactor kinetics for acid leaching of nickel that is used in the model and explain the curve-fitting of the kinetics. Furthermore, Section 7.4 describes the techno-economic and sensitivity analyses and shows the most relevant input of both. The Python code and the relevant Aspen Plus files for the curve-fitting, techno-economic and sensitivity analyses are provided on the following Github page: `https://github.com/Killian2412/MSc-Thesis-CNF-purification-process.git`.

7.1. Simulation Flowchart

Figure 7.1 shows the standard flowchart for the process simulation of the process plant. The simulation starts with specifying the input in Python. Part of the input are specifications for the equipment, the other part are economic specifications such as the buying price of HCl. The relevant input for the equipment is sent to Aspen Plus after which the simulation runs in Aspen Plus. The results from the Aspen Plus simulation are then retrieved in Python. For the equipment of the process plant that is not in the Aspen Plus flow sheet, both the simulation and calculations are conducted with Python. Using both the results from Aspen Plus and the extra equipment simulation with Python, the sizing calculations for the equipment are performed. Following the sizing calculations, all the techno-economic calculations are performed in Python. The final step is the visualisation of the results.

In the case of a Monte Carlo analysis, there is an additional step in-between the fifth and sixth step. The additional step is the change of the economic parameters that are varied in the Monte Carlo analysis. After the additional step, the sizing and techno-economic calculations are performed. Then, the flowchart loops back to the additional step. The calculations are performed for a new sample of values for the economic parameters. After looping n times, the Monte Carlo simulation is finished and the results are visualised. For certain sensitivity analyses, such as the reactor analysis, the first seven steps are looped. Once the loop is finished, the results are once again visualised in Python.

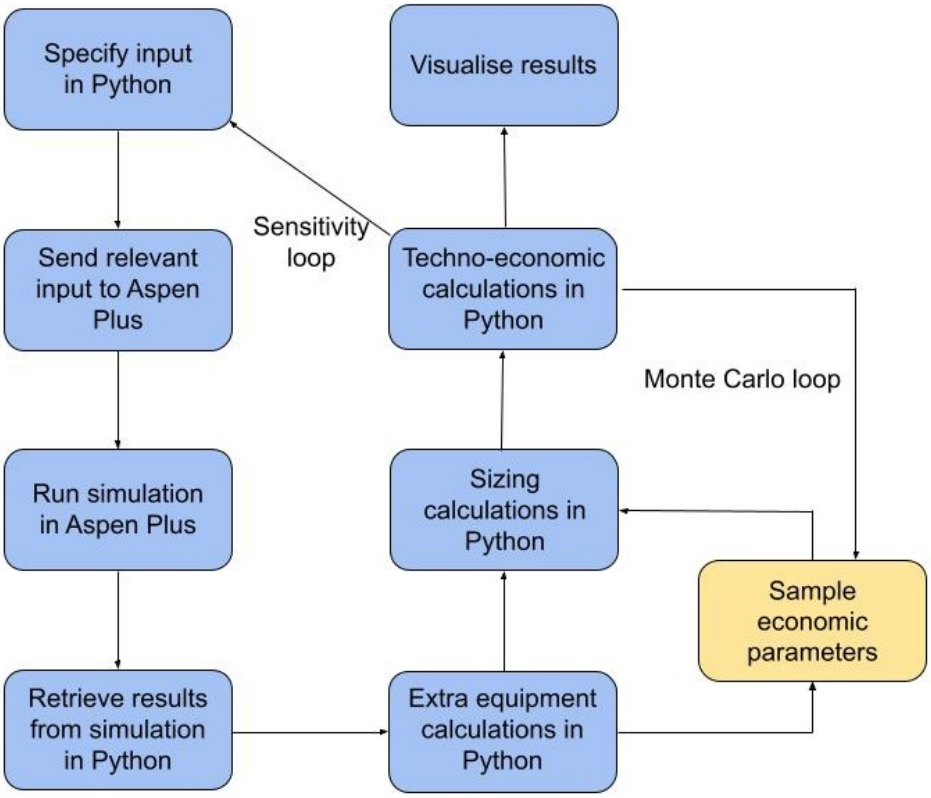

Figure 7.1: Standard flowchart of the process simulation. The simulation begins with specifying input in Python followed by sending the input to Aspen Plus, running Aspen Plus and retrieving results from Aspen Plus. Extra equipment calculations, sizing calculations and techno-economic calculations are carried out with Python. Finally, the results are visualised with Python. In the case of a Monte Carlo analysis, there is an additional step to sample the economic parameters in-between step five and six. Furthermore, the flowchart loops back to the additional step to carry out calculations for a new sample of values for the economic parameters. For certain sensitivity analyses, the first seven steps are looped.

7.2. Aspen Plus Input and Setup

The first important step to correctly set up Aspen Plus is to define all the relevant components, as shown in Figure 7.2. For some components, the type is manually set to solid. This is necessary for the component to be visible when defining a CISOLID substream, something that is treated later on in this section. Other components are left as their standard definition, which is 'Conventional'.

The next step is to define the property method. The property method defined is Aspen Plus is 'ELECNRTL'. The reason is that this property method is one of the best options available for handling complex chemistries with ions. The property method calculates the properties of the components and the streams in the process simulation.

After properly setting up all the properties, the Aspen Plus flow sheet is built, as shown in Figure 7.3. Note that the streams and names in the Aspen Plus flow sheet are not the same as those in the process flow sheet in Figure 5.2. Furthermore, the pump, steam generator and air filter have been left out. The necessary calculations and modelling of the missing equipment are in Python. Furthermore, an extra separator block is added after the second filter. This separator block, 'IONREMOV', removes the ions from the process stream. The ions Ni^{2+} and Cl^{-} cause errors in the dryer, hence they are forcibly removed from the stream. In the real process plant, the ion remover does not exist and therefore the ion remover is not taken into account in the techno-economic calculations.

Component ID	Type	Component name	Alias	CAS number
CARBON	Solid	CARBON-GRAPHITE	C	7440-44-0
H2O	Conventional	WATER	H2O	7732-18-5
HCL	Conventional	HYDROGEN-CHLORIDE	HCL	7647-01-0
SIO2	Solid	SILICON-DIOXIDE	SIO2	14808-60-7
NICL2	Solid	NICKEL-CHLORIDE	NICL2	
H2	Conventional	HYDROGEN	H2	1333-74-0
NI	Solid	NICKEL	NI	7440-02-0
CL-	Conventional	CL-	CL-	
NI++	Conventional	NI++	NI+2	
MG	Solid	MAGNESIUM	MG	7439-95-4
AL	Solid	ALUMINIUM	AL	7429-90-5
FE	Solid	IRON	FE	7439-89-6
CA	Solid	CALCIUM	CA	7440-70-2
AIR	Conventional	AIR	AIR	132259-10-0
SI	Solid	SILICON	SI	7440-21-3

Figure 7.2: Definition of the components for the process simulation in Aspen Plus. The type of the components is for a few manually set to 'Solid'.

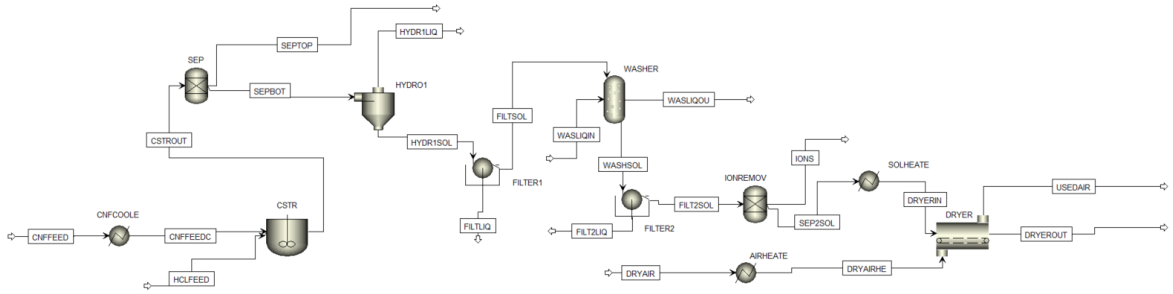

Figure 7.3: Aspen Plus flow sheet of the CNF purification process plant

After defining the process flow sheet in Aspen Plus, all input for the equipment and feed streams is to be specified. The input for the equipment is provided in Section 5.2. The composition of the HCl feed depends on the acid concentration and it is defined in the MIXED tab of the stream in Aspen Plus. In the case of the baseline acid concentration of 2 M, the mass fraction of H_2O is equal to 0.92941 and of HCl to 0.07059. Table 7.1 shows the composition of the CNF feed stream. The CNF feed stream is defined in the CISOLID tab of the stream in Aspen Plus. The composition is based on the results of the analysis of untreated CNF samples in Section 4.1. Only components that appear in both XRF and ICP are considered and the numbers in the composition are based on only the ICP analysis results. The mass flow of the H_2O feed is equal to the CNF feed mass flow and the composition is 100 % H_2O. The dry air mass flow is determined in Section 5.2 and the composition is 100 % air, which represents dry atmospheric air.

Table 7.1: Composition of the CNF feed in Aspen Plus. The components are defined in the CISOLID tab in Aspen Plus and the mass fractions are indicated. The composition is based on the results of the analysis of untreated CNF samples in Section 4.1

Component	Mass Fraction
C	0.994173
Ni	0.0047
Mg	0.000638
Al	0.000133
Fe	$3.3{\cdot}10^{-5}$
Ca	$3.3{\cdot}10^{-5}$
Si	0.00029

The next step is to define the particle size distribution (PSD) of the CISOLID stream in Aspen Plus. A PSD mesh is defined with 0.5 mm as the lower limit and 1.5 mm as the upper limit of the particle size. The mesh assumes equidistant spacing with a total of 10 intervals. The PSD is populated using a normal distribution function with an assumed mean of 1 mm and an assumed standard deviation of 0.1 mm. The size is based on the received CNF samples from the acid leaching experiments in Chapter 4. The PSD can be relevant for solid handling equipment like the hydrocyclone and filters. In this study, the PSD is not as relevant, since the equipment design is not of very high detail and the PSD does not affect the results. If the equipment design is very detailed, the PSD starts to play an important role.

A temperature drop of 0°C is assumed over the hydrocylone and both solid filters. In Aspen Plus either the temperature change, temperature or duty of the outlet flash of the hydrocyclone and filters is to be specified.

7.3. Reactor Kinetics

A very important step in Aspen Plus is to set up the reaction kinetics of the CSTR. The reaction kinetics are based on a study on acid leaching of Ni with hydrochloric acid by Parhi et al.[81] The study contains two important figures: Ni conversion versus residence time at different temperatures and Ni conversion versus residence time at different acid concentrations. The kinetic model that best describes the acid leaching of Ni in the study is the shrinking core model. However, the shrinking core model is not directly available in Aspen Plus as a reaction model for reaction kinetics. Therefore, a different method needs to be applied to correctly implement the reaction kinetics into Aspen Plus. The method that is applied is to curve fit a power law model to Figure 5 and 6 in the study by Parhi et al, and use the results from the curve fit as input for the Aspen Plus power law reaction. The Python code and related Aspen Plus model for curve-fitting the acid leaching kinetics are provided on the following Github page: `https://github.com/Killian2412/MSc-Thesis-CNF-purification-process.git`

The equations used for the curve fit are given in Equation 7.1 through 7.6. In Equation 7.1 the Arrhenius law is applied, where α is the pre-exponential factor, E_a is the activation energy in kJ mol^{-1}, R is the universal gas constant in kJ mol^{-1} K^{-1} and T is the temperature in K. Equation 7.2 describes the calculation of the instantaneous HCl concentration χ_{HCl} in kmol m^{-3} by dividing the number of kmol of HCl, n_{HCl}, by the reactor volume V. The instantaneous concentration of Ni in kmol m^{-3} is calculated in Equation 7.3 by multiplying the initial Ni concentration with $1 - X$. X represents the Ni conversion at a certain time point. Equation 7.4 describes the power law model used to model the kinetics. The rate of reaction is r, which is calculated by multiplying k with the concentration of HCl to the power n and the concentration of Ni to the power m. In Equation 7.5 the Ni conversion rate is described. Equation 7.5 is derived by rewriting $\frac{dn_{\mathrm{Ni}}}{dt} = -n_{\mathrm{Ni,0}} \cdot \frac{dX}{dt} = -r \cdot V$, where $n_{\mathrm{Ni,0}}$ represents the initial concentration of Ni in kmol. The last Equation is 7.6, which describes the rate of change of the HCl concentration in kmol.

$$k = \alpha \cdot \mathrm{e}^{\frac{-E_a}{R \cdot T}} \tag{7.1}$$

$$\chi_{\mathrm{HCl}} = \frac{n_{\mathrm{HCl}}}{V} \tag{7.2}$$

$$\chi_{\mathrm{Ni}} = \chi_{\mathrm{Ni,0}} \cdot (1 - X) \tag{7.3}$$

$$r = k \cdot \chi_{\mathrm{HCl}}^{n} \cdot \chi_{\mathrm{Ni}}^{m} \tag{7.4}$$

$$\frac{dX}{dt} = \frac{V}{n_{\mathrm{Ni,0}}} \cdot r \tag{7.5}$$

$$\frac{dn_{\mathrm{HCl}}}{dt} = -2 \cdot r \cdot V \tag{7.6}$$

The Scipy module in Python is used to perform a non-linear least squares fitting.[113] The Scipy function computes model predictions for a given set of parameters: α, E_a, m and n. The initial values for the set of parameters are: $\alpha = 4{\cdot}10^{-5}$, $E_a = 17$ kJ mol^{-1}, $n = 0.5$ and $m = 1$. The Scipy function then aims to minimize the sum of the squared residuals between $\frac{dX}{dt}$ from the curve fit and $\frac{dX}{dt}$ from the data in Figures 5 and 6 by Parhi et al. The values from the curve fit are: $\alpha = 6.422{\cdot}10^{-1}$, $E_a =$

17.14 kJ mol^{-1}, $n = 0.296$ and $m = 1.178$. The activation energy is very close to the value reported in Parhi et al, which is 17 ±3 kJ mol^{-1}.[81] To test the values of the curve fit, the experimental conditions and set up used by Parhi et al. are mimicked in Aspen Plus with a batch reactor. Parhi et al. uses a 500 mL round bottom flask with the same amount of acid. Per 100 mL of acid, 0.2 g of catalyst sample is added. Implementing the values into the Aspen Plus power law kinetic reaction for the Aspen Plus batch reactor does however not yield the same results. The reaction is too fast, so too much Ni is converted. The issue is the pre-exponential factor α. It is very likely that the value calculated with the curve fit has different units than the value should have in Aspen Plus, s^{-1}. To correctly implement the kinetics into Aspen Plus, the pre-exponential factor is curve fitted again. The curve fitting is now conducted with the help of Aspen Plus. The values for E_a, n and m are held constant and only the 353 K line of Figure 6 in Parhi et al is considered, as the fit yields the most accurate results for that line. The pre-exponential factor α, which is indicated with the symbol k in Aspen Plus and not to be confused with the k from Equation 7.1, is varied. For every value of k, an Aspen Plus simulation is run to test if the fit yields the same results as the experimental data. For each k value, the Ni conversion is calculated. Using the Scipy package, the value of k is fitted with the differential evolution method. The differential evolution method uses a stochastic algorithm to find the best fit for k. The best value for k found by the differential evolution method is $7.8771 \cdot 10^{-5}$. The value for k is then implemented in the reaction kinetics in Aspen Plus. Afterwards, the conversion versus time graphs at different temperatures and acid concentrations are constructed. In Figure 7.4 the conversion is plotted versus time at different temperatures for both the data from Parhi et al[81] and the curve fit with the power law model. In Figure 7.5 the conversion is plotted versus time at different acid concentrations, also for both the data from Parhi et al[81] and the curve fit with the power law model. The curve fit is accurate for the higher temperatures, 323 K and higher. The curve fit is also more accurate for the higher acid concentrations of 1 M and 2 M. For the lower temperatures and acid concentrations, the accuracy of the curve fit decreases a lot, with values of R^2 below 0.7.

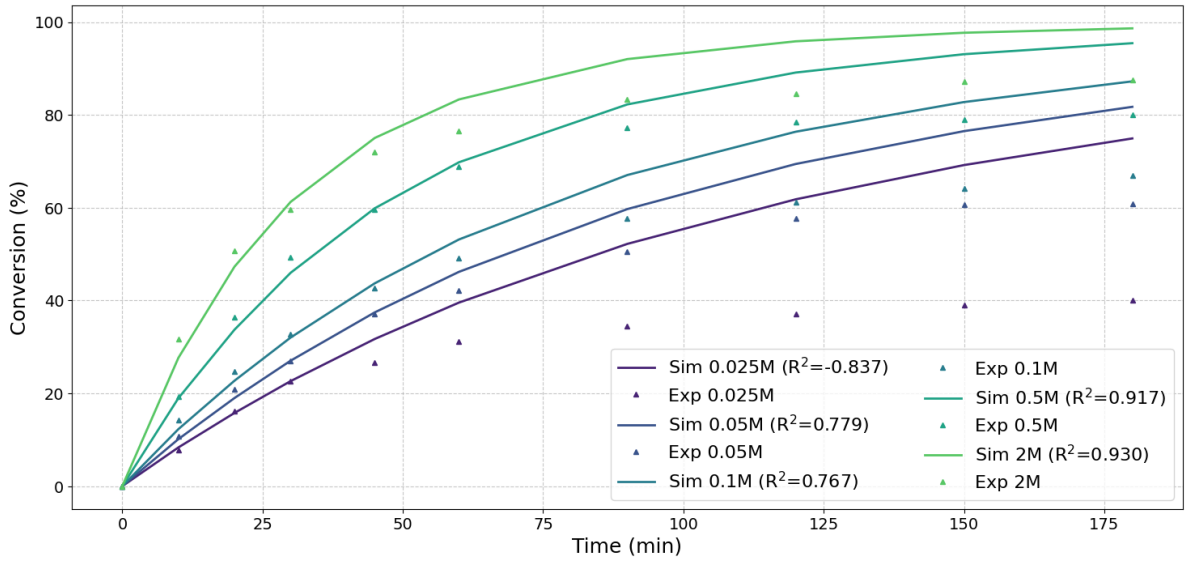

Figure 7.4: Curve fits of Ni acid leaching kinetics using the power law model and only Python for curve fitting. The conversion is plotted against the time at various temperatures for both the datapoints from literature by Parhi et al[81], and for the power law model. The power law data is represented by lines, the data from literature by dots. The acid concentration is 1 M. $k = 7.8771 \cdot 10^{-5}$, $E_a = 17.14$ kJ mol^{-1}, $n = 0.296$ and $m = 1.178$.

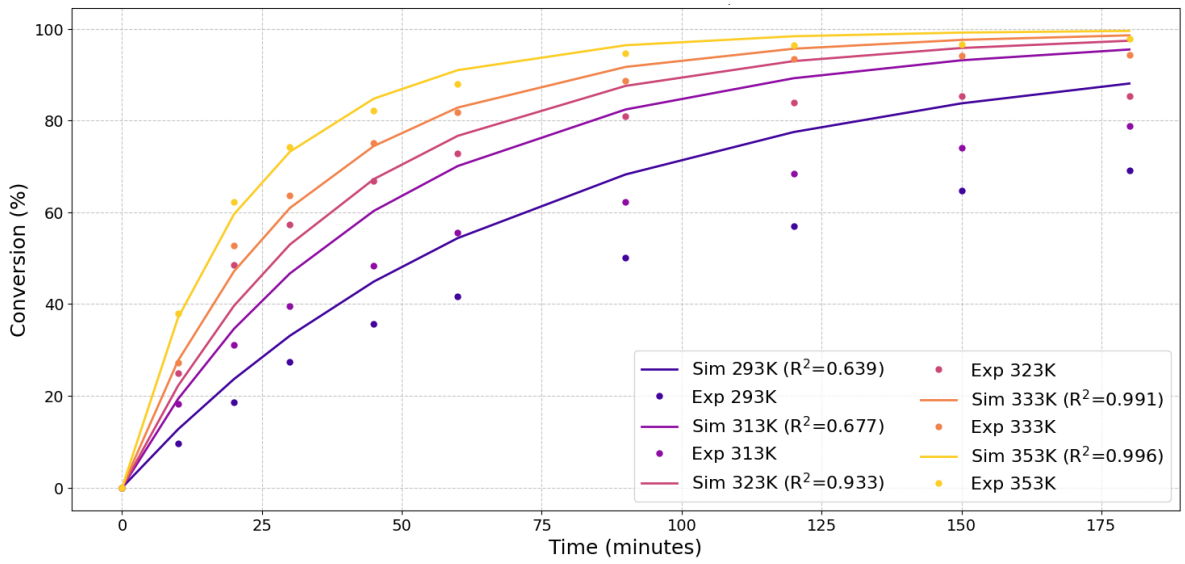

Figure 7.5: Curve fits of Ni acid leaching kinetics using the power law model and refitting in Aspen Plus. The conversion is plotted against the time at various HCl concentrations for both the datapoints from literature by Parhi et al[81], and for the power law model. The power law data is represented by lines, the data from literature by dots. The temperature is 323 K. $k = 7.8771 \cdot 10^{-5}$, $E_a = 17.14$ kJ mol^{-1}, $n = 0.296$ and $m = 1.178$.

In Figure 7.6 the conversion rate is plotted versus time for both the data from Parhi et al[81] and the curve fit with the power law model. As the time increases, the conversion rate decreases. The decrease of the conversion rate is logical, as both the Ni concentration and HCl concentration also decrease with time. The effect is a lower reaction rate r and therefore also a lower conversion rate.

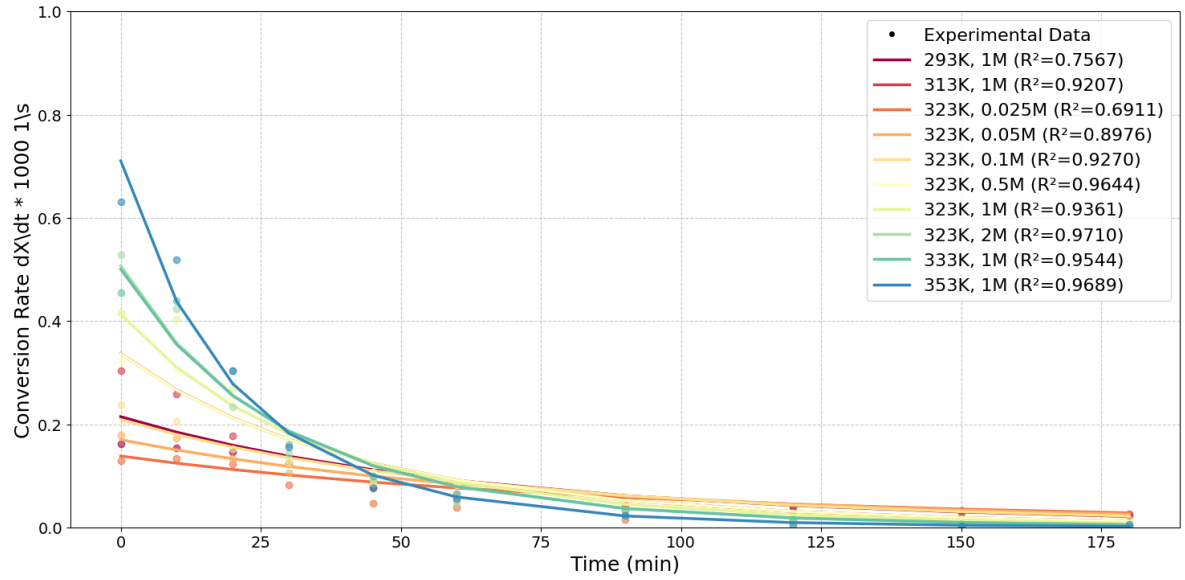

Figure 7.6: Conversion rate versus time (dX/dt) for both the data from Parhi et al[81] and the curve fit with the power law model. The power law data is represented by lines, the data from literature by dots. The conversion rate decreases with time.

7.4. Techno-economic Baseline and Sensitivity Analyses

7.4.1. Techno-economic Baseline Scenario

The baseline scenario is the standard scenario of the CNF purification process plant. The techno-economic analysis of the baseline scenario provides an overview of the techno-economics of the conceptual process plant. An important part of the baseline scenario is the input. Most of the input for the process plant and for the techno-economics is already given in Chapters 5 and 6. The Python code and the related Aspen Plus model for the techno-economic analysis are provided on the following Github page: `https://github.com/Killian2412/MSc-Thesis-CNF-purification-process.git`.

One of the most important parameters is the mass flow rate of the CNF feed. The mass flow rate of the CNF feed ultimately determines the total plant production capacity. The production capacity is based on the CNF market in 2020, which was expected to be 100,000 tonnes.[59] A production capacity that does not overload the market, but still allows the process plant to play a significant role on the CNF market is desired. Therefore, a baseline production capacity of 20,000 tonnes per year is assumed. In the case of 8000 operating hours per year, that equals an output mass flow rate of 2500 kg hr^{-1}. To achieve the desired output mass flow rate, the mass flow rate of the CNF feed has to be equal 3470 kg hr^{-1}. Table 7.2 gives an overview of the input for the baseline scenario. It is important to note for the baseline scenario that the best experimental conditions from Parhi et al[81] are retrieved and used as input for the reactor.

Table 7.2: The input for the baseline scenario of the CNF purification plant. This does not contain all of the input for the process plant.

Parameter	Value	Units	Source
CNF production	20,000	tonne/year	
CNF feed mass flow	3470	kg hr^{-1}	
CSTR temperature	80	°C	
CSTR residence time	3	hours	
Acid feed concentration	2	M	
Plant hours per year	8000	hours	
Project lifetime	20	years	
Acid waste price	316	$/tonne	[107]
Dust waste price	20	$/tonne	[107]
Electricity price	0.10	$/kWh	[106]
Water price	0.10	$/$m^3$	[104, 105]
Dry air price	0	$/$m^3$	
Operator salary	3850	$/month	[108–111]
Interest rate	10	%	
HCl price	112.03	$/tonne	[103]
CNF selling price	25,000	$/tonne	[59]
Tax rate	21	%	

The required outputs of the baseline scenario analysis are the NPV, LCOP, PBT, ROI and IRR. The economic parameters determine the economic viability of the process plant. Furthermore, an overview of the capital costs, VCOP and FCOP is desired. The effectiveness of the nickel removal and the final product composition are also important required outputs to help determine the viability of the process.

7.4.2. Sensitivity Analyses

To study the robustness of the process design and how various parameters influence the design and the economic viability, multiple sensitivity analyses are conducted. The python code for the sensitivity analyses and the related Aspen Plus model are supplied on the following Github page: `https://github.com/Killian2412/MSc-Thesis-CNF-purification-process.git`.

First off, a Monte Carlo analysis is conducted to determine how robust the process design is.[114] For each of the most important economic parameters, a Gaussian distribution is determined. Then, for each parameter a value is randomly selected from its respective probability distribution. Using the randomly selected values, the simulation is run in Python and the LCOP is calculated and stored. This process

repeats itself 1,000,000 times. Table 7.3 shows the economic parameters, their mean and the standard deviation (STD). The standard deviation of the electricity price is set to 0.0233 $/kWh and is based on the graph on the electricity price of EUENERGY.[106] The standard deviation of the water price is an estimate. For the operator salary, 99.7 % of the values are assumed to fall within 20 % of the mean. This leads to a standard deviation of 255 $/month. The standard deviation of the interest rate is based on the maximum value of 15 % for large projects.[78] Hence the standard deviation of the interest rate becomes 1.67. For the HCl price, graphs show that the price since May 2022 lies in-between 80 and 180 $/tonne.[103] Based on that, 3σ is set equal to 50 and the standard deviation becomes 16.67 $/tonne. The standard deviation of the project lifetime is 5 and is an assumption. Another assumption is made for the standard deviation of the operating hours per year, which is set to 250. The standard deviation of the acid waste price is 40 $/tonne and is also an assumption. The variance factors of the fixed capital costs and fixed production costs represent a multiplication with the respective costs. The standard deviations of the fixed capital and fixed production costs are based on the maximum and minimum literature values of the parameters that influence the respective costs. Hence, 99.7 % of the values for the fixed capital and fixed production cost lie within the minimum and maximum bounds provided by literature.

Table 7.3: The Monte Carlo parameters with their mean and standard deviation (STD) for a Gaussian distribution.

Parameter	**Mean**	**STD**	**Units**	**Source**
Electricity price	0.10	0.0233	$/kWh	[106]
Water price	0.10	0.03	$/m^3	[104]
Operator salary	3850	255	$/month	[108–111]
Interest rate	10	1.67	%	[78]
HCl price	112.03	16.67	$/tonne	[103]
Project lifetime	20	5	years	
Operating hours per year	8000	250	hours	
Acid waste price	316	40	$/tonne	[107]
Fixed capital costs variance factor	1	0.1		[78]
Fixed production costs variance factor	1	0.05		[78]

Next to the Monte Carlo analysis, a tornado plot is created for the impact of economic parameters on the LCOP. For each of the economic parameters from the Monte Carlo analysis, the value is varied with +50 % and -50 %, while holding the other parameters constant. While doing so, the LCOP is calculated. This shows which of the economic parameters has the largest impact on the LCOP in the form of a tornado plot.

The effect of the CNF feed mass flow rate, reactor temperature and reactor residence time on the LCOP is determined. For each of these parameters, their value is varied and the subsequent LCOP at each value is calculated. Only one parameter is varied at a time. The values used for the CNF feed mass flow rate are: 1500 to 20000 kg hr^{-1} in 38 steps. For the reactor temperature: 30 to 100 °C in 15 steps. And finally for the residence time: 1 to 24 hours in 24 steps.

Another sensitivity analysis is to study the effect of the reactor temperature, reactor residence time, reactor pressure, nickel mass fraction in the CNF feed and acid concentration in the acid feed on the reactor conversion. For each of the parameters, their value is varied and the subsequent reactor conversion is retrieved from Aspen Plus. Only one parameter is varied at a time. The values used for the reactor temperature are 50 to 100 °C in 51 steps. For the residence time of the reactor: 0.1 to 24 hours in 240 steps. For the reactor pressure: 1 to 50 atm in 50 steps. The Ni mass fraction in the CNF feed is varied from 0.001 to 0.20 in 200 steps. Finally, the acid concentration is varied from a mass fraction of 0.01 to 0.5 in 60 steps.

The effect of the CNF selling price on the IRR, ROI, PBT and NPV is also to be determined. The CNF selling price is varied from 10 to 113 $/kg in 104 steps. In addition, the effect of the interest rate and project lifetime on the NPV is determined. Five different values for the lifetime are used: 10, 15, 20, 25 and 30 years. For each value of the lifetime, the interest rate is varied between 5 and 100 % in 20 steps.

8

Research Results and Discussion

This chapter shows and discusses the results of the techno-economic and sensitivity analyses. First, the baseline scenario is discussed in Section 8.1, followed by a description of the sensitivity analyses in Section 8.2. The following sensitivity analyses are conducted: sensitivity analysis of various parameters on the economic outcome, reactor volume analysis, reactor conversion analysis, tornado plot and finally a Monte Carlo analysis. After the sensitivity analyses, the improved process design cases are shown and discussed in Section 8.3.

8.1. Baseline Scenario

The baseline scenario is based on the process design in Chapter 5, the techno-economic framework in Chapter 6 and the input as described in Section 7.4.1. The results for the the equipment sizes are shown in Appendix B and for the process streams in Appendix C.

The first set of results are the main economic parameters, see Table 8.1. The LCOP of CNF is equal to 10.09 $/kg, which is a realistic result. The range of the selling price is 25 to 113 $/kg, therefore there is still plenty of margin. The much higher selling price, set to 25 $/kg for the baseline scenario, also explains the very high values for the ROI and IRR: 467.95 % and 185.10 % respectively. The high selling price also leads to a very low PBT of 0.20 years and a high NPV of 1.48 billion $. The main economic parameters show a very profitable process, but that is mainly due to the high selling price. It is very important to note that the selling price is now based on the lowest value of a range provided in literature by Dagle et al.[59]

Table 8.1: The output of the main economic parameters for the baseline scenario of the CNF purification plant.

Parameter	Value	Units
LCOP	10.09	$/kg
ROI	467.95	%
IRR	185.10	%
PBT	0.20	years
NPV	1,482,232,825	$

It is also important to consider the purity of the final CNF product and the remaining Ni content. The purity of the final CNF product is 99.47 wt%, which is very high and could lead to an even higher selling price already used in the baseline scenario. Literature mentioned in Section 2.3 also indicates that a higher purity is beneficial to the selling price. The remaining Ni content in the CNF product is equal to 4460 ppm or 0.446 wt%, which indicates a conversion of only 5.15 %. The remaining Ni content is much too high. The Ni content should not be higher than 300 ppm, as mentioned in Section 2.3. Furthermore, a conversion of 5.15 % is very low and hence the acid leaching is not effective at all in the baseline scenario. Because of the remaining Ni content, the selling price of 25 $/kg also becomes unrealistic. It is not known what a realistic selling price would be instead, but using the

baseline scenario is not advised. Since only 5.15 % of Ni is removed, the quality of the product is barely improved and therefore its selling price is also barely improved.

The question arises what the cause of the low conversion of Ni is. The literature by Parhi et al.[81] shows conversions up to 80 to 90 %. The conversion was achieved by acid leaching of a catalyst with an initial Ni content of 12.75 wt%. However, in this study, CNF with an initial Ni content of only 0.47 wt% is to be purified. The kinetic model described in Section 7.3 indicates a large influence of the Ni content on the reaction rate. This helps explain the lower conversion due to the lower nickel content in the baseline scenario. Furthermore, in Parhi et al,[81] 100 mL of acid is used per 0.2 g of sample. In this study, only 10 mL per 1 g is used, which is much less acid per sample. If the initial Ni content of the CNF feed is set to 12.75 wt%, the Ni conversion still only reaches 9.65 %. If on top of increasing the Ni content the same acid to sample ratio is applied as in Parhi et al, the Ni conversion reaches 80 %, which is similar to the findings of Parhi et al. However, using such a high acid to sample ratio is not practical and leads to excessive acid feed costs. In that case, the process plant is not profitable anymore.

However, there is still a chance that the baseline scenario is effective for the removal of nickel from the CNF. The results of the preliminary acid leaching experiments in Section 4.3 show an average conversion of 70.3 %, with conversion as high as 83.0 %. The highest conversion is achieved with a temperature of 70 °C, a 4 hour residence time, 550 rpm stirring speed, 1 mL of acid for 0.25 g of CNF sample, a 4 M H_2SO_4 solution and 40 % sonication. The results of the preliminary experiments give a much more positive outlook for the baseline scenario. A limitation is that the preliminary experiments have only been conducted with a H_2SO_4 solution so far. Conducting the preliminary experiments with HCl may yield different results. Furthermore, the measured Ni concentration in the original sample of the experiments might not be accurate yet and therefore the measured conversion can not be fully trusted yet.

A possible reason for the difference in Ni conversion between the Aspen Plus model that uses the kinetics from Parhi et al[81] and the acid leaching experiments in our study is the composition of the sample used in the experiments. The study by Parhi et al[81] focused on the leaching of nickel from a Ni–Al_2O_3 spent catalyst, while our acid leaching experiments focus on the leaching of nickel from CNF. The use of the kinetics from Parhi et al[81] can be seen as a limitation of the study. In order to determine the exact reaction kinetics of the leaching of nickel from the CNF with different acids, it is important to continue the acid leaching experiments. The reaction kinetics should then be incorporated in the baseline scenario to provide more accurate results. A limitation of the acid leaching experiments is that the sonication is difficult to implement on an industrial scale. A potential solution is the addition of a crusher before the reactor.

To analyse the baseline scenario in further detail, the costs have to be mapped. Figure 8.1 shows the cost split of the VCOP, fixed capital costs and the FCOP for the baseline scenario. It is remarkable that the VCOP accounts for by far the largest share of the costs. Followed by the VCOP are the fixed capital costs and the FCOP. It is also interesting to see that the fixed capital costs are quite low for the baseline scenario, totalling around 20 million $.

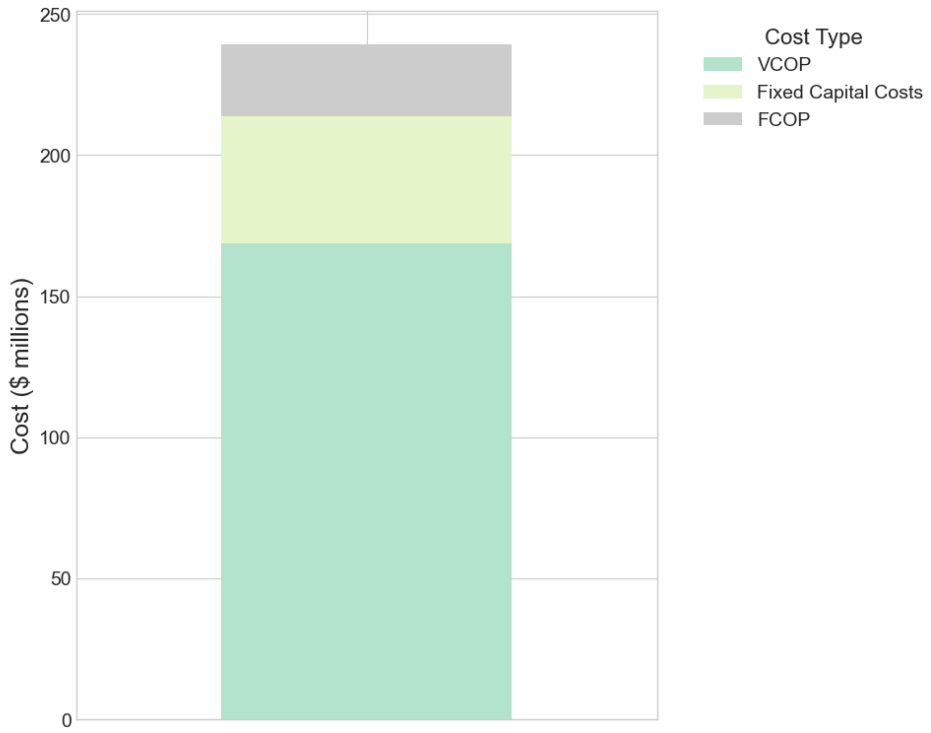

Figure 8.1: Cost split of the VCOP, Fixed Capital Costs and the FCOP for the baseline scenario. The cost is shown in $ millions. The VCOP represents the largest share of the costs, followed by the Fixed Capital Costs and the FCOP.

Figure 8.2 shows the breakdown of the VCOP. The acid waste cost accounts for just over half of the yearly VCOP. Furthermore, the raw material cost, which is the cost of buying the acid, is also quite large. The reason is that for each kg of CNF, 10 L of acid is used in the reactor. This means that if 3470 kg hr^{-1} of CNF is supplied, then 34,700 L hr^{-1} of acid is used. Combine the high use of acid with the acid feed price of $112.03/tonne and the acid waste price of $316/tonne and a high VCOP emerges. The high costs due to the acid consumption show a need for the implementation of an acid recycle to reduce the VCOP. In addition to the acid feed and waste cost, the cost of electricity is also quite significant due to the electricity needed for the steam boiler. The electricity price is not very high, at only $0.10/kWh. Therefore, around 400 million kWh of electricity is used in the baseline scenario. Furthermore, the water and dust waste cost are negligible. The water consumption is not very high in the baseline scenario and the dust waste flow is very low.

Figure 8.3 shows the breakdown of the equipment costs for the baseline scenario. The CSTR, dryer and steam boiler represent the largest share of the total equipment costs. For a reactor, it is quite common to represent a larger share of the equipment costs. The high cost of the dryer and steam generator originate from the final stage of the water removal. A large dryer is required and the steam is mostly required for the slurry heater. Each piece of equipment is only included once, except for the CSTR, of which 2 pieces are required. The reason is the limit of 100 m^3 for a CSTR. The sizes of the equipment are given in Appendix B. A limitation of the equipment cost calculation is that the lower limits for the size ranges of the cost correlations of the following equipment were lowered: solids cooler, filter1 and filter2, washer, dryer. Using a size below the usual range still provided reasonably accurate results for the equipment cost. The new ranges are provided in Chapter 6. In case the size of the hydrocyclone falls below the lower limit of the size range, the size is set to the value lower limit.

Figure 8.4 shows the breakdown of the FCOP for the baseline scenario. The FCOP is well spread across its cost components. The R&D, general and administrative, patents and royalties and selling and marketing costs make up over half of the FCOP. On the other side, the land rent, property taxes, insurance cost and environmental charges make up only a small portion of the FCOP.

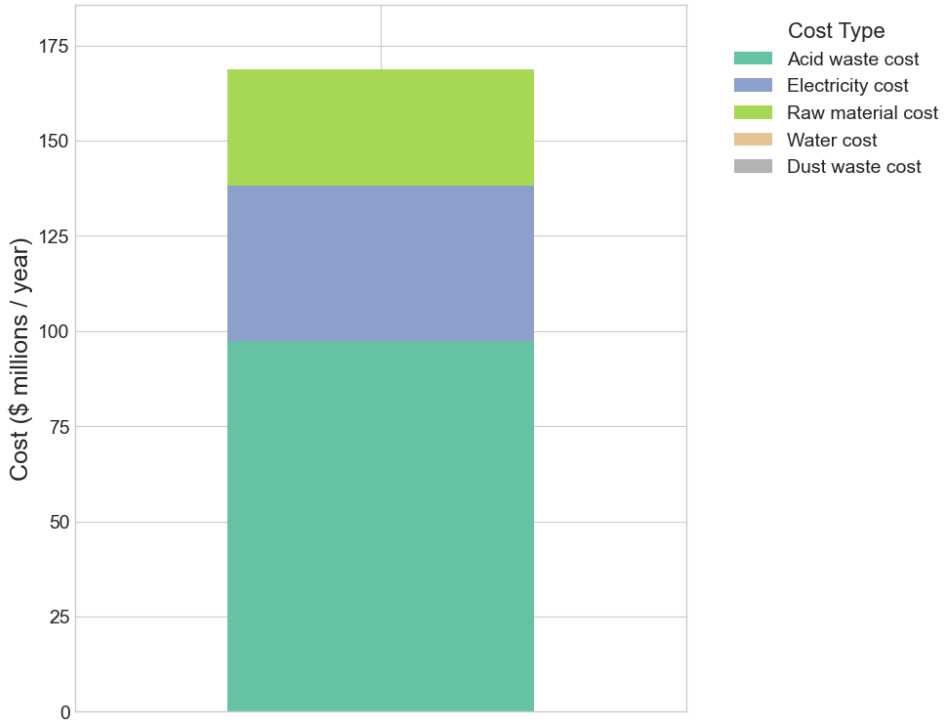

Figure 8.2: VCOP breakdown of the baseline scenario. The raw material cost, which is the cost of buying the acid, and the acid waste cost represent the largest share of the VCOP. Electricity costs are mainly because of the Steam Boiler. The water and dust waste costs are negligible.

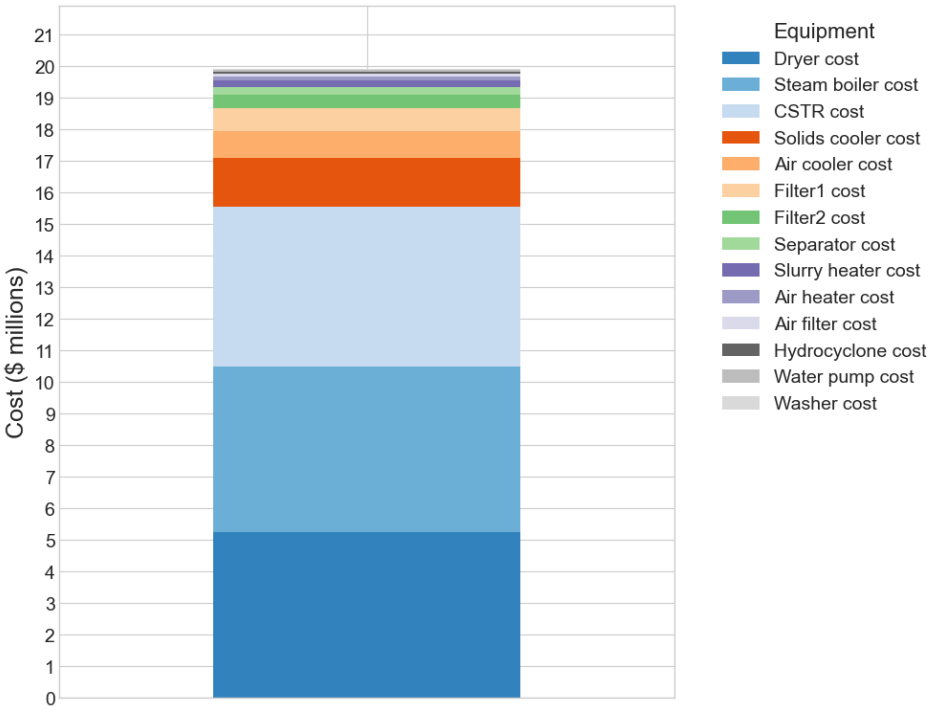

Figure 8.3: Total equipment cost breakdown of the baseline scenario. The CSTR, dryer and steam boiler are the largest share of the capital costs. The ISBL costs are included.

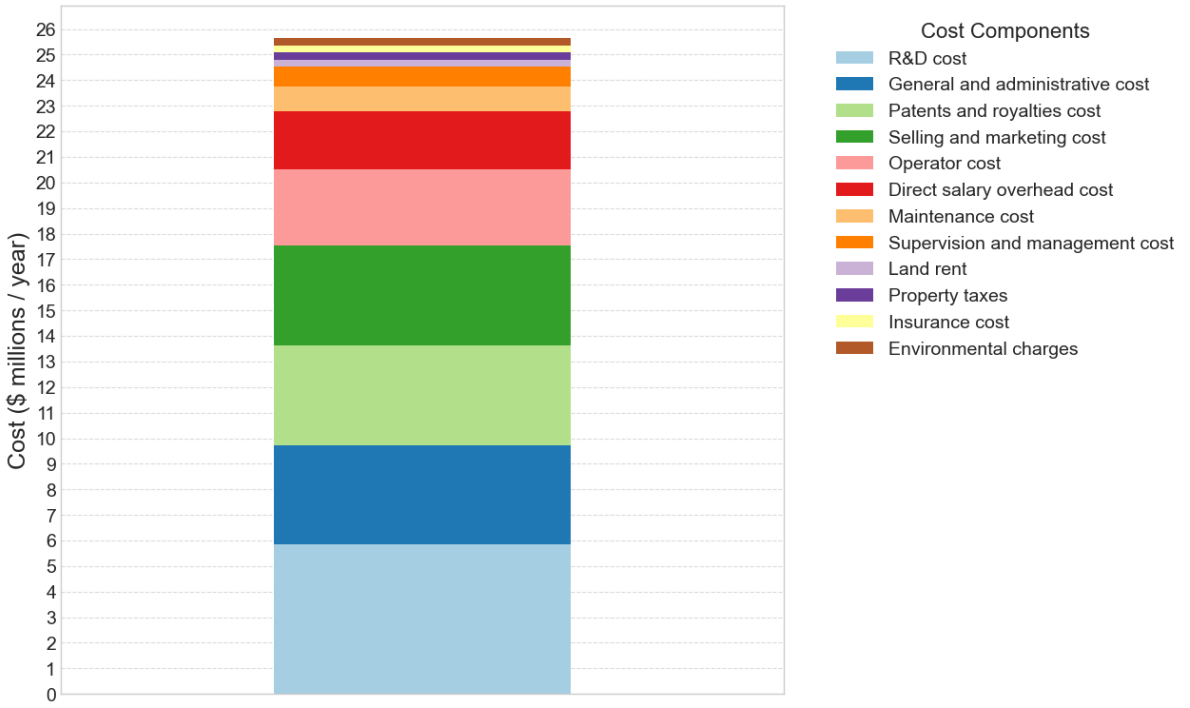

Figure 8.4: FCOP breakdown of the baseline scenario. The FCOP is spread very well across the cost components. The highest costs are for R&D and the lowest are for the environmental charges.

8.2. Sensitivity Analyses

The setup of the sensitivity analyses is described in Section 7.4.2. The goal of the sensitivity analyses is to study the robustness of the baseline scenario and how various parameters influence the design and the economic viability. In Section 8.2.1 the impact of various process design parameters on the economics is analysed. Section 8.2.2 shows the impact of the total reactor volume on the LCOP, CSTR cost and number of reactors. In addition, Section 8.2.3 shows the impact of reactor parameters on the conversion. Section 8.2.4 contains the tornado plot of the impact of economic parameters on the LCOP and Section 8.2.5 contains the results of the Monte Carlo analysis.

8.2.1. Sensitivity Analyses on Economic Output Parameters

The first set of sensitivity analyses is the variation of process parameters to determine the effect on the economics of the baseline scenario. First off, Figure 8.5 shows the effect of the annual CNF production on the LCOP. The CNF production in the baseline scenario is 20 kilotonnes. The results show that increasing the CNF production to above 20 kilotonnes has a positive effect on the LCOP. In the CNF production range of 10 to 30 kilotonnes, the LCOP decreases steeply. After 30 kilotonnes, the LCOP decreases less rapidly until it almost flattens out. The baseline scenario production level of 20 kilotonnes is therefore not the most optimal production level.

Figure 8.6 shows the influence of the interest rate on the NPV at different project lifetimes. The results show that the curve flattens out to 0 for all project lifetimes. A logical effect, as increasing the interest rate leads to a lower NPV value. Once the IRR value is surpassed, the NPV starts to become negative. For longer project lifetimes, the NPV is higher around interest rates between at least 10 to 30 %. It is logical that the NPV is higher for longer projects, as more revenue is generated in the extra years of the lifetime.

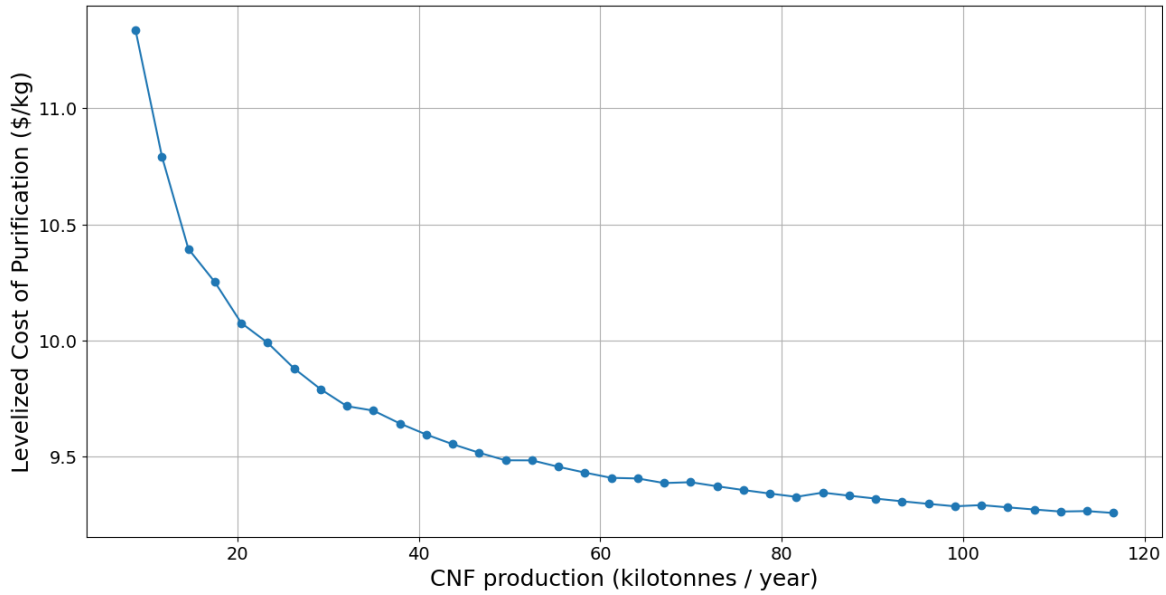

Figure 8.5: Effect of the annual CNF production on the LCOP. As the CNF production increases, the LCOP first decreases steeply and later on almost flattens out.

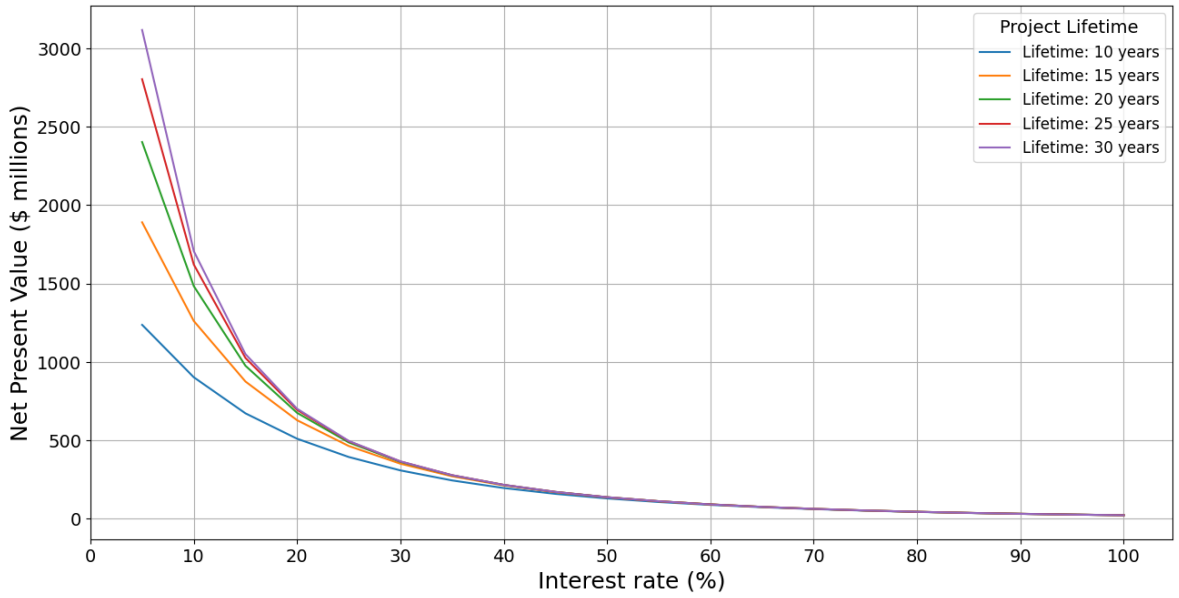

Figure 8.6: Influence of the interest rate on the NPV at different project lifetimes. For longer project lifetimes, the NPV is higher at interest rates between 10 to 30 % because more revenue is generated in the extra years of the lifetime.

Figure 8.7 shows the effect of the CNF selling price on the IRR, ROI, PBT and NPV. Results show that increasing the CNF selling price has a very positive and linear effect on both the NPV and the ROI. The ROI can even become above 2000 % for a selling price above 70 $/kg, which are both very large numbers. The effect of the CNF selling price on the IRR is very positive and becomes linear at increasingly high CNF selling prices. The results show an IRR around 550 % for a selling price of 100 $/kg, which is very high. The interest rate would need to be 550 % for the NPV to be equal to 0. Furthermore, the CNF selling price has a very positive effect on the PBT. The PBT first drops very steeply as the selling price increases and eventually converges to 0 years. The reason for the very positive economic numbers is due to the fact that the LCOP in the baseline scenario is only equal to 10.09 $/kg. The LCOP has a low value compared to the selling prices included in the sensitivity

analysis.

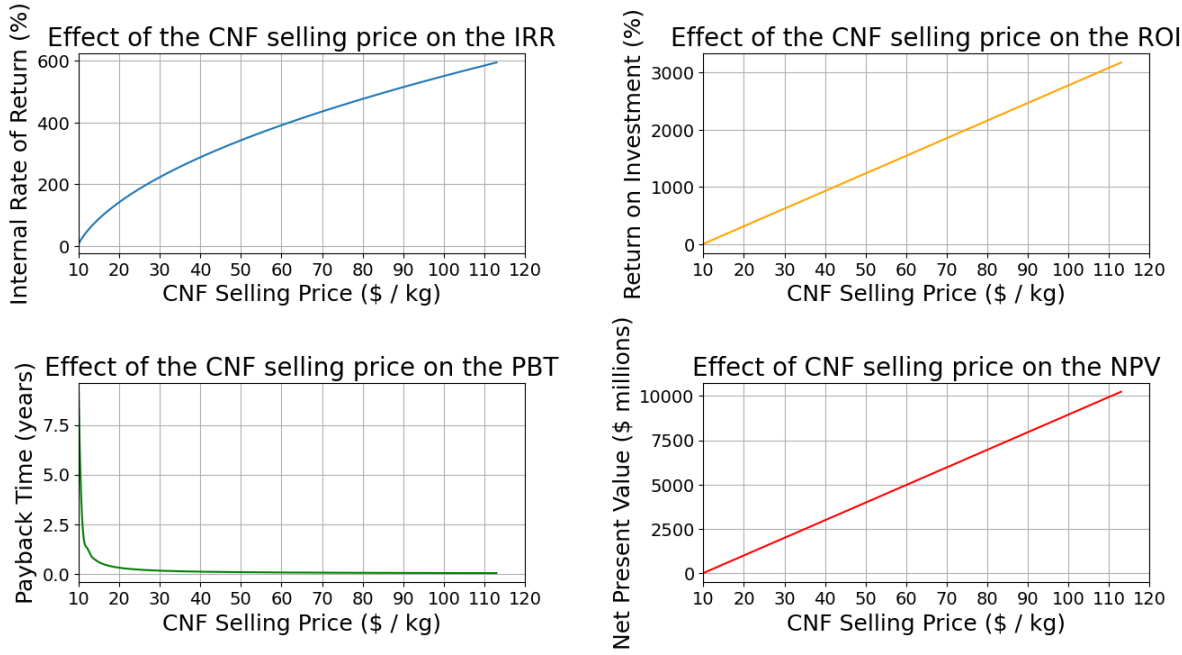

Figure 8.7: Effect of the CNF selling price on the IRR, ROI, PBT and NPV. The results indicate that increasing the CNF selling price has a linear positive effect on the NPV and ROI. The effect of the selling price on the IRR is positive and becomes linear at increasingly high selling prices. The selling price has a strong influence on the PBT, as the PBT first decreases very steeply and then converges to 0.

Figure 8.8 shows the effect of the CSTR residence time on the LCOP. As the residence time increases, the LCOP also increases. However, the line is not smooth. The reason for the jagged line is explained in Appendix 8.2.2. For the average increase of the residence time compared to the LCOP, a linear increasing line becomes visible. It is also interesting to note that the LCOP only increases by just over 1 $/kg if the residence time is increased from 1 to 24 hours. The increase of LCOP is to be expected, as a longer residence time leads to a larger reactor volume and therefore a more expensive reactor.

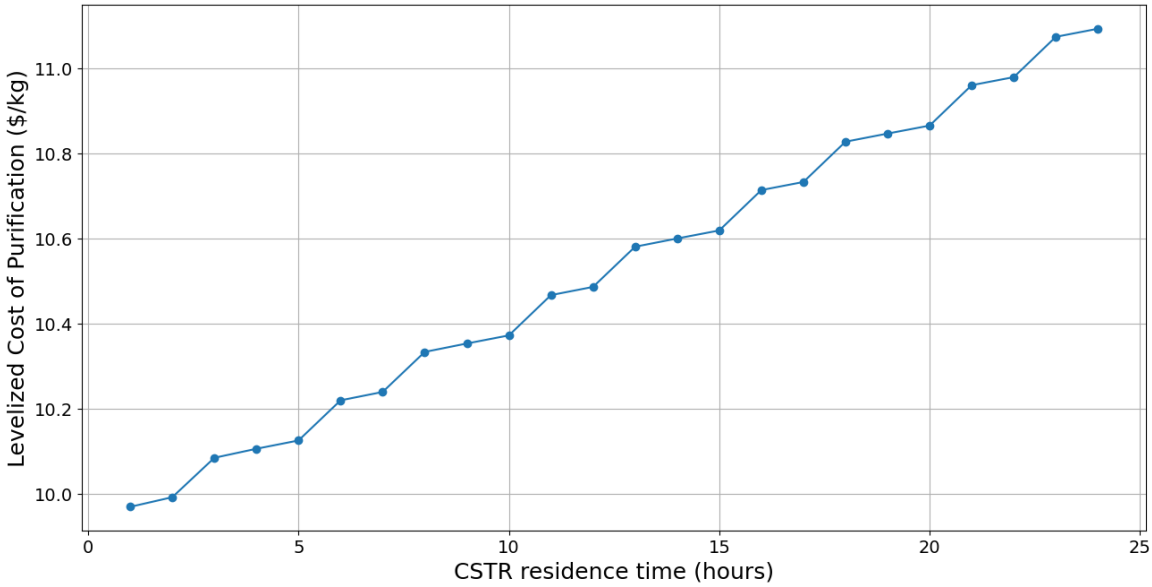

Figure 8.8: Effect of the CSTR residence time on the LCOP. The LCOP increases with the residence time, but the increase is not smooth. The average increase does yield a linear line.

Figure 8.9 shows the effect of the CSTR temperature on the LCOP. The LCOP increases linearly from 8.5 to 10.6 \$/kg. The increase of the LCOP is due to the heat duty of the CSTR, which increases with the temperature. An increase of the heat duty also leads to a higher steam supply and a larger steam generator. All of which increase the costs and therefore the LCOP.

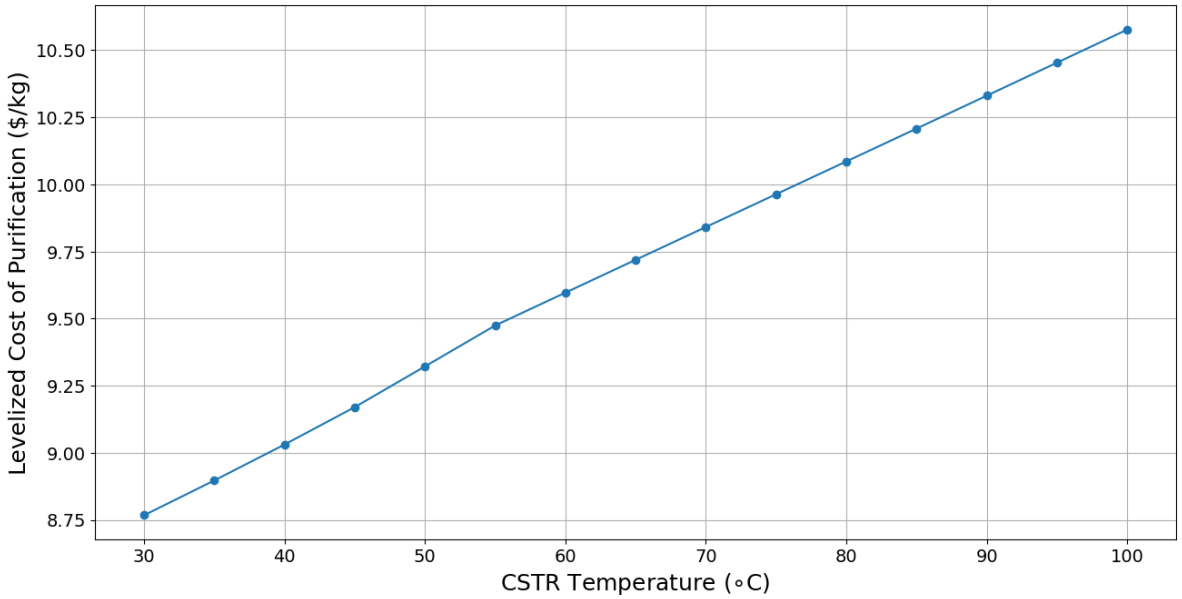

Figure 8.9: Effect of the CSTR temperature on the LCOP. The LCOP increases linearly with the CSTR temperature.

8.2.2. Reactor Volume Analysis

To explain the jagged line in Figure 8.8, further analysis on the reactor is required. Three important analysis are conducted: the effect of the reactor volume on the LCOP, on the CSTR cost and on the number of reactors.

Figure 8.10 shows the effect of the total calculated reactor volume on the LCOP when only the reactor residence time is varied. Exactly the same pattern as in Figure 8.8 emerges, where the LCOP increases in a rough pattern. When only the CNF feed flow instead of the residence time is varied, the LCOP actually decreases as the total calculated CSTR volume increases. That is in line with the findings in Figure 8.5.

The calculated reactor volume is plotted against the CSTR cost in Figure 8.11. Once again, there is a rough pattern. The CSTR cost increases with the total CSTR volume, which is to be expected. It is noteworthy that at every hundred m^3 of reactor volume, there is a jump in the CSTR cost. A possible reason is the maximum volume of a single CSTR, which is 100 m^3. At every hundred m^3, an extra CSTR is added to the process plant and the size of every CSTR is the total calculated CSTR volume divided by the number of CSTR.

To further look into the number of reactors, Figure 8.12 shows the effect of the total CSTR volume on the number of reactors. Indeed, at every hundred m^3 a reactor is added. It appears that just when an extra reactor is added, the total CSTR cost makes a jump and hence the LCOP in Figures 8.8 and 8.10 also makes a jump when an extra reactor is added.

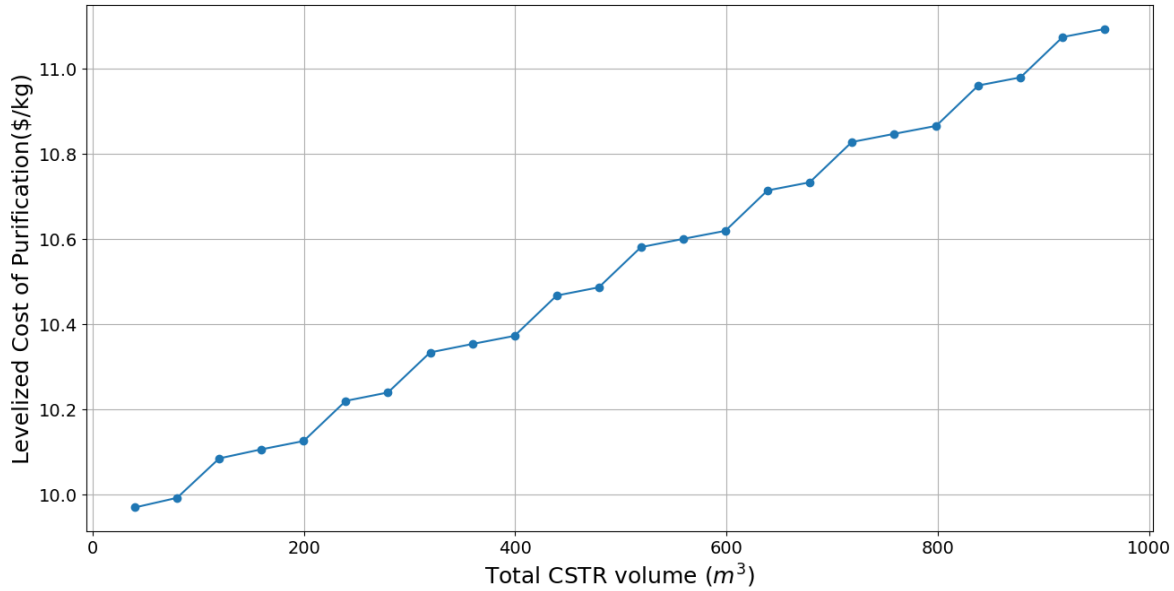

Figure 8.10: Effect of the total CSTR volume on the LCOP when only the residence time of the CSTR is varied. The LCOP increases in a jagged pattern as the total CSTR volume increases. At every 100 m^3 added, the line makes a larger jump than usual.

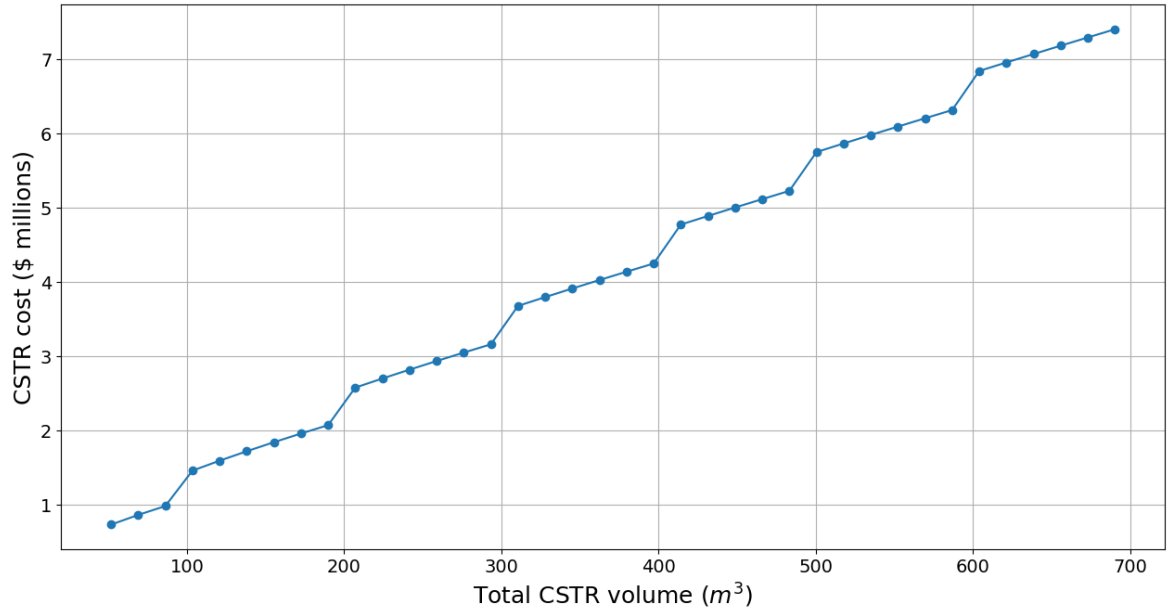

Figure 8.11: Effect of the total CSTR volume on the CSTR cost. The cost increases in a jagged pattern and at every 100 m^3 added, the line makes a larger jump than usual.

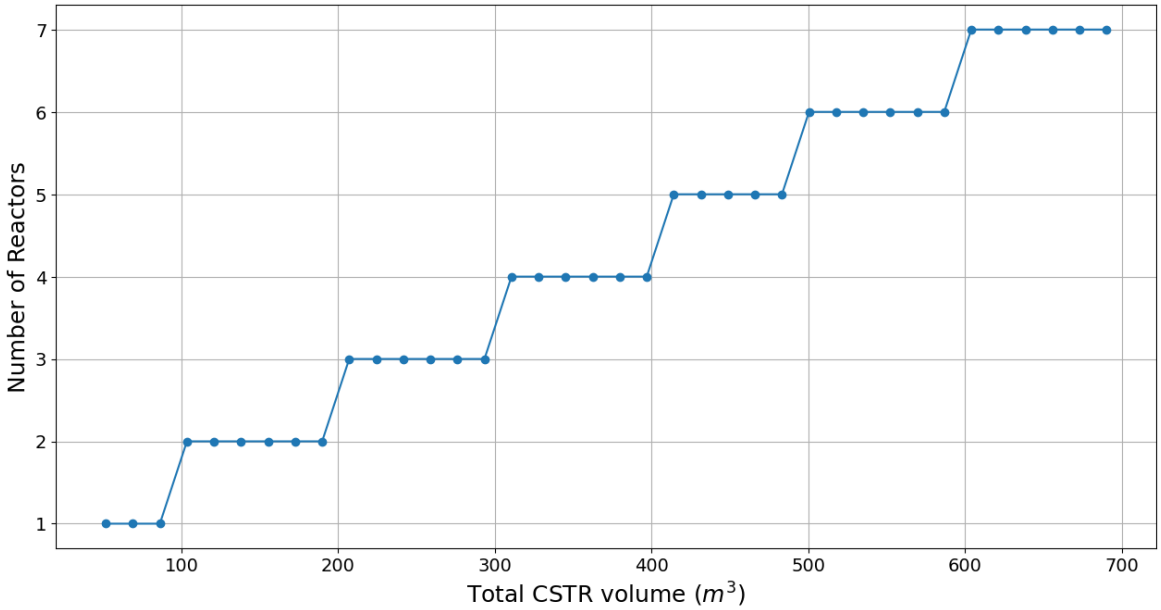

Figure 8.12: Effect of the total CSTR volume on the number of reactors. The total number of reactors increases by 1 at every 100 m^3 added. The reason is that the maximum volume of one reactor is exactly 100 m^3.

8.2.3. Reactor Conversion Analysis

Section 8.1 showed a Ni conversion of only 5.15 % for the baseline scenario of the process plant. 5.15 % is a very low number and a reason to study the Ni conversion. This section details the reactor conversion analysis. The goal of the reactor conversion analysis is to determine how relevant parameters of the reactor and reactor feed influence the Ni conversion. The relevant parameters studied are: the reactor temperature, reactor residence time, reactor pressure, the HCl mass fraction in the acid feed and the Ni mass fraction in the CNF feed. The reactor conversion analysis can give important insights into the reactor kinetics in Aspen Plus and on how to improve the Ni conversion.

Figure 8.13 shows the effect of the reactor temperature on the Ni conversion. The Ni conversion increases nearly linear with a very slight upward curve. The increase in Ni conversion with the reactor temperature follows directly from the Arrhenius law, described in Section 7.3. The temperature has a positive effect on the reaction rate and hence on the Ni conversion. The downside of increasing the reactor temperature is an increase of the LCOP, as illustrated in Figure 8.9.

Figure 8.14 shows the effect of the reactor residence time on the Ni conversion. The effect of the residence time is significant, as the baseline Ni conversion can be increased to up to almost 30 %. The downside is that a very high residence time of 24 hours is required to achieve the almost 30 % conversion. Furthermore, increasing the residence time also means an increase of the LCOP, as Figure 8.8 demonstrated.

Figure 8.15 shows the effect of the reactor pressure on the Ni conversion. The results show that the influence of the reactor pressure on the Ni conversion is negligible. Altering the reactor pressure would therefore not be a good measure to increase the Ni conversion.

Figure 8.16 shows the effect of the HCl mass fraction in the acid feed on the Ni conversion. The effect of the HCl mass fraction flattens out as the mass fraction increases. Remarkable is that the largest increase of the conversion happens before the HCl mass fraction reaches 0.1. A mass fraction of 0.1 is roughly equal to a 3 M HCl acid mixture. The results are in line with the findings of Parhi et al.[81] Parhi et al show that the largest increase in Ni conversion occurs below 1 M. Increasing the molarity above 1 M, then 2 M shows less profound effects on the Ni conversion. Figure 8.16 becomes less accurate for acid concentrations below 1 M, because the curve fit is increasingly less accurate at those acid concentrations. The results also confirm that less acid in the feed is one of the causes of the lower conversion in the baseline scenario as compared to Parhi et al.

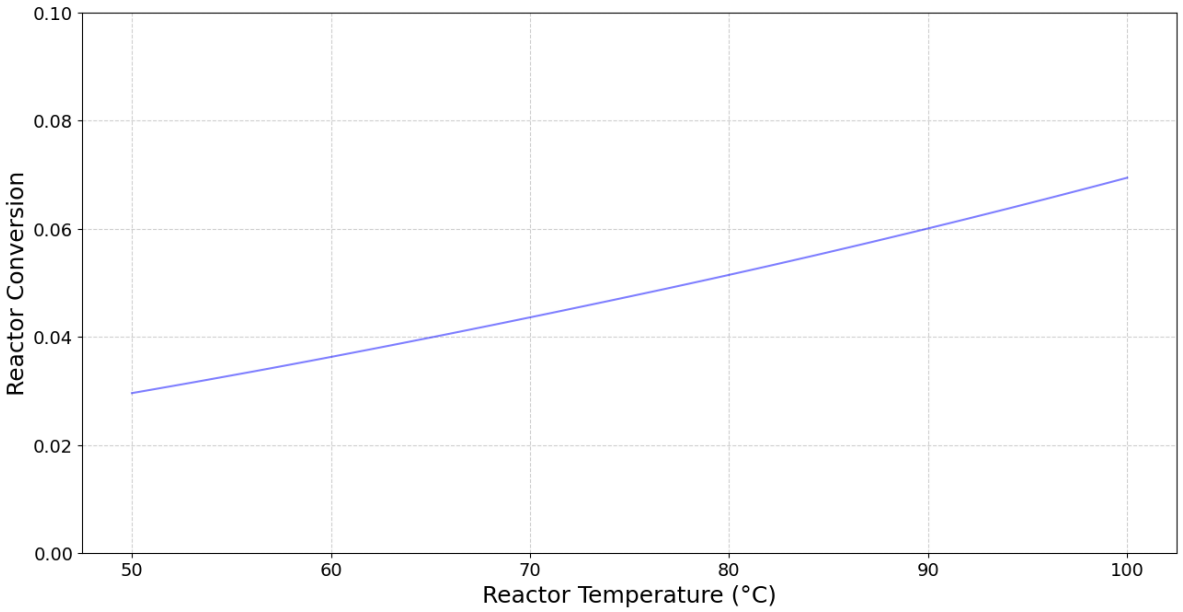

Figure 8.13: Effect of the reactor temperature on the Ni conversion. The Ni conversion increases with the reactor temperature, but the increase is small.

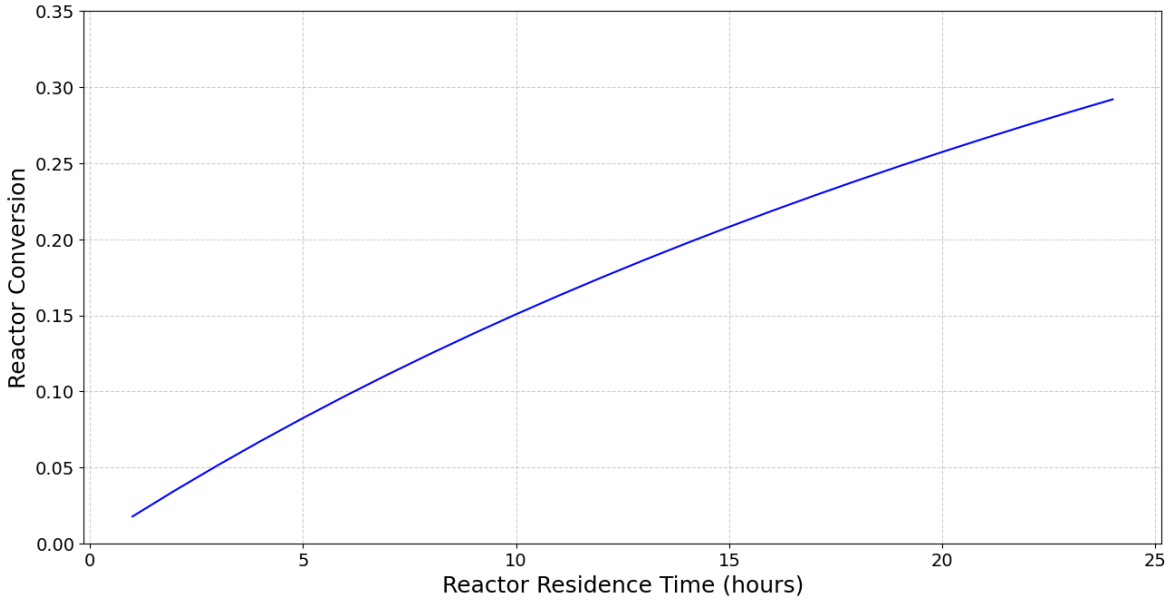

Figure 8.14: Effect of the reactor residence time on the Ni conversion. The effect of the residence time is clearly visible, as the baseline Ni conversion can be increased from 5 % to almost 30 %.

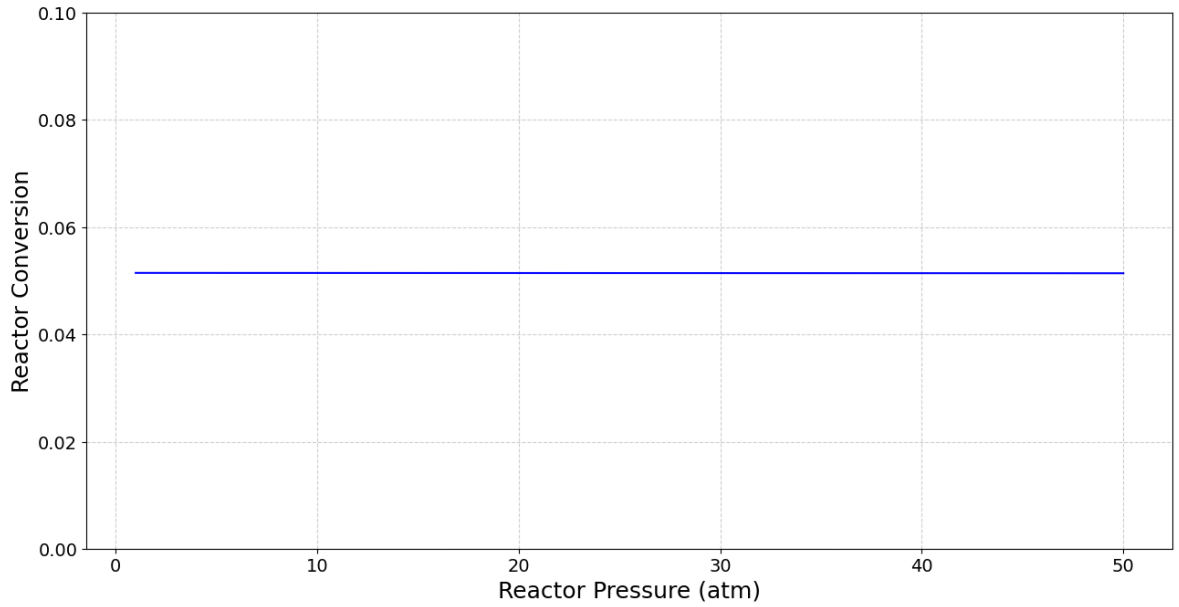

Figure 8.15: Effect of the reactor pressure on the Ni conversion. The influence of the reactor pressure is negligible.

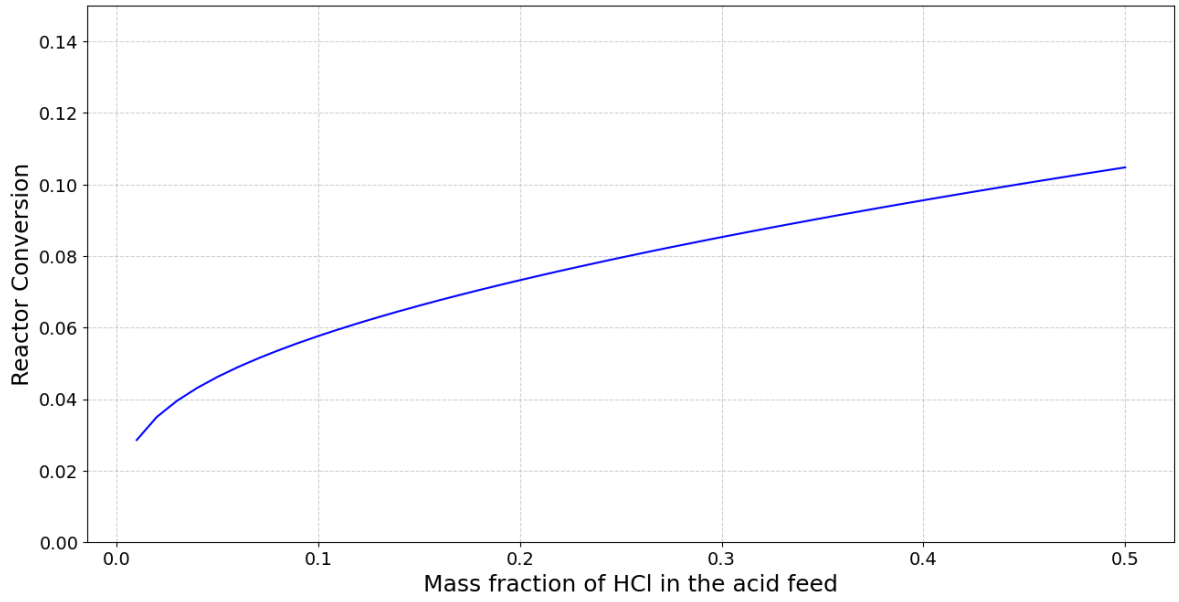

Figure 8.16: Effect of the HCl mass fraction in the acid feed on the Ni conversion. The effect of the HCl mass fraction is small and flattens out. The largest increase is when the HCl mass fraction is smaller than 0.1.

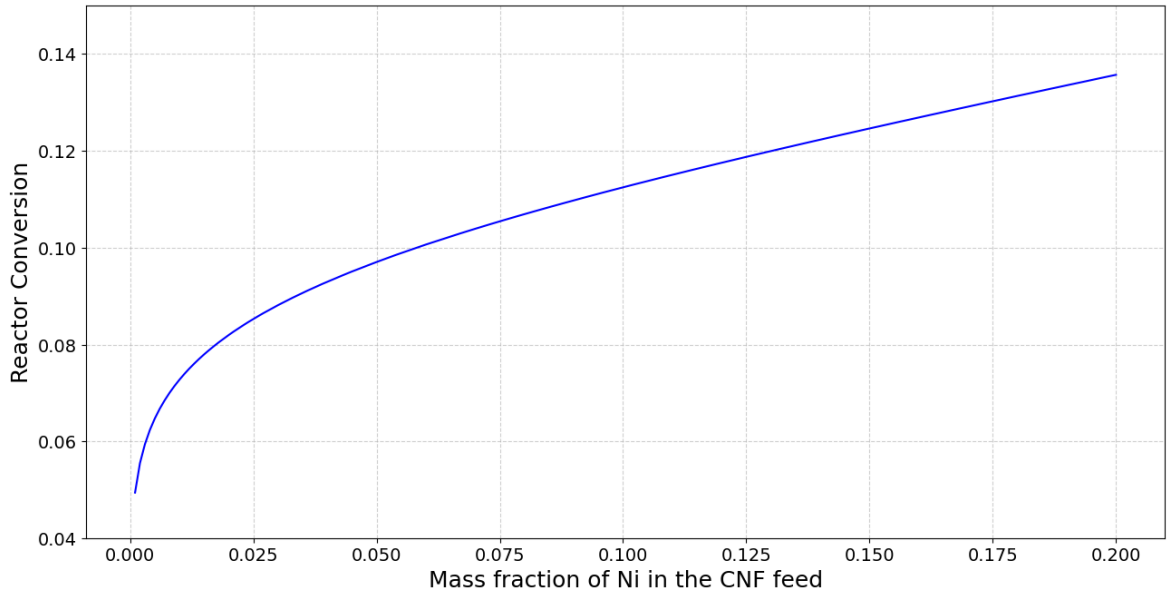

Figure 8.17: Effect of the Ni mass fraction in the CNF feed on the Ni conversion. The conversion increases with the Ni mass fraction in the CNF feed.

Figure 8.17 shows the impact of the Ni mass fraction in the CNF feed on the Ni conversion. A higher initial Ni concentration leads to a higher reactor conversion. According to the kinetics described in Section 7.3, the result is expected as the Ni concentration directly impacts the Ni conversion. Furthermore, the result confirms that the lower Ni content in the CNF of the baseline scenario compared to the catalyst purified in the study by Parhi et al[81] is one of the causes of the lower conversion.

The reactor conversion analysis clearly shows that increasing the residence time of the reactor has the largest effect on the Ni conversion, followed by increasing the Ni content in the CNF feed. However, the Ni content in the CNF feed is not a variable for the process design, as it is fixed. Additionally, increasing the reactor temperature and the HCl mass fraction in the feed have the largest impact on the reactor conversion. The reactor pressure has a negligible effect on the Ni conversion. The findings of the reactor conversion analysis can be taken into account to improve the baseline scenario and reactor setup, of which the results are shown in Section 8.3.

8.2.4. Tornado Plot

A tornado plot is created for the baseline scenario to show the impact of economic parameters on the LCOP. The value for each of the economic parameters is varied with +50 % and -50 %. Figure 8.18 shows the tornado plot with the impact of the economic parameters on the LCOP. The acid waste price has the largest impact on the LCOP, with a variation of ±2.5 $/kg on the LCOP. The reason is that the acid waste price is very high: $316/tonne. Furthermore, the acid waste flow is also high as no acid is recycled in the baseline scenario. Following the acid waste price is the electricity price, with an impact of ±1 $/kg on the LCOP. The impact of the electricity price is due to the high demand of electricity in the process plant, as the steam is generated with an electric steam generator. The required electricity for the heating of steam could possibly be lowered with a steam recycle as the steam recycle stream would have a higher temperature than the water entering the steam generator. The impact of the HCl buying price is also significant and is linked to the high flow rate of the acid feed. The high impact of the acid waste price and the HCl buying price shows a need for an acid recycle stream. An acid recycle would have to include the removal of the metals from the acid, after which the acid can be fed back into the reactor.

On the other hand of the spectrum, the impact on the LCOP of the water price is negligible. Therefore, leaving out the water recycle in the model has no large impact on the LCOP. The impact of the interest rate and fixed capital costs variance factor is also small. In addition, it is important to note

that the variance factors of the fixed capital costs and fixed production costs represent a multiplication with the respective costs. The mean values of the variance factors are equal to 1. Furthermore, the project lifetime and the plant operating hours increase the LCOP when their values are lowered. For the project lifetime, the reason is that the LCOP is calculated as an average over the lifetime. Increasing the project lifetime means the capital costs can be spread over a longer period and therefore the LCOP increases. For the plant operating hours per year, the annual CNF production decreases with less operating hours at the same feed flow rates. Figure 8.5 showed that the LCOP increases as the annual CNF production is lowered. For that reason, lowering the plant operating hours per year increases the LCOP of the process.

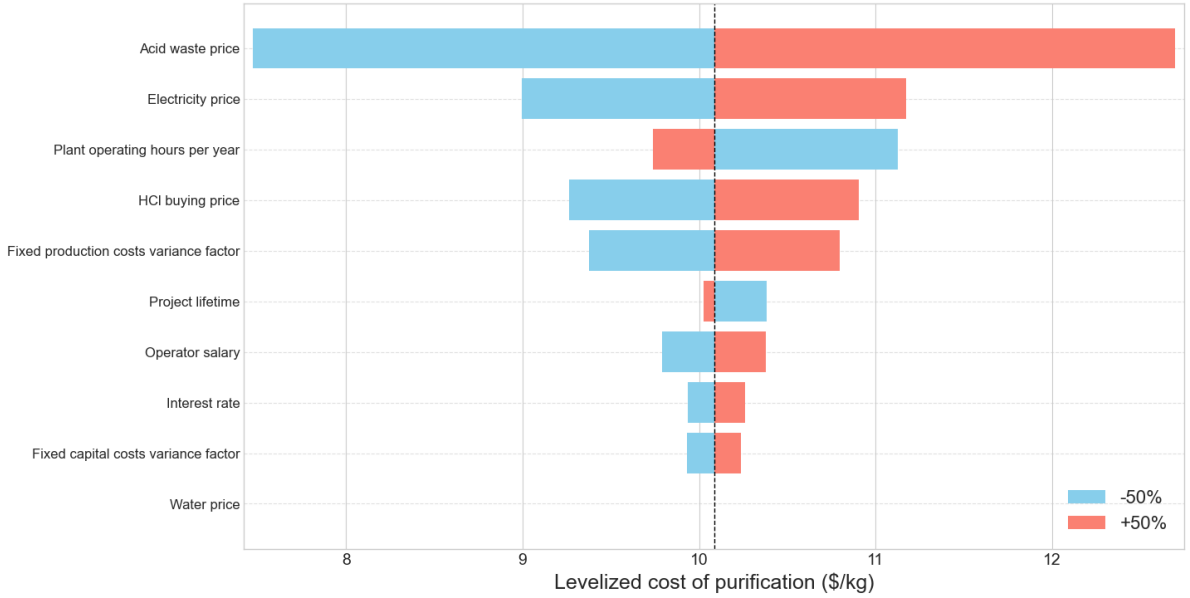

Figure 8.18: Tornado plot of the impact of economic parameters on the LCOP of the process. The economic parameters are varied with +50 % and -50 %. The acid waste and electricity price have the largest impact on the LCOP. On the other hand, the impact of the water price is negligible. The plant operating hours and the project lifetime are the only economic parameters for which lowering their value increases the LCOP of the process.

8.2.5. Monte Carlo Analysis

A Monte Carlo analysis is conducted on the baseline scenario to determine the robustness of the process design. For the most important economic parameters a Gaussian distribution is determined. The Monte Carlo analysis is run with 1,000,000 iterations. In each iteration, a value is randomly selected for each parameter from its respective probability distribution. Finally, the LCOP is calculated and stored for each iteration.

Figure 8.19 shows the resulting probability distributions of the economic parameters. The probability distributions of the economic parameters clearly follow a Gaussian distribution, as expected. The mean and standard deviation of the resulting probability distributions of all parameters is equal or very close to to those determined in Section 7.4.2.

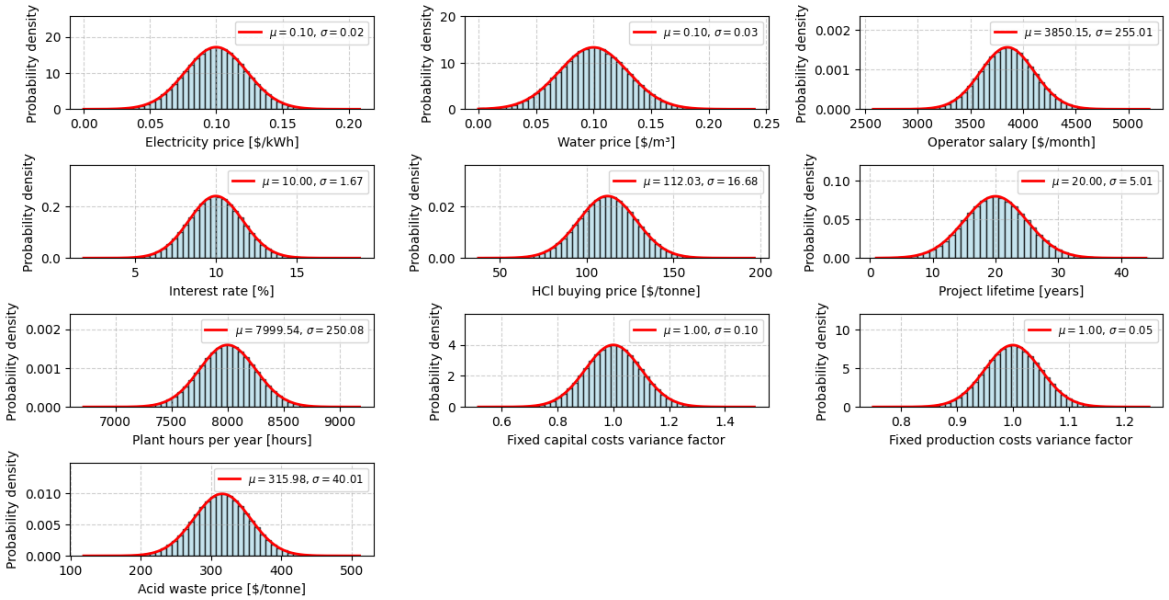

Figure 8.19: Resulting probably distributions from the Monte Carlo analysis of the economic parameters. The distributions are Gaussian. The mean and standard deviation of all parameters is equal or very close to those calculated in Section 7.4.2.

Figure 8.20 shows the resulting probability distribution of the LCOP. The LCOP probability distribution is Gaussian. The mean of the LCOP is equal to 10.12 $/kg, which is very close to the calculated LCOP of the baseline scenario in Section 8.1: 10.09 $/kg. The standard deviation of the LCOP is equal to 0.90. The LCOP variation is relatively small and compared to the variation of the LCOP in the tornado plot, the variation is only slightly larger. Because the standard deviation is low, it can be concluded that the process design of the baseline scenario is indeed robust. Furthermore, the selling price in the baseline scenario, 25 $/kg, is much higher than the highest value of the LCOP in the Monte Carlo analysis.

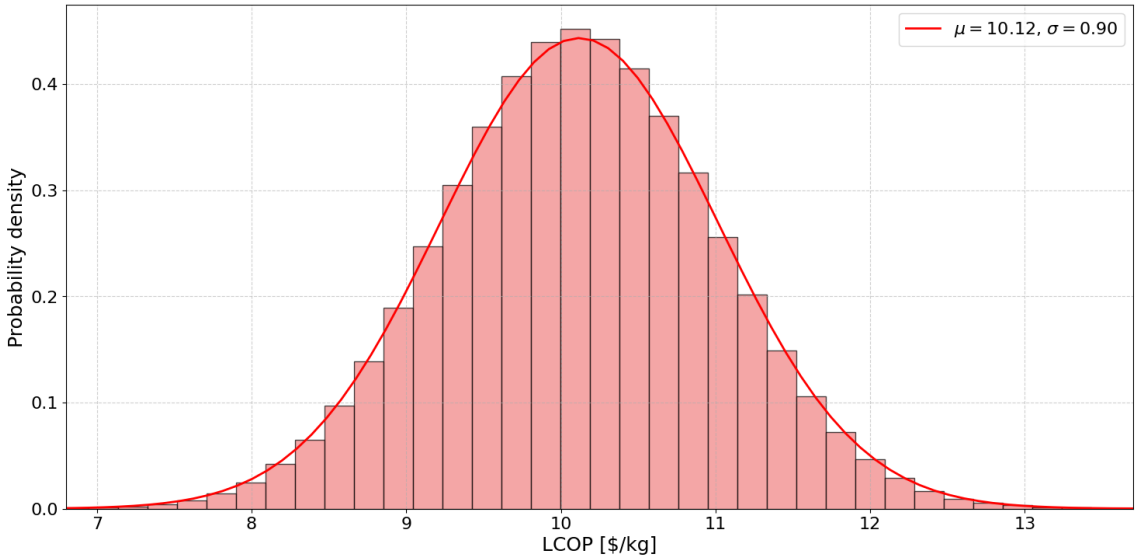

Figure 8.20: Resulting probability distribution of the LCOP from the Monte Carlo analysis. The distribution is Gaussian and the low standard deviation shows a robust process design for the baseline scenario.

8.3. Improved Process Design Cases

This section details the improved process design cases. The goal of the improved process design cases is to increase the nickel conversion while keeping the process economically viable. The focus of the cases is theoretical. There are two improved process design cases: the improved baseline scenario discussed in Section 8.3.1 and the improved baseline with new reactor setup scenario discussed in Section 8.3.2. The improvements are mainly based on the findings of the sensitivity analyses in Section 8.2.

8.3.1. Improved Baseline Scenario

The baseline scenario has a nickel conversion of only 5.15 % and 4460 ppm of nickel remains in the CNF product. That is too high, as <300 ppm of nickel is desired in the CNF product. The sensitivity analyses in Section 8.2 show that the nickel conversion can be improved by increasing the reactor temperature, residence time and HCl concentration of the acid feed. Another potential factor that can improve the conversion is to increase of ratio of the volumetric flow of the acid feed to the mass flow of the CNF feed.

A first improvement to the baseline is implemented by increasing the reactor temperature from 80 °C to 100 °C, increasing the residence time from 3 to 8 hours, increasing the HCl concentration from 2 to 4 M and increasing the ratio of CNF mass flow to acid feed volumetric flow from 1:10 to 1:20. The result is an increase of the reactor conversion to 31.85 %, leaving 3209 ppm of nickel in the final product. The final CNF product purity is 99.60 wt%. The number of reactors required does increase from 2 to 7 and the LCOP is increased from 10.09 to 19.38 $/kg. The PBT is increased to 0.93 years. The first improvement to the baseline clearly improves the nickel conversion, but also increases the LCOP.

Another improvement to the baseline is the implementation of an acid recycle. The tornado plot in Section 8.2.4 shows that the acid waste price has the largest impact on the LCOP and the HCl buying price also has a significant impact on the LCOP. Implementing a HCl recycle stream means that the impact of the acid waste price and HCl buying price on the LCOP is reduced. An acid recycle, where 90 % of the acid is recycled, is added to the original baseline scenario. The acid recycle is modelled by lowering both the fresh HCl feed and the acid waste flow by 90 %. The costs related to implementing an acid recycle are not considered, which is a limitation. The ratio of the CNF feed mass flow to the acid feed volumetric flow rate is increased from 1:10 to 1:95. The results show that the reactor conversion is increased to 31.96 %, leaving 3204 ppm of nickel with a CNF product purity of 99.60 wt%. The number of reactors increases to 11, the number of water pumps to 2 and the LCOP to 23.95 $/kg. The PBT becomes 3.84 years. Implementing an acid recycle allows for a higher acid use in the reactor, which has a positive effect on the reactor conversion. Using more acid does increase the LCOP and the feed ratio of 1:95 would not be economically viable without an acid recycle.

The final improved baseline scenario is achieved by combining the first two improvement scenarios. The reactor temperature is set to 100 °C, the residence time to 8 hours, The HCl concentration to 4 M, the ratio of CNF feed mass flow to acid feed volumetric flow to 1:75 and 90 % of the acid is recycled. The ratio of 1:75 is lower than the aforementioned 1:95, else the LCOP would be higher than the selling price and the process would not be viable. The results show a nickel conversion of 61.04 %, leaving 1836.92 ppm of Ni with a final CNF product purity of 99.73 wt%. In total, 25 reactors are required, and the number of water pumps is increased to 2. The new LCOP is equal to 24.68 $/kg, the PBT becomes 6.75 years, with an ROI of 9.65 % and IRR of 10.77 %. The final NPV is 13,533,462 $. The final improved baseline scenario shows a significant increase in conversion, which comes at the cost of an increased LCOP and less profit.

An important note is that the final improved baseline scenario may not be the best possible improved version of the baseline scenario, which is a limitation. Slightly altering the input parameters may positively influence the results. However, finding the best possible improved version is out of scope. Additionally, the costs of the acid recycle are not considered and this also proves to be a limitation of the analysis. Moreover, the reaction kinetics from the study by Parhi et al[81] are still used. Using reaction kinetics from the acid leaching experiments with CNF could lead to different and improved conversion results.

The final nickel concentration is still not below 300 ppm. However, the nickel conversion of the

baseline scenario can not be improved much further without altering the process design or implementing reaction kinetics from the acid leaching experiments with CNF. Since the latter is not possible yet, the next focus in our study is altering the process design. Specifically, the goal is to change the reactor setup.

8.3.2. Improved Baseline and Reactor Setup

The improved baseline and reactor setup scenario builds on the findings of Section 8.3.1. To further increase the nickel conversion to the required level, the reactor setup has to be altered. Figure 8.21 shows the altered process design in Aspen Plus with the new reactor setup. The new reactor setup contains three reactors in series. For each reactor, the temperature is set to 100 °C and the residence time to 20 hours. The acid feed concentration is 4 M of HCl, 90 % of the acid is recycled and the ratio of the CNF feed mass flow rate to the acid feed volumetric flow rate is 1:35. Costs for recycling the acid are not considered, which is a limitation. The lower CNF to acid feed ratio and higher residence time are a large difference compared to the final version of the improved baseline scenario in Section 8.3.1. Decreasing the CNF to acid feed ratio lowers the LCOP, but it also lowers the conversion below the required level. Increasing the residence time improves the conversion again, but also increases the LCOP. However, the LCOP increase from increasing the residence time is less than the LCOP decrease by decreasing the CNF to acid feed ratio. Through iterative parameter adjustment, the residence time ends up being higher and the CNF to acid feed ratio lower than the final version of the improved baseline scenario.

The results of the improved baseline and reactor setup scenario show a reactor conversion of 93.95 %. Only 285.66 ppm of Ni remains in the CNF product and the final purity is 99.89 wt%. The required Ni content is now below 300 ppm. The LCOP is equal to 21.84 $/kg with a PBT of 5.33 years. The ROI is 13.44 %, the IRR is 14.93 % and the NPV is equal to 271,355,174 $. The downside is the need for a total of 90 reactors: 30 for CSTR1, 30 for CSTR2 and 30 for CSTR3. The conclusion is a profitable process design with a desired low Ni content, but the process design contains 90 reactors. The question arises whether the improved design is practical or not. Another important remark is that multiple reactors in series essentially model a plug flow reactor.

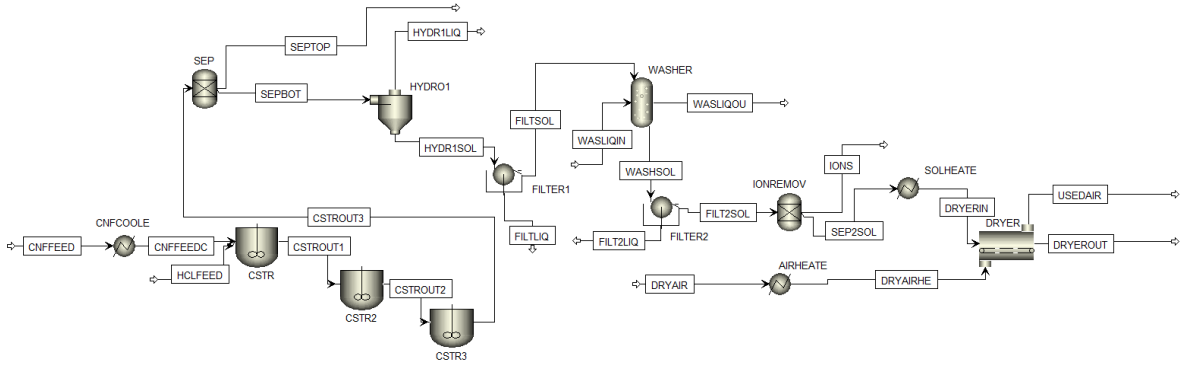

Figure 8.21: Aspen Plus flow sheet of the improved baseline and reactor setup scenario with three reactors in series. The CNF feed is first cooled to the reactor temperature in the solids cooler 'CNFCOOLE', after which it is fed to the first reactor. Acid leaching occurs in three serial reactors and is followed by the removal of the generated H_2 gas in a three-phase separator 'SEP'. The slurry is fed to the hydrocyclone 'HYDRO1' and vacuum drum filter 'FILTER1' for the liquid removal, after which washing with water occurs to remove as much acid leftover as possible. After washing, the main stream is fed to another rotary drum filter 'FILTER2' for liquid removal. The main stream is fed to the 'IONREMOV", which removes the Ni and Cl ions in Aspen Plus to prevent errors in the dryer during the simulation. The 'IONREMOV' block is not present in the actual process. The main stream is then fed to the slurry heater and finally to the drier to obtain a fully dry CNF product. The incoming dry air is heated in the air heater and supplied to the dryer. The water pump, steam generator, air filter, air condenser and recycle streams are not included in the Aspen Plus flow sheet.

9

Conclusion

9.1. Conclusion

A purification process for CNF produced by CMP with a Ni-SiO_2 catalyst has been designed, modelled and analysed. The main outcome of the process design is a baseline scenario, and two improved process design cases are presented. The model includes a Python code for all the techno-economic calculations, part of the equipment calculations and sizing and the sensitivity analyses. In addition to the Python code, the model includes an Aspen Plus flow sheet. The analyses concern a techno-economic analysis to determine the economic viability and a sensitivity analysis to determine the key parameters affecting the economic viability and process conditions. The techno-economic analysis is class 4, meaning the accuracy is ±30 %. A class 4 estimate is based on limited cost data and design detail.

The nanocarbons typically formed by CMP are CNF, CNT, CB and amorphous carbon. CNT has the highest selling price, followed by CNF, CB and amorphous carbon. As the current nanocarbon market is expected to grow significantly towards 2030, more research should be conducted into the production and purification of nanocarbons. Research by Hadian et al[14] on CMP with a Ni-SiO_2 catalyst shows the formation of CNF with a fish bone structure and diameters between 15 to 80 nm. This specific CNF is used as the basis for this study.

Using the hierarchy method as a framework, and using acid leaching for the removal of Ni from the CNF as a basis, the purification process of CNF is designed. HCl is used for acid leaching, the output is set to 20,000 tonnes of CNF per year and the location of the plant is the Netherlands. The result of the process design is a process flow sheet containing all the equipment and process streams. The process includes acid leaching and liquid removal steps such as filtration, washing and drying to achieve the final CNF product. Recycling of the acid is not considered. The recycling of steam and water is indicated in the process flow sheet, but is not included in the model for analysis of the process plant. However, the impact of the water price on the LCOP is very low. Including a steam recycle could potentially reduce the electricity cost required for the heating of steam, since the steam recycle stream would probably have a higher temperature than the water entering the steam generator.

Since no kinetics have followed from the acid leaching experiments yet, kinetic data from literature by Parhi et al[81] on the acid leaching of nickel from a Ni–Al_2O_3 spent catalyst is used. The kinetics are converted to a power law model using curve fitting to Figure 5 and 6 provided by Parhi et al.[81] The final curve fit shows a high R^2 value for the highest acid concentrations 1 M and 2 M in the experiments by Parhi et al[81], as well as for the highest temperatures of 323 K, 333 K and 353 K in the experiments. The R^2 for a temperature of 323 K is 0.933, with R^2 for 353 K equal to 0.996, both with 1 M acid concentration. For temperatures below 323 K and acid concentrations below 1 M, the curve fit becomes increasingly less accurate with R^2 values below 0.7. However, the curve fit is only used for a reactor temperature of 80 °C and a 2 M acid concentration, except in the sensitivity analyses where the temperature or HCl mass fraction is varied.

For the baseline scenario of the process design, a LCOP of 10.09 $/kg follows from the techno-

economic analysis. The ROI is equal to 467.95 %, the IRR to 185.10 %, the PBT to 0.20 years and the NPV to 1,482,232,825 $. The economic parameters indicate a very profitable process, which is mainly due to the selling price of 25 $/kg assumed for the baseline scenario. The baseline scenario shows a final product purity of 99.47 wt%. The nickel conversion is only 5.15 %, leaving 4460 ppm of Ni in the final CNF product. The desired Ni content in the product is 300 ppm or lower. Because of the remaining Ni content, the selling price of 25 $/kg becomes unrealistic, but it is unknown what a realistic selling price would be instead. However, using the baseline scenario with the current conditions is not advised, as the quality of the CNF is barely increased.

The acid leaching experiments for the removal of nickel from CNF show a more promising nickel conversion than the leaching kinetics of Parhi et al[81] show for the specific CNF. So far, preliminary experiments with the following conditions have been conducted: a temperature of 70 °C, 4 hour residence time, a 4 M H_2SO_4 solution, and varying sonication between none, 20 % and 40 %. The results of the preliminary experiments show an average nickel conversion of 70.9 %, with 83.0 % for the preliminary experiments with 40 % sonication. However, difficulties arise with the analysis of the solid CNF samples. To prepare the CNF sample for ICP analysis, the CNF sample is mixed with HNO_3. The problem is that not all of the solid dissolves into the acid. Therefore, during ICP analysis, only the part of the solid dissolved into the acid is analysed. A part of the metals that remains in the undissolved solid is therefore not accounted for. The ICP analysis of the solid CNF sample can be inaccurate and the consequence could be that the current results show a higher conversion than in reality. A possible solution is to use a microdigester to dissolve all of the solid CNF sample as preparation for ICP analysis.

The sensitivity analyses of the baseline scenario show that increasing the CNF production lowers the LCOP, while increasing the reactor residence time and reactor temperature increases the LCOP. The reactor residence time has the largest positive impact on the nickel conversion, followed by the reactor temperature and the HCl mass fraction in the feed. The reactor pressure has a negligible effect on the nickel conversion. The tornado plot analysis of the baseline scenario shows the impact of economic parameters on the LCOP by varying the paremeters with ±50 %. The acid waste price has the largest impact on the LCOP with ±2.5 $/kg variation, followed by the electricity price. The acid buying price also has a significant impact on the LCOP. The impact of the acid waste price and acid buying price shows a need for an acid recycle, as a recycle would reduce the impact of both. The water price, fixed capital costs and interest rate have the smallest impact on the LCOP. The Monte Carlo analysis is conducted on the baseline scenario with 1,000,000 iterations. The resulting probability density of the LCOP is Gaussian. The mean is equal to 10.12 $/kg, with a standard deviation of 0.90 $/kg, which is relatively low. The Monte Carlo analysis indicates a robust process design under economic uncertainties.

To improve the baseline scenario, two improved process design cases are presented. The first improved baseline scenario includes the following changes: a reactor temperature of 100 °C, a reactor residence time of 8 hours, 4 M HCl concentration of the acid feed, a 1:75 ratio of the CNF feed mass flow to the acid feed volumetric flow and a 90 % acid recycle. The conversion of the first improved baseline scenario is equal to 61.04 %, leaving 1836.92 ppm of nickel with a final product purity of 99.73 wt %. The new LCOP is equal to 24.68 $/kg with a positive NPV. While the process is economically viable, the conversion is still too low as too much nickel remains in the final product. The second improved baseline scenario also includes a change in the reactor setup: instead of using only one reactor, three reactors are placed in series. For each reactor, the temperature is set to 100 °C and the residence time to 20 hours. 4 M HCl concentration is used with a ratio of 1:35 for the CNF feed mass flow to the acid feed volumetric flow and with a 90 % acid recycle. The result is a conversion of 93.95 %, leaving only 285.66 ppm of Ni which is below the desired maximum of 300 ppm. The final CNF product purity is 99.89 wt%. with an LCOP equal to 21.84 $/kg. However, in total 90 reactors are required. So while the process is profitable and the product has a desired low nickel content, questions arise whether the improved design is practical or not.

9.2. Recommendations

Future research should focus on the acid leaching experiments of nickel from CNF to determine the leaching effectiveness and the leaching kinetics. The reactor is currently modelled with the kinetics provided by Parhi et al[81], which gives a nickel conversion of only 5.15 %. However, the preliminary acid

leaching experiments give a nickel conversion of 70.9 %, which is a very large difference compared to the nickel conversion of the model with the kinetics from Parhi et al.[81] Using the leaching kinetics from the acid leaching experiments will provide different and more accurate results, as these are conducted on the CNF and not on a Ni–Al_2O_3 spent catalyst. The acid leaching experiments should also be expanded to other acids than only H_2SO_4, such as HCl and HNO_3. This will help determine which acid gives the highest nickel conversion.

In addition to the acid leaching experiments, future research should focus on the implementation of a recycle for the used acid. To recycle the used acid, the Ni and Cl ions should be removed. Afterwards, the acid can be fed back into the process. Possible methods to remove the metal ions are electrolysis and adsorption. However, research should not limit itself to those two methods. Agboola et al[17] show another possible method for acid regeneration by removing $FeCl_2$ from HCl with oxidation in an acid regeneration column followed by a centrifuge separator. For the removal of $NiCl_2$, so Ni and Cl ions, a similar oxidation method may be possible.

The model of the process plant can also be further improved by including the water and steam recycling streams. Although the water cost has a small effect on the LCOP, including the water recycle could decrease the LCOP a little bit and make the model more complete. Including a steam recycle also reduces the water cost and potentially also a part of the heating cost of the steam generator.

Further research should be conducted into the purification of other types of nanocarbons with the current process design. The current process design, with possibly a few adjustments where necessary, could be economically viable for CNT and other nanocarbon types. Especially for CNT, where the selling price is in range of 100,000 to 60,000,000 $/tonne.[59] This leads to the last recommendation. Conducting more research into the CNF and CNT selling price will give more clarity about the impact of the purity and nickel content on the selling price. Since there is not a lot of literature on the CNF and CNT selling price, companies should be contacted to gather data on the purity and selling price.

References

(1) Wang, I.-W.; Dagle, R. A.; Khan, T. S.; Lopez-Ruiz, J. A.; Kovarik, L.; Jiang, Y.; Xu, M.; Wang, Y.; Jiang, C.; Davidson, S. D.; Tavadze, P.; Li, L.-L.; Hu, J. Catalytic Decomposition of Methane into Hydrogen and High-Value Carbons: Combined Experimental and DFT Computational Study. *Catalysis Science & Technology* **2021**, *11*, 4911–4921, DOI: 10.1039/D1CY00287B.

(2) International Energy Agency *Global Hydrogen Review 2024*; Report; International Energy Agency, 2024, https://www.iea.org/reports/global-hydrogen-review-2024.

(3) Sánchez-Bastardo, N.; Schlögl, R.; Ruland, H. Methane Pyrolysis for Zero-Emission Hydrogen Production: A Potential Bridge Technology from Fossil Fuels to a Renewable and Sustainable Hydrogen Economy. *Industrial & Engineering Chemistry Research* **2021**, *60*, 11855–11881, DOI: 10.1021/acs.iecr.1c01679.

(4) Machhammer, O.; Bode, A.; Hormuth, W. Financial and Ecological Evaluation of Hydrogen Production Processes on Large Scale. *Chemical Engineering & Technology* **2016**, *39*, 1185–1193, DOI: 10.1002/ceat.201600023.

(5) Qian, J. X.; Chen, T. W.; Enakonda, L. R.; Liu, D. B.; Basset, J.-M.; Zhou, L. Methane decomposition to pure hydrogen and carbon nano materials: State-of-the-art and future perspectives. *International Journal of Hydrogen Energy* **2020**, *45*, 15721–15743, DOI: 10.1016/j.ijhydene.2020.04.100.

(6) Hantoko, D.; Khan, W. U.; Osman, A. I.; Nasr, M.; Rashwan, A. K.; Gambo, Y.; Al Shoaibi, A.; Chandrasekar, S.; Hossain, M. M. Carbon–neutral hydrogen production by catalytic methane decomposition: a review. *Environmental Chemistry Letters* **2024**, *22*, 1623–1663, DOI: 10.1007/s10311-024-01732-4.

(7) Eatemadi, A.; Daraee, H.; Karimkhanloo, H.; Kouhi, M.; Zarghami, N.; Akbarzadeh, A.; Abasi, M.; Hanifehpour, Y.; Joo, S. W. Carbon nanotubes: Properties, synthesis, purification, and medical applications. *Nanoscale research letters* **2014**, *9,* 393, DOI: 10.1186/1556-276X-9-393.

(8) Zemtsova, E. G.; Arbenin, A. Y.; Sidorov, Y. V.; Morozov, N. F.; Korusenko, P. M.; Semenov, B. N.; Smirnov, V. M. The Use of Carbon-Containing Compounds to Prepare Functional and Structural Composite Materials: A Review. *Applied Sciences* **2022**, *12,* 9945, DOI: 10.3390/app12199945.

(9) Arora, D.; Attri, P. Carbon Nanotubes (CNTs): A Potential Nanomaterial for Water Purification. *Journal of Composites Science* **2020**, *4*, 135, DOI: 10.3390/jcs4030135.

(10) Hughes, K. J.; Iyer, K. A.; Bird, R. E.; Ivanov, J.; Banerjee, S.; Georges, G.; Zhou, Q. A. Review of Carbon Nanotube Research and Development: Materials and Emerging Applications. *ACS Applied Nano Materials* **2024**, *7*, 18695–18713, DOI: 10.1021/acsanm.4c02721.

(11) Yahyazadeh, A.; Nanda, S.; Dalai, A. K. Carbon Nanotubes: A Review of Synthesis Methods and Applications. *Reactions* **2024**, *5*, 429–451, DOI: 10.3390/reactions5030022.

(12) Chen, D.; Christensen, K. O.; Ochoa-Fernández, E.; Yu, Z.; Tøtdal, B.; Latorre, N.; Monzon, A.; Holmen, A. Synthesis of carbon nanofibers: Effects of Ni crystal size during methane decomposition. *Journal of Catalysis* **2005**, *229*, 82–96, DOI: 10.1016/j.jcat.2004.10.017.

(13) Modekwe, H. U.; Olaitan Ayeleru, O.; Onu, M. A.; Tobias, N. T.; Mamo, M. A.; Moothi, K.; Daramola, M. O.; Olubambi, P. A. In *Handbook of Carbon Nanotubes*, Abraham, J., Thomas, S., Kalarikkal, N., Eds.; Springer International Publishing: Cham, 2022, pp 619–633, DOI: 10.1007/978-3-030-91346-5_73.

(14) Hadian, M.; Marrevee, D. P. F.; Buist, K. A.; Reesink, B. H.; Bos, A. N. R.; van Bavel, A. P.; Kuipers, J. A. M. Kinetic study of thermocatalytic decomposition of methane over nickel supported catalyst in a fluidized bed reactor. *Chemical Engineering Science* **2022**, *260*, 117938, DOI: 10.1016/j.ces.2022.117938.

(15) Ahmad, A.; Hamdani, I. R.; Srinivasakannan, C.; Al Shoaibi, A.; Hossain, M. M. Catalytic cracking of methane to hydrogen and carbon: Scale-up perspective. *International Journal of Hydrogen Energy* **2024**, *54*, 1212–1230, DOI: 10.1016/j.ijhydene.2023.12.042.

(16) Parmar, K. R.; Pant, K. K.; Roy, S. Blue hydrogen and carbon nanotube production via direct catalytic decomposition of methane in fluidized bed reactor: Capture and extraction of carbon in the form of CNTs. *Energy Conversion and Management* **2021**, *232*, 113893, DOI: 10.1016/j.enconman.2021.113893.

(17) Agboola, A. E.; Pike, R. W.; Hertwig, T. A.; Lou, H. H. Conceptual design of carbon nanotube processes. *Clean Technologies and Environmental Policy* **2007**, *9*, 289–311, DOI: 10.1007/s10098-006-0083-2.

(18) Fromm, C. Hydrogen Production via Methane Pyrolysis: An Overview of 'Turquoise' Hydrogen https://www.chemengonline.com/hydrogen-production-via-methane-pyrolysis-an-overview-of-turquoise-h2/ (accessed 02/17/2025).

(19) Korányi, T. I.; Németh, M.; Beck, A.; Horváth, A. Recent Advances in Methane Pyrolysis: Turquoise Hydrogen with Solid Carbon Production. *Energies* **2022**, *15,* 6342, DOI: 10.3390/en15176342.

(20) Punetha, M.; Bhagat, J.; Pathak, R.; Bhatt, S.; Sanghani, P.; Punetha, V. D. In *Handbook of Functionalized Carbon Nanostructures: From Synthesis Methods to Applications*, Barhoum, A., Deshmukh, K., Eds.; Springer International Publishing: Cham, 2024, pp 2743–2800, DOI: 10.1007/978-3-031-32150-4_75.

(21) Abraham, J.; Thomas, S.; Kalarikkal, N., *Handbook of Carbon Nanotubes*; Springer Cham: 2022, DOI: https://doi.org/10.1007/978-3-030-91346-5.

(22) Dubey, R.; Dutta, D.; Sarkar, A.; Chattopadhyay, P. Functionalized carbon nanotubes: synthesis, properties and applications in water purification, drug delivery, and material and biomedical sciences. *Nanoscale Advances* **2021**, *3*, 5722–5744, DOI: 10.1039/D1NA00293G.

(23) Huang, J.; Liu, Y.; You, T. Carbon nanofiber based electrochemical biosensors: A review. *Analytical Methods* **2010**, *2*, 202–211, DOI: 10.1039/B9AY00312F.

(24) Celzard, A. What are the differences between carbon nanotubes (CNTs) and carbon nanofibers (CNFs)? https://www.researchgate.net/post/What_are_the_differences_between_carbon_nanotubes_CNTs_and_carbon_nanofibers_CNFs (accessed 10/02/2025).

(25) Terrones, M. Science and Technology of the Twenty-First Century: Synthesis, Properties, and Applications of Carbon Nanotubes. *Annual Review of Materials Research* **2003**, *13*, 419–501, DOI: 10.1146/annurev.matsci.33.012802.100255.

(26) Li, D.; Chen, J.; Li, Y. Evidence of composition deviation of metal particles of a Ni–Cu/Al2O3 catalyst during methane decomposition to COx-free hydrogen. *International Journal of Hydrogen Energy* **2009**, *34*, 299–307, DOI: 10.1016/j.ijhydene.2008.09.106.

(27) Toebes, M. L.; Bitter, J. H.; van Dillen, A. J.; de Jong, K. P. Impact of the Structure and Reactivity of Nickel Particles on the Catalytic Growth of Carbon Nanofibers. *Catalysis Today* **2002**, *76*, 33–42, DOI: 10.1016/S0920-5861(02)00209-2.

(28) Serp, P.; Corrias, M.; Kalck, P. Carbon nanotubes and nanofibers in catalysis. *Applied Catalysis A: General* **2003**, *253*, 337–358, DOI: 10.1016/S0926-860X(03)00549-0.

(29) Hamdan, M.; Halawy, L.; Abdel Karim Aramouni, N.; Ahmad, M. N.; Zeaiter, J. Analytical review of the catalytic cracking of methane. *Fuel* **2022**, *324*, 124455, DOI: 10.1016/j.fuel.2022.124455.

(30) Hantoko, D.; Khan, W. U.; Putra, A. F. P.; Al Shoaibi, A.; Chandrasekar, S.; Hossain, M. M. Fe–Ce–Al Catalysts for Decomposition of Methane to High Purity Hydrogen and High-Value Carbon. *Industrial & Engineering Chemistry Research* **2024**, *63*, 18869–18878, DOI: 10.1021/acs.iecr.4c02856.

(31) Chufa, B. M.; Anandy Murthy, H. C.; Gonfa, B. A.; Anshebo, T. Y. Carbon nanotubes: a review on green synthesis, growth mechanism and application as a membrane filter for fluoride remediation. *Green Chemistry Letters and Reviews* **2021**, *14*, 647–664, DOI: 10.1080/17518253.2021.1991484.

(32) Wang, I.-W.; Ayillath Kutteri, D.; Gao, B.; Hu, J. Methane Pyrolysis for Carbon Nanotubes and COx-Free H2 over Transition-Metal Catalysts. *Energy & Fuels* **2018**, *33*, 197–205, DOI: 10.1021/acs.energyfuels.8b03502.

(33) Välimäki, E.; Yli-Varo, L.; Romar, H.; Lassi, U. Carbons Formed in Methane Thermal and Thermocatalytic Decomposition Processes: Properties and Applications. *Journal of Carbon Research* **2021**, *7,* 50, DOI: 10.3390/c7030050.

(34) Liang, W.; Yan, H.; Chen, C.; Lin, D.; Tan, K.; Feng, X.; Liu, Y.; Chen, X.; Yang, C.; Shan, H. Revealing the Effect of Nickel Particle Size on Carbon Formation Type in the Methane Decomposition Reaction. *Catalysts* **2020**, *10*, 890, DOI: 10.3390/catal10080890.

(35) Raza, J.; Khoja, A. H.; Anwar, M.; Saleem, F.; Naqvi, S. R.; Liaquat, R.; Hassan, M.; Javaid, R.; Qazi, U. Y.; Lumbers, B. Methane decomposition for hydrogen production: A comprehensive review on catalyst selection and reactor systems. *Renewable and Sustainable Energy Reviews* **2022**, *168*, 112774, DOI: 10.1016/j.rser.2022.112774.

(36) Mitoura dos Santos Junior, J.; Gomes, J. G.; de Freitas, A. C. D.; Guirardello, R. An Analysis of the Methane Cracking Process for CO2-Free Hydrogen Production Using Thermodynamic Methodologies. *Methane* **2022**, *1*, 243–261, DOI: 10.3390/methane1040020.

(37) Fan, Z.; Weng, W.; Zhou, J.; Gu, D.; Xiao, W. Catalytic decomposition of methane to produce hydrogen: A review. *Journal of Energy Chemistry* **2021**, *58*, 415–430, DOI: 10.1016/j.jechem.2020.10.049.

(38) Gamal, A.; Eid, K.; El-Naas, M. H.; Kumar, D.; Kumar, A. Catalytic Methane Decomposition to Carbon Nanostructures and COx-Free Hydrogen: A Mini-Review. *Nanomaterials* **2021**, *11,* 1226, DOI: 10.3390/nano11051226.

(39) Hou, P.-X.; Liu, C.; Cheng, H.-M. Purification of carbon nanotubes. *Carbon* **2008**, *46*, 2003–2025, DOI: 10.1016/j.carbon.2008.09.009.

(40) Rahatwan, I. D.; Wulan, P. P. D. K.; Solahudin, M. Techno-economic analysis of pilot scale carbon nanotube production from LPG with Fe-Co-Mo/MgO catalyst in Indonesia. *AIP Conference Proceedings* **2020**, *2230*, 030013, DOI: 10.1063/5.0002357.

(41) Chiang, I. W.; Brinson, B. E.; Smalley, R. E.; Margrave, J. L.; Hauge, R. H. Purification and Characterization of Single-Wall Carbon Nanotubes. *The Journal of Physical Chemistry B* **2001**, *105*, 1157–1161, DOI: 10.1021/jp003453z.

(42) Wang, J. S.; Wai, C. M.; Shimizu, K.; Cheng, F.; Boeckl, J. J.; Maruyama, B.; Brown, G. Purification of Single-Walled Carbon Nanotubes Using a Supercritical Fluid Extraction Method. *The Journal of Physical Chemistry C* **2007**, *111*, 13007–13012, DOI: 10.1021/jp073374o.

(43) Harutyunyan, A. R.; Pradhan, B. K.; Chang, J.; Chen, G.; Eklund, P. C. Purification of Single-Wall Carbon Nanotubes by Selective Microwave Heating of Catalyst Particles. *The Journal of Physical Chemistry B* **2002**, *106*, 8671–8675, DOI: 10.1021/jp0260301.

(44) Thiên-Nga, L.; Hernadi, K.; Ljubović, E.; Garaj, S.; Forró, L. Mechanical Purification of Single-Walled Carbon Nanotube Bundles from Catalytic Particles. *Nano Letters* **2002**, *2*, 1349–1352, DOI: 10.1021/nl025740f.

(45) Kang, J. H.; Park, J.-K. Magnetophoretic Continuous Purification of Single-Walled Carbon Nanotubes from Catalytic Impurities in a Microfluidic Device. *Small* **2007**, *3*, 1784–1791, DOI: 10.1002/smll.200700334.

(46) Georgakilas, V.; Voulgaris, D.; Vázquez, E.; Prato, M.; Guldi, D. M.; Kukovecz, A.; Kuzmany, H. Purification of HiPCO Carbon Nanotubes via Organic Functionalization. *Journal of the American Chemical Society* **2002**, *124*, 14318–14319, DOI: 10.1021/ja0260869.

(47) Bandow, S.; Rao, A. M.; Williams, K. A.; Thess, A.; Smalley, R. E.; Eklund, P. C. Purification of Single-Wall Carbon Nanotubes by Microfiltration. *The Journal of Physical Chemistry B* **1997**, *101*, 8839–8842, DOI: 10.1021/jp972026r.

(48) Shelimov, K. B.; Esenaliev, R. O.; Rinzler, A. G.; Huffman, C. B.; Smalley, R. E. Purification of single-wall carbon nanotubes by ultrasonically assisted filtration. *Chemical Physics Letters* **1998**, *282*, 429–434, DOI: 10.1016/S0009-2614(97)01265-7.

(49) Bonard, J.-M.; Stora, T.; Salvetat, J.-P.; Maier, F.; Stöckli, T.; Duschl, C.; Forró, L.; de Heer, W. A.; Châtelain, A. Purification and size-selection of carbon nanotubes. *Advanced Materials* **1997**, *9*, 827–831, DOI: 10.1002/adma.19970091014.

(50) Tohji, K.; Takahashi, H.; Shinoda, Y.; Shimizu, N.; Jeyadevan, B.; Matsuoka, I.; Saito, Y.; Kasuya, A.; Ito, S.; Nishina, Y. Purification Procedure for Single-Walled Nanotubes. *The Journal of Physical Chemistry B* **1997**, *101*, 1974–1978, DOI: 10.1021/jp962888c.

(51) Sato, Y.; Ogawa, T.; Motomiya, K.; Shinoda, K.; Jeyadevan, B.; Tohji, K.; Kasuya, A.; Nishina, Y. Purification of MWNTs Combining Wet Grinding, Hydrothermal Treatment, and Oxidation. *The Journal of Physical Chemistry B* **2001**, *105*, 3387–3392, DOI: 10.1021/jp002817k.

(52) Hernadi, K.; Fonseca, A.; Nagy, J. B.; Bernaerts, D.; Riga, J.; Lucas, A. Catalytic synthesis and purification of carbon nanotubes. *Synthetic Metals* **1996**, *77*, 31–34, DOI: 10.1016/0379-6779(96)80051-8.

(53) Hou, P. X.; Bai, S.; Yang, Q. H.; Liu, C.; Cheng, H. M. Multi-step purification of carbon nanotubes. *Carbon* **2002**, *40*, 81–85, DOI: 10.1016/S0008-6223(01)00075-6.

(54) Wang, Y.; Gao, L.; Sun, J.; Liu, Y.; Zheng, S.; Kajiura, H.; Li, Y.; Noda, K. An integrated route for purification, cutting and dispersion of single-walled carbon nanotubes. *Chemical Physics Letters* **2006**, *432*, 205–208, DOI: 10.1016/j.cplett.2006.10.054.

(55) Li, F.; Cheng, H. M.; Xing, Y. T.; Tan, P. H.; Su, G. Purification of single-walled carbon nanotubes synthesized by the catalytic decomposition of hydrocarbons. *Carbon* **2000**, *38*, 2041–2045, DOI: 10.1016/S0008-6223(00)00061-0.

(56) Montoro, L. A.; Rosolen, J. M. A multi-step treatment to effective purification of single-walled carbon nanotubes. *Carbon* **2006**, *44*, 3293–3301, DOI: 10.1016/j.carbon.2006.06.018.

(57) Liu, Y.; Gao, L.; Sun, J.; Zheng, S.; Jiang, L.; Wang, Y.; Kajiura, H.; Li, Y.; Noda, K. A multi-step strategy for cutting and purification of single-walled carbon nanotubes. *Carbon* **2007**, *45*, 1972–1978, DOI: 10.1016/j.carbon.2007.06.009.

(58) Kim, Y.; Luzzi, D. E. Purification of Pulsed Laser Synthesized Single Wall Carbon Nanotubes by Magnetic Filtration. *The Journal of Physical Chemistry B* **2005**, *109*, 16636–16643, DOI: 10.1021/jp0522359.

(59) Dagle, R. A.; Dagle, V.; Bearden, M. D.; Holladay, J. D.; Krause, T. R.; Ahmed, S. *An Overview of Natural Gas Conversion Technologies for Co-Production of Hydrogen and Value-Added Solid Carbon Products*; tech. rep.; Pacific Northwest National Lab. (PNNL), Richland, WA (United States); Argonne National Lab. (ANL), Argonne, IL (United States), 2017, DOI: 10.2172/1411934.

(60) Yang, M.; Baeyens, J.; Li, S.; Zhang, H. Hydrogen and carbon produced by fluidized bed catalytic methane decomposition. *Chemical Engineering Research and Design* **2024**, *204*, 67–80, DOI: 10.1016/j.cherd.2024.01.069.

(61) Statista Research Department. Carbon black market size worldwide in 2018 and 2023, with a forecast for 2030. Statista, https://www.statista.com/statistics/1350339/global-carbon-black-market-size/#statisticContainer (accessed 02/18/2025).

(62) Mordor Intelligence Research & Advisory. Carbon Black Market Report - Industry Growth, Size & Forecast Analysis (2025 - 2030). https://www.mordorintelligence.com/industry-reports/carbon-black-market (accessed 02/18/2025).

(63) Statista Research Department. Market value of nanofiber products worldwide in 2018 and 2023. Statista, https://www.statista.com/statistics/967727/global-nanofiber-market-value/ (accessed 02/18/2025).

(64) Alhamed, H.; Behar, O.; Saxena, S.; Angikath, F.; Nagaraja, S.; Yousry, A.; Das, R.; Altmann, T.; Dally, B.; Sarathy, S. M. From methane to hydrogen: A comprehensive review to assess the efficiency and potential of turquoise hydrogen technologies. *International Journal of Hydrogen Energy* **2024**, *68*, 635–662, DOI: 10.1016/j.ijhydene.2024.04.231.

(65) Statista Research Department. Carbon nanotube market value worldwide in 2021 with a forecast to 2030. Statista, https://www.statista.com/statistics/714463/global-market-value-of-carbon-nanotubes/ (accessed 02/19/2025).

(66) Statista Research Department. Market value of carbon nanotubes worldwide from 2018 to 2026, by region. Statista, https://www.statista.com/statistics/1037740/global-carbon-nanotube-market-value-by-region/ (accessed 02/20/2025).

(67) Nanografi. Carbon Nanofibers, Purity: >95%, Outside Diameter: 50-150nm https://shop.nanografi.com/carbon-nanotubes/carbon-nanofibers-purity-95-outside-diameter-50-150-nm/?searchid=908702&search_query=carbon+nanofiber (accessed 10/01/2025).

(68) Verschoor, A. *Update of ecological risk limits of nickel in soil*; RIVM Letter Report 2015-0137; Rijksinstituut voor Volksgezondheid en Milieu (RIVM), 2015, https://www.rivm.nl/bibliotheek/rapporten/2015-0137.pdf.

(69) Gates, A.; Jakubowski, J. A.; Regina, A. C., *Nickel Toxicology*; StatPearls Publishing: 2023, https://www.ncbi.nlm.nih.gov/books/NBK592400/.

(70) Nanografi. Graphitized Carbon Nanofibers (purity 99.9%, outside diameter 50–150 nm, length 1–15 µm). https://shop.nanografi.com/carbon-nanotubes/graphitized-carbon-nanofibers-purity-99-9-outside-diameter-50-150-nm-length-1-15-m/ (accessed 10/01/2025).

(71) Sigma-Aldrich. Carbon Nanofibers, Pyrolitically Stripped, Platelets (Conical), >98% Carbon Basis, D × L 100 nm × 20–200 µm. https://www.sigmaaldrich.com/NL/en/product/aldrich/719811 (accessed 10/01/2025).

(72) Sigma-Aldrich. Carbon Nanofibers, Graphitized, Platelets (Conical), >98 % Carbon Basis, D × L 100 nm × 20–200 µm. https://www.sigmaaldrich.com/NL/en/product/aldrich/719803 (accessed 10/01/2025).

(73) US Research Nanomaterials, Inc. Carbon NanoFibers, Purity: >95%, Diameter 200-600nm, length 20-50um. https://www.us-nano.com/inc/sdetail/317 (accessed 03/31/2025).

(74) ACS Material. Carbon nanofibers. https://www.acsmaterial.com/carbon-nanofibers.html (accessed 03/31/2025).

(75) Nanografi. Single Walled Carbon Nanotubes, Purity: > 96%, Dia: 1.0 nm. https://shop.nanografi.com/carbon-nanotubes/single-walled-carbon-nanotubes-purity-96-dia-1-0-nm/ (accessed 10/01/2025).

(76) Nanografi. Single Walled Carbon Nanotubes, Purity: > 92%, OD: 1-2 nm. https://shop.nanografi.com/carbon-nanotubes/single-walled-carbon-nanotubes-purity-92-od-1-2-nm/ (accessed 10/01/2025).

(77) Nanografi. Short Single Walled Carbon Nanotubes, Purity: > 65%, SSA: 400 m2/g. https://shop.nanografi.com/popular-products/short-single-walled-carbon-nanotubes-purity-65-ssa-400-m2-g/?searchid=909950&search_query=single+walled (accessed 10/01/2025).

(78) Towler, G.; Sinnott, R., *Chemical Engineering Design: Principles, Practice and Economics of Plant and Process Design*, 3th ed.; Butterworth-Heinemann: 2021, DOI: 10.1016/C2019-0-02025-0.

(79) Dimian, A. C.; Bildea, C. S.; Kiss, A. A., *Process Synthesis by the Hierarchical Approach*; Computer Aided Chemical Engineering, Vol. 35; Elsevier: 2014, pp 253–300, DOI: 10.1016/B978-0-444-62700-1.00007-3.

(80) Douglas, J. M., *Conceptual Design of Chemical Processes*; McGraw-Hill: 1988.

(81) Parhi, P. K.; Park, K. H.; Senanayake, G. A kinetic study on hydrochloric acid leaching of nickel from Ni–Al2O3 spent catalyst. *Journal of Industrial and Engineering Chemistry* **2013**, *19*, 589–594, DOI: 10.1016/j.jiec.2012.09.028.

(82) The Engineering ToolBox Solids – Specific Heats https://www.engineeringtoolbox.com/specific-heat-solids-d_154.html (accessed 11/18/2025).

(83) Trojosky, M. Rotary drums for efficient drying and cooling. *Drying Technology* **2019**, *37*, 632–651, DOI: 10.1080/07373937.2018.1552597.

(84) Zeng, L.; Li, L.; Xiao, J.; Zhou, P.; Han, X.; Shen, B.; Dai, L. Microplastics in the Environment: A Review Linking Pathways to Sustainable Separation Techniques. *Separations* **2025**, *12,* 82, DOI: 10.3390/separations12040082.

(85) Acharya, P.; Ives, P. Incineration at Bayou Bounfouca remediation project. *Waste Management* **1994**, *14*, 13–26, DOI: 10.1016/0956-053X(94)90017-5.

(86) Mohanty, S.; Chalavadi, G.; Majumdar, A. K. In *Proceedings of the XVI International Seminar on Mineral Processing Technology (MPT 2017)*, Mahabalipuram, Chennai, India, 2017, https://eprints.nmlindia.org/7875/.

(87) Svarovsky, L., *Solid-Liquid Separation*, 4th ed; Butterworth-Heinemann: Oxford, 2000.

(88) Bickert, G. In *The Coal Handbook (Second Edition)*, Osborne, D., Ed., 2nd Edition; Woodhead Publishing Series in Energy, Vol. 1; Woodhead Publishing: 2023, pp 491–510, DOI: 10.1016/B978-0-12-824328-2.00013-3.

(89) Sutherland, K. S., *Filters and Filtration Handbook*, 5th ed; Elsevier/Butterworth-Heinemann: 2007.

(90) Mujumdar, A. S., *Handbook of Industrial Drying*, 2nd ed., revised and expanded; Marcel Dekker Inc.: 1995.

(91) Statista Research Department. Relative Humidity in the Netherlands. Statista, https://www.statista.com/statistics/1012972/relative-humidity-in-the-netherlands/ (accessed 09/23/2025).

(92) The Engineering ToolBox. Water Vapor Saturation Pressure: Data, Tables & Calculator. https://www.engineeringtoolbox.com/water-vapor-saturation-pressure-d_599.html (accessed 09/23/2025).

(93) World Health Organization, *WHO Global Air Quality Guidelines: Particulate Matter ($PM_{2.5}$ and PM_{10}), Ozone, Nitrogen Dioxide, Sulfur Dioxide and Carbon Monoxide*; World Health Organization: Geneva, 2021.

(94) Çengel, Y. A.; Ghajar, A. J., *Heat and Mass Transfer: Fundamentals and Applications*, 6th ed., Table 11.1; McGraw-Hill Education: 2020, p 683.

(95) US Research Nanomaterials, Inc. Graphitized Carbon NanoFibers, Purity >99.9%, Diameter 200–600 nm, Length 20–50 µm, https://www.us-nano.com/inc/sdetail/984, Accessed: 2025-09-24, 2025.

(96) Moran, M. J.; Shapiro, H. N., *Fundamentals of Engineering Thermodynamics*, 7th ed.; Wiley: 2010, p 927.

(97) Murugan, P.; Dhanushkodi, S.; Sudhakar, K.; Wilson, V. H. Industrial and Small-Scale Biomass Dryers: An Overview. *Energy Engineering* **2021**, *118*, 435–446, DOI: 10.32604/EE.2021.013491.

(98) Mujumdar, A. S., *Classification and Selection of Industrial Dryers*, 2nd ed; Marcel Dekker Inc.: 2000, p 40.

(99) Martínez, I. *Heat of Solution Data for Aqueous Solutions*; Technical Report; Universidad Politécnica de Madrid, ETSIAE, 2025, http://imartinez.etsiae.upm.es/~isidoro/dat1/Heat%20of%20solution%20data.pdf (accessed 11/18/2025).

(100) Woods, D. R., *Rules of Thumb in Engineering Practice*; Wiley-VCH Verlag GmbH & Co. KGaA: 2007.

(101) Department of Chemical Engineering, University of Manchester. Chemical Engineering Plant Cost Index. https://www.training.itservices.manchester.ac.uk/public/gced/CEPCI.html?reactors/CEPCI/index.html (accessed 07/15/2025).

(102) Industrial Assessment Center Program *IAC Decarb Tipsheet 3: High-Temperature Heat Pumps*; tech. rep.; Lawrence Berkeley National Laboratory for the U.S. Department of Energy, 2023, https://industrialapplications.lbl.gov/sites/default/files/pdf-embeds/IAC%20Decarb%20Tipsheet%203.pdf (accessed 06/20/2025).

(103) Mike | Price Indexes. Hydrochloric Acid Price Index. BusinessAnalytiq., https://businessanalytiq.com/procurementanalytics/index/hydrochloric-acid-price-index/ (accessed 08/04/2025).

(104) Turton, R.; Bailie, R. C.; Whiting, W. B.; Shaeiwitz, J. A., *Analysis, Synthesis, and Design of Chemical Processes*, 3rd ed.; Pearson Education (Prentice Hall): 2009.

(105) The Global Economy. Netherlands: Consumer Price Index (CPI). https://www.theglobaleconomy.com/Netherlands/cpi/ (accessed 08/13/2025).

(106) EUEnergy. Electricity prices Netherlands. https://euenergy.live/country.php?a2=NL (accessed 08/04/2025).

(107) Hjort, M.; Spence, M. *2013 Survey of Waste Production and Management at European Refineries*; Technical Report 12/17; Brussels: Concawe / NewFields Consultants, 2017, DOI: 10.13140/RG.2.2.32241.79206.

(108) Nationale Beroepengids. Salaris Procesoperator. https://www.nationaleberoepengids.nl/salaris/procesoperator (accessed 09/24/2025).

(109) Procestechniek.nl. Procesoperator Salaris. https://www.procestechniek.nl/werken-in-de-procestechniek/procesoperator/salaris/ (accessed 09/24/2025).

(110) Indeed Nederland. Procesoperator Salaris in Nederland. https://nl.indeed.com/career/procesoperator/salaries (accessed 09/24/2025).

(111) Werkzoeken.nl. Salaris Procesoperator. https://www.werkzoeken.nl/salaris/proces-operator/ (accessed 09/24/2025).

(112) Bloomberg L.P. EUR/USD Exchange Rate. https://www.bloomberg.com/quote/EURUSD:CUR (accessed 07/02/2025).

(113) Virtanen, P. et al. SciPy 1.0: Fundamental Algorithms for Scientific Computing in Python. *Nature Methods* **2020**, *17*, 261–272, DOI: 10.1038/s41592-019-0686-2.

(114) Metropolis, N.; Ulam, S. The Monte Carlo Method. *Journal of the American Statistical Association* **1949**, *44*, 335–341, DOI: 10.1080/01621459.1949.10483310.

A

Acid Leaching Experimental Procedure

The experimental procedure of the acid leaching experiments of CNF samples containing nickel is shown in this Appendix. The procedure has been outlined in collaboration with P.B. Tamarona.

Experimental procedure for the purification of carbon nanofibres containing a Ni/SiO_2 catalyst using acid leaching

1. Scanning Electron Microscopy (SEM)

PIC: Prasad Gonugunta

Goal: To compare the structural condition of nanocarbons before and after the acid leaching process, determining whether the acid has any effect on the nanocarbon structure.

This technique will be used to observe the internal structure, morphology, and compositional contrast of the nanocarbon samples before and after acid leaching.

2. X-ray Diffraction (XRD) Analysis

PIC: Prasad Gonugunta

Goal: To characterize the structure and species of the nanocarbons, including trace amounts of catalyst, before and after the acid leaching process, determining whether there is a shift in carbon forms or metal content.

This technique is a non-destructive technique, based on the constructive interference of monochromatic X-rays and a crystalline sample, that

3. X-ray Fluorescence (XRF) Analysis

PIC: Prasad Gonugunta

Goal: To measure how effective the leaching process to extract the Ni and other impurities from the nanocarbons.

This technique uses the interaction of X-rays with a material (non-destructive) to determine its elemental composition (qualitative and quantitative analysis). This analysis will be done before and after the leaching process.

4. Inductively Coupled Plasma (ICP) Analysis

PIC: Michel van den Brink

Goal: To measure the nickel contents in before and after the leaching and determine the effectiveness of the leaching.

This technique requires prior burning of the carbon sample, such that the nickel remains. ICP analysis is suitable for samples with very low concentrations. It atomizes the sample and creates small atomic ions which can then be detected.

5. Acid Leaching of The Nanocarbons

PIC: Panji Tamarona

Goal: To study the effectiveness of acid leaching for purifying nanocarbons from traces of metal catalysts, at various concentrations, temperature, reactor type and the help of sonicator.

Raw materials:

a. Nanocarbon samples (+/- 100 gr)
b. Acids: HCl, H_2SO_4
c. Ammonium acids/salts: ammonium hydroxide and ammonium sulfate salt
d. Water

Equipment:

a. Thermoshaker (IKA Matrix Orbital Delta plus Package)
b. 2 ml x 24 vials attachment
c. 5 ml x 8 vials attachment
d. Sonicator
e. Plastic vials 1.5 ml x 48 pcs
f. Plastic vials 2 ml x 48 pcs
g. Plastic vials 3 ml x 20 pcs
h. Plastic vials 5 ml x 16 pcs
i. Funnel x 15 pcs: ideally glass, with small stem.
j. Paper filter x 500 pcs: Whatman Grade 42
k. Dropper x 4 pcs: NL: pipetten
l. Water heater: ideally a heating bath because it has temperature gauge. Else: water cooker?
m. Oven
n. Petri dish x 48 pcs: glass, 60-100 mm diameter with 15 mm height.
o. Platinum crucible x 4 pcs: 30-50 mL
p. Lid cover for crucible x 4 pcs: size follows the crucibles.
q. Sticker labels for the vials: 150 pcs

Safety gear:

a. Lab coat
b. Safety goggles
c. Fume hood

Chemical reactions:

Nickel with hydrochloric acid:
$Ni + HCl \rightarrow NiCl_2 + H_2$
Safety concern: beware of hydrogen coming out. So it can be recommended to put the thermoshaker in the fume hold.

Nickel with nitric acid:
$Ni + 4HNO_3 \rightarrow Ni(NO_3)_2 + 2H_2O + 2NO_2$

Nickel with sulphuric acid:
$Ni + H_2SO_4 \rightarrow NiSO_4 + H_2$
Ionic: $Ni + 2H^+ + SO_4^{2-} \rightarrow Ni^{2+} + SO_4^{2-} + H_2$

Nickel with ammonium salt:
$Ni + 2NH_4Cl \rightarrow NiCl_2 + 2NH_4$

Procedure:

A. Preliminary experiments

- Leaching the nanocarbon with thermoshaker using 6 Vials of 2 ml for 4 hours with >500 rpm.
- **Nanocarbons samples required**: 0.2 gr/vials x 6 vials/exp. = **1.2 gr**
- **Acid samples required**: **~12 ml for each acid**
- Use H_2SO_4 as acid
- 4M acid concentration, 70 °C and 4 h residence time.
- Each sample is washed with water before XRF, XRD, ICP and SEM analyses.
- The goal is to determine whether the leaching will actually work.

Important Rule:

Write down on the label when something has undergone the purification, the filtration, the drying etc.

Steps:

1. Conduct XRF, XRD and SEM analyses on untreated samples.
2. Burn the carbon for the untreated samples at 950*C for 12 min in the oven.
3. Conduct ICP analysis
    - Use a platinium crucible for holdig the sample. If not available, use quartz/silica/alumina
    - Use a lid to cover the crucible so that the Ni nanoparticles do not fly away
    - Use HCL or HNO3 as the solution for the ICP analysis
4. Prepare the acid mixture of water + acid with the correct concentration
    a. M1*V1 = M2*V2, M is molarity, V is volume. Is equation to use for mixing.
5. Make holes in the lids of the vials that will be used.
6. Label the vials with stickers. Write acid concentration, temperature, residence time and contents on it.
7. Put the vials in the thermoshaker, do not turn on the thermoshaker yet.
8. Add the acid mixture using a dropper to the vials and heat it to the specified temperature using the thermoshaker.
9. Add the carbon samples to the vials
10. Sonicate the samples using a sonicater for a predefined time and frequency if necessary
11. Let the thermoshaker run for the specified time and at the specified temperature
12. After the thermoshaker is finished, remove the vials
13. Filter the acid/nanocarbon mixture for each vial:
    a. Measure weight of an empty vial
    b. Put a funnel with paper filter on top of a vial
    c. Pour the acid/nanocarbon mixture in the funnel. The nanocarbon will stay behind on the paper filter and the acid will drop into the empty vial
    d. Collect the nanocarbon
    e. Measure the remaining acid
14. Heat water to 70-100*C.

15. For each sample, wash the nanocarbon by pouring hot water (70*C-100*C) with a dropper on the nanocarbon. Minimum of three times/drops.
16. Dry the nanocarbon in the oven at 120*C for 4 hours. Use a petri dish to hold a sample.
17. Conduct XRF, XRD and SEM measurements on the samples.
18. Burn the carbon for each sample at 950*C for 12 min in the oven.
19. Conduct ICP analysis on each sample
    - Use a platinium crucible for holdig the sample. If not available, use quartz/silica/alumina
    - Use a lid to cover the crucible so that the Ni nanoparticles do not fly away
    - Use HCL or HNO3 as the solution for the ICP analysis

B. Acid concentration effects

- Leaching the nanocarbon with thermoshaker using the 2 ml x 24 vials attachment → three times using HCl, H_2SO_4 and ammonium sulfate salt.
- **Nanocarbons samples required**: 0.2 gr/vials x 24 vials/exp. x 3 exp. = **14.4 gr**
- **Acid samples required**: ~**16.8 ml for each acid**
- Each sample is washed with water before XRF, XRD, ICP and SEM analyses.

Important Rule:

Write down on the label when something has undrgone the purification, the filtration, the drying etc.

Steps:

1. Prepare the acid mixture of water + acid with the correct concentration
    a. M1*V1 = M2*V2, M is molarity, V is volume. Is equation to use for mixing.
2. Make holes in the lids of the vials that will be used.
3. Label the vials with stickers. Write acid concentration, temperature, residence time and contents on it.
4. Put the vials in the thermoshaker, do not turn on the thermoshaker yet.
5. Add the acid mixture using a dropper to the vials and heat it to the specified temperature using the thermoshaker.
6. Add the carbon samples to the vials
7. Sonicate the samples using a sonicater for a predefined time and frequency if necessary
8. Let the thermoshaker run for the specified time and at the specified temperature
9. After the thermoshaker is finished, remove the vials
10. Filter the acid/nanocarbon mixture for each vial:
    a. Measure weight of an empty vial
    b. Put a funnel with paper filter on top of a vial
    c. Pour the acid/nanocarbon mixture in the funnel. The nanocarbon will stay behind on the paper filter and the acid will drop into the empty vial

d. Collect the nanocarbon
e. Measure the remaining acid

11. Heat water to 70-100*C.
12. For each sample, wash the nanocarbon by pouring hot water (70*C-100*C) with a dropper on the nanocarbon. Minimum of three times/drops.
13. Dry the nanocarbon in the oven at 120*C for 4 hours. Use a petri dish to hold a sample.
14. Conduct XRF, XRD and SEM measurements on the samples.
15. Burn the carbon for each sample at 950*C for 12 min in the oven.
16. Conduct ICP analysis on each sample
    - Use a platinium crucible for holdig the sample. If not available, use quartz/silica/alumina
    - Use a lid to cover the crucible so that the Ni nanoparticles do not fly away
    - Use HCL or HNO3 as the solution for the ICP analysis

Vials	Samples (gr)	Solvent vol. (ml)	Temperature (°C)	Residence time (h)	Acid conc. (M)
1	0.2	2	60	1	1
2	0.2	2	60	1	1
3	0.2	2	60	1	1
4	0.2	2	60	1	1
5	0.2	2	60	1	2
6	0.2	2	60	1	2
7	0.2	2	60	1	2
8	0.2	2	60	1	2
9	0.2	2	60	1	3
10	0.2	2	60	1	3
11	0.2	2	60	1	3
12	0.2	2	60	1	3
13	0.2	2	60	1	4
14	0.2	2	60	1	4
15	0.2	2	60	1	4
16	0.2	2	60	1	4
17	0.2	2	60	1	5
18	0.2	2	60	1	5
19	0.2	2	60	1	5
20	0.2	2	60	1	5
21	0.2	2	60	1	6
22	0.2	2	60	1	6
23	0.2	2	60	1	6
24	0.2	2	60	1	6

C. Temperature and residence time effects

- Leaching the nanocarbon with thermoshaker using the 2 ml x 24 vials attachment → at temperatures (°C) of 30, 50, 70 and 90.
- **Nanocarbons samples required**: 0.2 gr/vials x 24 vials/exp. x 4 exp. = **19.2 gr**
- **Acid samples required**: **---**
  (type and concentration of acid is TBD, based on the results of experiment A)
- Each sample is washed with water before XRF, XRD, ICP and SEM analyses.

Important Rule:

Write down on the label when something has undrgone the purification, the filtration, the drying etc.

Steps:

1. Prepare the acid mixture of water + acid with the correct concentration
   b. M1*V1 = M2*V2, M is molarity, V is volume. Is equation to use for mixing.
2. Make holes in the lids of the vials that will be used.
3. Label the vials with stickers. Write acid concentration, temperature, residence time and contents on it.
4. Put the vials in the thermoshaker, do not turn on the thermoshaker yet.
5. Add the acid mixture using a dropper to the vials and heat it to the specified temperature using the thermoshaker.
6. Add the carbon samples to the vials
7. Sonicate the samples using a sonicater for a predefined time and frequency if necessary
8. Let the thermoshaker run for the specified time and at the specified temperature
9. After the thermoshaker is finished, remove the vials
10. Filter the acid/nanocarbon mixture for each vial:
    a. Measure weight of an empty vial
    b. Put a funnel with paper filter on top of a vial
    c. Pour the acid/nanocarbon mixture in the funnel. The nanocarbon will stay behind on the paper filter and the acid will drop into the empty vial
    d. Collect the nanocarbon
    e. Measure the remaining acid
11. Heat water to 70-100*C.
12. For each sample, wash the nanocarbon by pouring hot water (70*C-100*C) with a dropper on the nanocarbon. Minimum of three times/drops.
13. Dry the nanocarbon in the oven at 120*C for 4 hours. Use a petri dish to hold a sample.
14. Conduct XRF, XRD and SEM measurements on the samples.
15. Burn the carbon for each sample at 950*C for 12 min in the oven.
16. Conduct ICP analysis on each sample

- Use a platinium crucible for holdig the sample. If not available, use quartz/silica/alumina
- Use a lid to cover the crucible so that the Ni nanoparticles do not fly away
- Use HCL or HNO3 as the solution for the ICP analysis

Vials	Samples (gr)	Solvent vol. (ml)	Temperature (°C)	Residence time (h)	Acid conc. (M)
1	0.2	2	30/50/70/90	0.5	x
2	0.2	2	30/50/70/90	0.5	x
3	0.2	2	30/50/70/90	0.5	x
4	0.2	2	30/50/70/90	0.5	x
5	0.2	2	30/50/70/90	1	x
6	0.2	2	30/50/70/90	1	x
7	0.2	2	30/50/70/90	1	x
8	0.2	2	30/50/70/90	1	x
9	0.2	2	30/50/70/90	1.5	x
10	0.2	2	30/50/70/90	1.5	x
11	0.2	2	30/50/70/90	1.5	x
12	0.2	2	30/50/70/90	1.5	x
13	0.2	2	30/50/70/90	2.0	x
14	0.2	2	30/50/70/90	2.0	x
15	0.2	2	30/50/70/90	2.0	x
16	0.2	2	30/50/70/90	2.0	x
17	0.2	2	30/50/70/90	2.5	x
18	0.2	2	30/50/70/90	2.5	x
19	0.2	2	30/50/70/90	2.5	x
20	0.2	2	30/50/70/90	2.5	x
21	0.2	2	30/50/70/90	3.0	x
22	0.2	2	30/50/70/90	3.0	x
23	0.2	2	30/50/70/90	3.0	x
24	0.2	2	30/50/70/90	3.0	x

D. Sonication effects

- Leaching the nanocarbon with thermoshaker using the 5 ml x 8 vials attachment → 1 vial without sonication, 2 vials with sonication of 5 mins, 2 vials with sonication of 10 mins, 2 vials with sonication of 15 mins, 1 vial with sonication during the leaching.
- **Nanocarbons samples required**: 0.5 gr/vials x 8 vials/exp. x 2 exp. = **8 gr**
- **Acid samples required**: **---**
  (type and concentration of acid is TBD, based on the results of experiment A)
- Each sample is washed with water before XRF, XRD, ICP and SEM analyses.
  The leaching temperature is TBD, based on the results of experiment B

Important Rule:

Write down on the label when something has undrgone the purification, the filtration, the drying etc.

Steps:

1. Prepare the acid mixture of water + acid with the correct concentration
   c. M1*V1 = M2*V2, M is molarity, V is volume. Is equation to use for mixing.
2. Make holes in the lids of the vials that will be used.
3. Label the vials with stickers. Write acid concentration, temperature, residence time and contents on it.
4. Put the vials in the thermoshaker, do not turn on the thermoshaker yet.
5. Add the acid mixture using a dropper to the vials and heat it to the specified temperature using the thermoshaker.
6. Add the carbon samples to the vials
7. Sonicate the samples using a sonicater for a predefined time and frequency if necessary
8. Let the thermoshaker run for the specified time and at the specified temperature
9. After the thermoshaker is finished, remove the vials
10. Filter the acid/nanocarbon mixture for each vial:
    a. Measure weight of an empty vial
    b. Put a funnel with paper filter on top of a vial
    c. Pour the acid/nanocarbon mixture in the funnel. The nanocarbon will stay behind on the paper filter and the acid will drop into the empty vial
    d. Collect the nanocarbon
    e. Measure the remaining acid
11. Heat water to 70-100*C.
12. For each sample, wash the nanocarbon by pouring hot water (70*C-100*C) with a dropper on the nanocarbon. Minimum of three times/drops.
13. Dry the nanocarbon in the oven at 120*C for 4 hours. Use a petri dish to hold a sample.
14. Conduct XRF, XRD and SEM measurements on the samples.
15. Burn the carbon for each sample at 950*C for 12 min in the oven.

16. Conduct ICP analysis on each sample
    - Use a platinium crucible for holdig the sample. If not available, use quartz/silica/alumina
    - Use a lid to cover the crucible so that the Ni nanoparticles do not fly away
    - Use HCL or HNO3 as the solution for the ICP analysis

Vials	Samples (gr)	Solvent vol. (ml)	Temperature (°C)	Residence time (h)	Acid conc. (M)
1	0.5	2	x	1	y
2	0.5	2	x	1	y
3	0.5	2	x	1	y
4	0.5	2	x	1	y
5	0.5	2	x	1	y
6	0.5	2	x	1	y
7	0.5	2	x	1	y
8	0.5	2	x	1	y

E. Water absorption by CNF

Conduct water absorption experiments to determine how well the CNF absorbs water and what the required drying time and temperature are.

Steps:

1. Weigh the CNF sample
2. Put the sample in the oven at 120*C for a specified amount of time. The sample will then surely be dry before conducting the experiment.
3. Drench the sample in water for 10 minutes
4. Weigh the sample
5. Determine how much water the sample has absorbed
6. Put the sample in the oven again at 120*C for a specified amount of time
7. Take the sample out of the oven and weigh the sample.
8. Determine how much water has been evaporated during the drying.

B

Baseline Equipment Overview

This Appendix gives an overview of the equipment sizes for the baseline scenario of the process design, see Table B.1

Table B.1: Equipment size overview for the baseline scenario. First the equipment name in the process flow sheet is given, followed by the names in Aspen.

Equipment	**Name in Aspen**	**Size**	**Unit**
Rotary solids cooler	CNFCOOLE	43.1	m^2
CSTR	CSTR	127.3	m^3
Three phase separator	SEP	11.8	L s^{-1}
Hydrocyclone	HYDRO1	11.6	L s^{-1}
Vacuum drum filter 1	FILTER1	19.2	m^2
Washer	WASHER	0.6	L s^{-1}
Vacuum drum filter 2	FILTER2	5.8	m^2
Slurry heater	SOLHEATE	84.8	m^2
Rotary dryer	DRYER	171.7	m^2
Air condenser	/	569.9	m^2
Air filter	/	3.8	Nm^3 s^{-1}
Air heater	AIRHEATE	143.3	m^2
Pump	/	18.4	L s^{-1}
Steam generator	/	46.7	MMBtu hr^{-1}

C

Process Stream Overview

This Appendix shows the process stream details for the baseline scenario of the process plant. For each stream the name in the flow sheet and, if relevant, the Aspen name is given. The temperature, pressure, flow rates and composition of the streams are also indicated. For non-coloured streams, the details have been directly retrieved from Aspen. For yellow streams, the details have been extracted from the Python code for the baseline scenario or from calculations by hand. For orange streams, the details have not been calculated.

While the recycle streams of water and steam are detailed in the process flow sheet in Figure 5.2, the recycle streams are not considered in the techno-economic model.

Stream	Main-1	Main-2	Main-3	Main-4	Main-5
Aspen stream name	CNFFEED	CNFFEEDC	CSTROUT	SEPBOT	HYDR1SOL
Temperature (*C)	600	80	80	67,2797083	67,2797083
Pressure (atm)	1,01325	1,01325	1,01325	1,01325	1,01325
Liquid flow rate (kg/hr)			34158,14464	34158,1158	1405,00989
Liquid mass fractions					
H2O			0,92938715	0,92938794	0,92938794
HCL			0,070557718	0,07055778	0,07055778
CL-			2,97E-05	2,97E-05	2,97E-05
NI++			2,46E-05	2,46E-05	2,46E-05
H2			8,44E-07		
Solid flow rate (kg/hr)	3470	3470	3469,160217	3469,16022	3122,24419
Solid mass fractions					
C	0,994173	0,994173	0,994413661	0,99441366	0,99441366
NI	0,0047	0,0047	0,004459067	0,00445907	0,00445907
MG	0,000638	0,000638	0,000638154	0,00063815	0,00063815
AL	0,000133	0,000133	0,000133032	0,00013303	0,00013303
FE	3,30E-05	3,30E-05	3,30E-05	3,30E-05	3,30E-05
CA	3,30E-05	3,30E-05	3,30E-05	3,30E-05	3,30E-05
SI	0,00029	0,00029	0,00029007	0,00029007	0,00029007
Dust waste					
Vapor flow rate (kg/hr)					
Vapor mass fractions					
H2O					
HCL					
H2					
AIR					

Stream	Main-6	Main-7	Main-8	Main-9	Main-10	Acid-1
Aspen stream name	FILTSOL	WASHSOL	FILT2SOL	DRYERIN	DRYEROUT	HCLFEED
Temperature (*C)	67,279708	32,8479821	32,847982	100	100	20
Pressure (atm)	1,01325	1,01325	1,01325	1,01325	1,01325	1,01325
Liquid flow rate (kg/hr)	702,50494	843,005933	632,25445			34157,3
Liquid mass fractions						
H2O	0,9293879	0,98332885	0,9833288			0,92941
HCL	0,0705578	0,01665833	0,0166583			0,07059
CL-	2,97E-05	7,01E-06	7,01E-06			
NI++	2,46E-05	5,80E-06	5,80E-06			
H2						
Solid flow rate (kg/hr)	2810,0198	2810,01978	2529,0178	2528,2842	2528,28421	
Solid mass fractions						
C	0,9944137	0,99441366	0,9944137	0,9947022	0,99470219	
NI	0,0044591	0,00445907	0,0044591	0,0044604	0,00446036	
MG	0,0006382	0,00063815	0,0006382	0,0006383	0,00063834	
AL	0,000133	0,00013303	0,000133	0,0001331	0,00013307	
FE	3,30E-05	3,30E-05	3,30E-05	3,30E-05	3,30E-05	
CA	3,30E-05	3,30E-05	3,30E-05	3,30E-05	3,30E-05	
SI	0,0002901	0,00029007	0,0002901	0	0	
Dust waste						
Vapor flow rate (kg/hr)				632,24635		
Vapor mass fractions						
H2O				0,9833415		
HCL				0,0166585		
H2						
AIR						

Stream	Waste-1	Waste-2	Waste-3	Waste-4	Waste-5	Waste-6
Aspen stream name	HYDR1LIQ	FILTLIQ	WASLIQOU	FILT2LIQ		
Temperature (*C)	67,279708	67,27971	32,8479821	32,847982		
Pressure (atm)	1,01325	1,01325	1,01325	1,01325		
Liquid flow rate (kg/hr)	32753,106	702,5049	3329,49901	210,75148	36995,86	632
Liquid mass fractions						
H2O	0,9293879	0,929388	0,98932228	0,9833288		
HCL	0,0705578	0,070558	0,01066951	0,0166583		
CL-	2,97E-05	2,97E-05	4,49E-06	7,01E-06		
NI++	2,46E-05	2,46E-05	3,72E-06	5,80E-06		
H2						
Solid flow rate (kg/hr)	346,91602	312,2244		281,00198	940,1424	
Solid mass fractions						
C	0,9944137	0,994414		0,9944137		
NI	0,0044591	0,004459		0,0044591		
MG	0,0006382	0,000638		0,0006382		
AL	0,000133	0,000133		0,000133		
FE	3,30E-05	3,30E-05		3,30E-05		
CA	3,30E-05	3,30E-05		3,30E-05		
SI	0,0002901	0,00029		0,0002901		
Dust waste						
Vapor flow rate (kg/hr)						
Vapor mass fractions						
H2O						
HCL						
H2						
AIR						

Stream	Air-1	Air-2	Air-3	Air-4	Air-5	Air-6	Air-7
Aspen stream name	DRYAIR		DRYAIRHE	USEDAIR			
Temperature (*C)	20		100	100			
Pressure (atm)	1,01325		1,01325	1,01325			
Liquid flow rate (kg/hr)							
Liquid mass fractions							
H2O							
HCL							
CL-							
NI++							
H2							
Solid flow rate (kg/hr)							
Solid mass fractions							
C							
NI							
MG							
AL							
FE							
CA							
SI							
Dust waste							
Vapor flow rate (kg/hr)	18881		18881	19513,25			
Vapor mass fractions							
H2O				0,031861			
HCL				0,00054			
H2							
AIR	1		1	0,967599			

Stream	Gas-1	Dust-1	Water-1	Water-2	Water-3	Water-4	Water-5
Aspen stream name	SEPTOP						
Temperature (*C)	67,27971						
Pressure (atm)	1,01325						
Liquid flow rate (kg/hr)			167821	12238		66246	
Liquid mass fractions							
H2O			1	1		1	
HCL							
CL-							
NI++							
H2							
Solid flow rate (kg/hr)		0,000195					
Solid mass fractions							
C							
NI							
MG							
AL							
FE							
CA							
SI							
Dust waste		1					
Vapor flow rate (kg/hr)	0,028845						
Vapor mass fractions							
H2O							
HCL							
H2	1						
AIR							

Stream	Water-6	Water-7	Water-8	Steam-1	Steam-2	Steam-3	Steam-4
Aspen stream name	WASLIQIN						
Temperature (*C)	20						
Pressure (atm)	1,01325						
Liquid flow rate (kg/hr)	3470	85861					
Liquid mass fractions							
H2O	1	1					
HCL							
CL-							
NI++							
H2							
Solid flow rate (kg/hr)							
Solid mass fractions							
C							
NI							
MG							
AL							
FE							
CA							
SI							
Dust waste							
Vapor flow rate (kg/hr)				66246	48445		17801
Vapor mass fractions							
H2O				1	1		1
HCL							
H2							
AIR							

Stream	Steam-5	Steam-6	Steam-7	Steam-8
Aspen stream name				
Temperature (*C)				
Pressure (atm)				
Liquid flow rate (kg/hr)				
Liquid mass fractions				
H2O				
HCL				
CL-				
NI++				
H2				
Solid flow rate (kg/hr)				
Solid mass fractions				
C				
NI				
MG				
AL				
FE				
CA				
SI				
Dust waste				
Vapor flow rate (kg/hr)	9413		8387	
Vapor mass fractions				
H2O	1		1	
HCL				
H2				
AIR				